ECCENTRICITY BASED ANALYSIS OF CONFINED REINFORCED CONCRETE CIRCULAR COLUMNS

by

AHMED MOHSEN ABD EL FATTAH

B.Sc., Cairo University, Egypt, 2000.

A THESIS

Submitted in partial fulfillment of the requirements for the degree

MASTER OF SCIENCE

Department of Civil Engineering
College of Engineering

KANSAS STATE UNIVERSITY
Manhattan, Kansas

2008

Approved by:

Major Professor
Hayder Rasheed

Copyright

Abstract

The development of column interaction diagrams for unconfined concrete is a standard analysis procedure. However, the need to develop analysis tools for the actual ultimate capacity of columns is evident. Modern codes and standards are introducing the need to perform extreme event analysis. In previous studies, various models were implemented to assess the ultimate confined capacity of columns under concentric axial loads. On the other hand, the effect of confinement in case of the eccentric axial load and the corresponding bending moment are not investigated in such models. So it is demanded to relate the strength and ductility to the degree of confinement utilization in a new model. The more the eccentricity the less the confinement engaged till the effect of the confinement vanishes at pure bending. Accordingly, the ultimate confined strength and the maximum strain range between the fully confined values f'_{cc} and ε_{cu} (at zero eccentricity) and the unconfined values f'_c and 0.003 (at infinite eccentricity) depending on the level of eccentricity.

$$\overline{f_{cc}} = \frac{1}{1+\frac{e}{H}} f'_{cc} + \frac{1}{1+\frac{H}{e}} f_{co}$$

Where $\overline{f_{cc}}$ = ultimate confined strength for the eccentric column.

H = diameter of the column.

Radial loading with constant eccentricity is followed in the nonlinear moment of area concept that considers the finite layer procedure and the secant stiffness approach, to achieve

equilibrium points of P-ε and M-φ up to failure. Three different comparisons are made to ensure the accuracy of the analysis. The first is to compare the unconfined analysis results with the well-known software (CSI-Section Builder). Secondly, the ultimate capacity of the confined section is compared with experimental data. Finally, the new eccentricity model is compared with the widely used Mander model, which is applicable to concentric columns, to examine the accuracy versus safety.

Table of Contents

List of Figures

List of Tables

Acknowledgements

"All the praises and thanks be to Allah, the lord of mankind, jinn and all that exists"

I wish to thank my mother Dr. Amany Aboellil

I would like to express my deepest and sincere gratitude to my advisor Dr. Hayder Rasheed who provided me with advising, and was a main reason of research completion. I wiould like to thank him for affording me the opportunity to gain my master degree at Kansas State University.

I extend my thanks to Dr Asad Esmaeily who supported me during different phases of project development, and was a main assistant in understanding programming concepts. I'd like to thank Dr Hani Melhem for serving in my committee members.

I would like to thank my wife for her assistant.

Finally, I would like to acknowledge Kansas department of transportation (KDot) for sponsoring this research.

Dedication

To the memory of my LATE FATHER

CHAPTER 1 - Introduction

1-1 Background

The importance of the analysis of circular columns to predict their load carrying capacity was recognized by the architects of the Roman Empire. The analysis of reinforced concrete circular columns is subject of interest since the turn of the twentieth century up to now. Despite the early introduction of the concept of confinement and its effects and despite the extensive research effort to model this phenomenon accurately, the analysis of confined concrete has not found its way to design practice of new columns or assessment routines of existing columns. It wasn't until very recently that design specifications and codes of practice, like AASHTO LRFD, started realizing the importance of introducing extreme event load cases that necessitates accounting for advanced behavioral aspects like confinement. Accordingly the literature is still lacking analysis tools that take into account confinement despite the availability of all kinds of confinement models.

1-2 Objectives

This study is intended to develop a 3-step analysis of reinforced concrete circular columns subjected to eccentric loading. First, the well-known ultimate capacity analysis of unconfined concrete is developed as a benchmarking step. Secondly, the unconfined ultimate interaction diagram is scaled down based on the Φ factors of the AASHTO LRFD to the design interaction diagram. Finally, the actual confined concrete ultimate analysis is developed based on a new eccentricity model accounting for partial confinement effect under eccentric loading. It is important to note that the present analysis procedure will be benchmarked against a wide range of experimental and analytical studies to establish its accuracy and reliability.

It is also the objective of this study to furnish interactive software with a user-friendly interface having analysis and design features that will facilitate the preliminary design of circular columns based on the actual demand.

1-3 Scope

This thesis is composed of seven chapters covering the development of material models, analysis procedures, benchmarking and practical applications.

Chapter one introduces the work highlighting the objectives and scope of the report. Chapter two details the literature reviews as it relates to the confinement models, experimental and analysis studies addressing the behavior of circular columns and the software available in the market to analyze and design the same type of columns. Chapter three describes the current confinement models used for concentric and eccentric loading in the present analysis procedures. Chapter four presents the formulation of the unconfined and confined analysis methods of the circular concrete columns cross sections. Chapter five is all about reporting on the results and comparisons providing the necessary discussions and comments. Chapter six briefs the reader on the software development, program interface deign and features. Chapter seven lists the conclusions and provides recommendations for future relevant work.

.

CHAPTER 2 - Literature Review

2-1 Overview

This chapter is divided into four main sections. The first section reviews the available confinement models with brief explanation for each, and viewing the circular confinement models. Then, experimental studies for columns, under concentric and eccentric load, take place. The third part covers eccentricity participation in literature. Finally, . The last section shows numerical and mathematical analysis done for unconfined and confined concrete analysis

2-2 Confined Models

Failure of reinforced concrete structures can be categorized by material failure, mechanical failure or combination between material and mechanical failure. Unlike the simple approach used for analyzing the behavior of plain concrete, the more complicated analysis of confined concrete has been conducted for about a hundred years and many models have been proposed. In 1899, Considere(Martinez et al. 1984). was the first to suggest the beneficial effect to confine axially loaded columns with spiral confinement. Morsch, Talbot, Bach, Graf, Withey, Emperger and Von Thullie made many contributions between 1900 and 1916(Martinez et al. 1984). The mother source equation for most of the models is having the form

$$f_{cc} = f_c^{'} + kf_l \tag{2-1}$$

where the maximum confined strength f_{cc} is related to the peak unconfined strength f'_c and the effective lateral confined pressure f_l with a coefficient k. This coefficient varies based on the concrete mix and the lateral confinement pressure and it was derived or obtained from the analytical and experimental work. The confinement models available in the literature are presented chronologically regardless of their comparative importance. Common notation is used for all the equations for the sake of consistency and comparison

Richart, Brandtzaeg and Brown (1928)

Richart et al. Model (Richart et al. 1928) was the first to capture the proportional relation between the lateral confined pressure and the ultimate compressive strength.

$$f_{cc} = f_c^{'} + k_1 f_l \tag{2-2}$$

The average value for the coefficient k_1, which was derived from a series of short column specimen tests, came out to be (4.1). The strain corresponding to the peak strength ε_{cc} is obtained from

$$\varepsilon_{cc} = \varepsilon_{co}\left[1 + k_2\left(\frac{f_l}{f_c^{'}}\right)\right] \qquad k_2 = 5k_1 \tag{2-3}$$

where ε_{cc} *is the strain corresponding to* $f'c$, k_2 is the strain coefficient of the effective lateral confinement pressure. No stress-strain curve was proposed by Richart et al.

Chan 1955

A tri-linear curve describing the stress-strain relationship was suggested by Chan (1955) based on experimental work. The ratio of the volume of steel ties to concrete core volume was the only variable in the experimental work done. Chan assumed that OA approximates the elastic stage and ABC approximates the plastic stage.

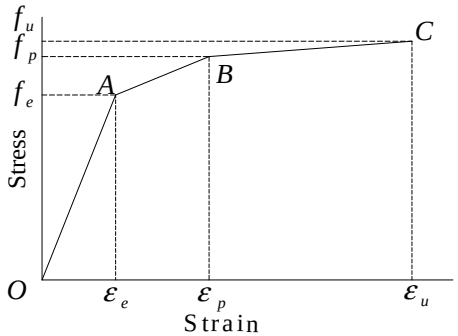

Figure 2-1 General Stress-Strain curve by Chan

Blume, Newmark and Corning (1961)

Blume et al. (1961) were the first to impose the effect of the yield strength for the transverse steel f_{yh} in different equations defining the model, The model generated has ascending straight line with steep slope starting from the origin till the plain concrete peak strength f'$_c$ and the corresponding strain ε_{co}, then a less slope straight line connect the latter point and the confined concrete peak strength f_{cc} and ε_{cc}

$$f_{cc} = 0.85 f_c^{'} + 4.1 \frac{A_s f_{yh}}{ah} \tag{2-4}$$

$$\varepsilon_{co} = \frac{0.22 f_c^{'} + 400 psi}{10^6 psi} \tag{2-5}$$

$$\varepsilon_{cc} = 5\varepsilon_y \tag{2-6}$$

where ε_y is the strain at yielding for the transverse reinforcement, A_s is the cross sectional area of transverse steel reinforcement and h is the cross section height.

Roy and Sozen (1965)

Based on their experimental results, which were controlled by two variables; ties spacing and amount of longitudinal reinforcement, Roy and Sozen (1965) concluded that there is no enhancement in the concrete capacity by using square ties. They proposed a bilinear ascending-descending stress strain curve that has a peak of the maximum strength of plain concrete f'_c and corresponding strain ε_{co} with a value of 0.002. On the other hand there was significant increase in ductility. The ultimate strain ε_{cu} was suggested to be a function of the volumetric ratio of ties to concrete core ρ_s, tie spacing s and the effective height of the cross section h.

$$\varepsilon_{cu} = \frac{3\rho_s h}{4s} \tag{2-7}$$

Soliman and Yu (1967)

Another model emerged from experimental results. The main parameters involved in the work done were tie spacing *s*, a new term represents the effectiveness of ties s_o, the area of ties A_s, and finally section geometry, which has three different variables; A_b the area of bond concrete under compression, A_c the area of concrete under compression and *b* which represents the effective width of the section. The model has three different portions as shown in Figure (2-2). The ascending portion that is represented by a curve till the peak point (f'_c, ε_{ce}). The flat straight-line portion with its length varying depending on the degree of confinement. The last portion is a descending straight line till (0.85 f_{cc}, ε_{cf}) then it extends down till the maximum strain.

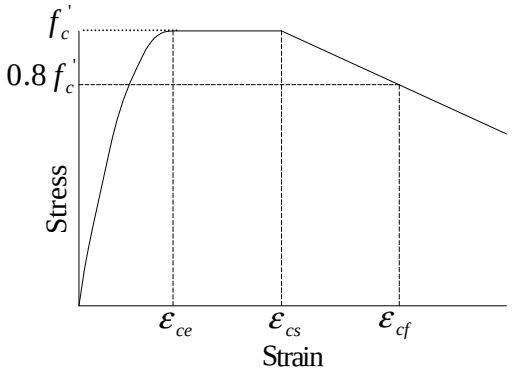

Figure 2-2 General Stress-Strain curve by Soliman and Yu.

$$q = \left(1.4\frac{A_b}{A_c} - 0.45\right)\frac{A_s\left(s_o - s\right)}{A_s s + 0.0028 b s^2} \tag{2-8}$$

$$f_{cc} = 0.9u_{cyl}\left(1 + 0.05q\right) \tag{2-9}$$

$$\varepsilon_{cc} = 0.55\, f_{cc} * 10^{-6} \tag{2-10}$$

$$\varepsilon_{cs} = 0.0025(1 + q) \tag{2-11}$$

$$\varepsilon_{cf} = 0.0045(1 + 0.85q) \tag{2-12}$$

Where *q* refers to the effectiveness of the transverse reinforcement.

Sargin (1971)

Sargin conducted experimental work on low and medium strength concrete with no longitudinal reinforcement. The transverse steel that was used had different size and different yield and ultimate strength. The main variable affected the results were the volumetric ratio of lateral reinforcement to concrete core ρ_s, the strength of plain concrete f'_c, the ratio of tie spacing to the width of the concrete core and the yield strength of the transverse steel f_{yh}.

$$f_c = k_3 f_c^{'}\left[\frac{Ax + (D-1)x^2}{1 + (A-2)x + Dx^2}\right] \tag{2-13}$$

where D is a constant controlling the slope of the descending branch:

$$D = 0.65 - 7.2 f_c^{'} * 10^{-3} \tag{2-14}$$

$$x = \frac{\varepsilon_c}{\varepsilon_{cc}} \tag{2-15}$$

$$A = \frac{E_c \varepsilon_{cc}}{k_3 f_c^{'}} \tag{2-16}$$

$$k_3 = 1 + 0.0145\left[1 - 0.245\frac{s}{b_c}\right]\frac{\rho_s f_{yh}}{\sqrt{f_c^{'}}} \tag{2-17}$$

$$\varepsilon_{cc} = 0.0024 + 0.0374\left[1 - \frac{0.734s}{b_c}\right]\frac{\rho_s f_{yh}}{\sqrt{f_c^{'}}} \tag{2-18}$$

$$f_{cc} = k_3 f_c^{'} \tag{2-19}$$

Where k_3 is concentric loading maximum stress ratio.

Kent and Park (1971)

As Roy and Sozen (1965) did, Kent and Park (1971) assumed that the maximum strength for confined and plain concrete is the same f'_c. The suggested curve starts from the origin then increases in a parabolic shape (Hognestad's Parabola) till the peak at f'_c and the corresponding strain ε_{co} at 0.002. Then it descends with one of two different straight lines. For the confined concrete, which is more ductile, it descends till the point (0.5 $f'c$, ε_{50c}) and continues descending to 0.2$f'c$ followed by a flat plateau. For the plain concrete it descends till the point (0.5 $f'c$, ε_{50u}) and continue descending to 0.2f'_c as well without a flat plateau. Kent and Park assumed that concrete could sustain strain to infinity at a constant stress of 0.2 $f'c$

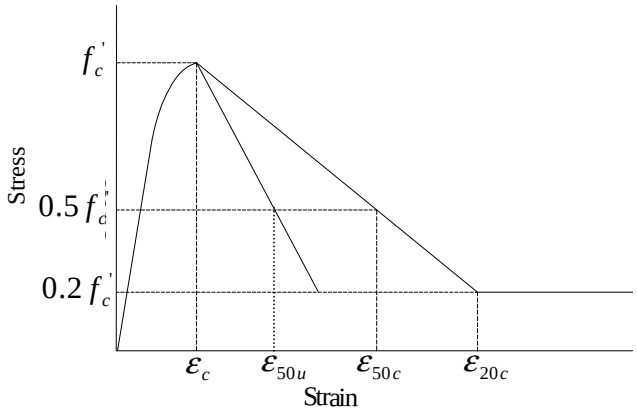

Figure 2-3 Stress-Strain curve by Kent et al.

$$f_c = f_c'\left[\frac{2\varepsilon_c}{\varepsilon_{co}} - \left(\frac{\varepsilon_c}{\varepsilon_{co}}\right)^2\right] \tag{2-20}$$

$$\varepsilon_{50u} = \frac{3 + 0.002 f_c'}{f_c' - 1000} \tag{2-21}$$

$$\rho_s = \frac{2(h+b)A_s}{hbs} \tag{2-22}$$

$$\varepsilon_{50h} = \varepsilon_{50c} - \varepsilon_{50u} \tag{2-23}$$

$$\varepsilon_{50h} = \frac{3}{4}\rho_l\sqrt{\frac{b}{s}} \tag{2-24}$$

$$Z = \frac{0.5}{\varepsilon_{50h} + \varepsilon_{50u} - \varepsilon_{co}} \tag{2-25}$$

where ρ_s is the ratio of lateral steel to the gross sectional area, z is constant controlling the slope of descending portion.

Vallenas, Bertero and Popov (1977)

The variables utilized in the experimental work conducted by Vallenas et al. (1977) were the volumetric ratio of lateral and longitudinal steel to concrete core ρ'', ratio of longitudinal steel to the gross area of the section ρ_l, ties spacing s, effective width size and strength of ties and size of longitudinal bars. The model generated was similar to Kent and Park model with improvement in the peak strength for confined concrete. For the ascending branch:

$$\frac{f_c}{f_c'} = \frac{\frac{E_c\varepsilon_{cc}}{f_c'}x - kx^2}{1 + \left(\frac{E_c\varepsilon_{cc}}{kf_c'} - 2\right)x} \qquad \varepsilon_c \le \varepsilon_{cc} \tag{2-26}$$

For the descending branch:

$$\frac{f_c}{f_c'} = k\left[1 - z\varepsilon_{cc}(x-1)\right] \qquad \varepsilon_{cc} \le \varepsilon_c \le \varepsilon_{cu} \tag{2-27}$$

$$\frac{f_c}{f_c'} = \varepsilon_{cu} \qquad \varepsilon_{cu} \le \varepsilon_c \qquad \varepsilon_{cu} = 0.3k \tag{2-28}$$

$$x = \frac{\varepsilon_c}{\varepsilon_{cc}} \tag{2-29}$$

$$f_{cc} = kf_c' \tag{2-30}$$

$$k = 1 + 0.0091\left[1 - 0.245\frac{s}{h}\right]\frac{\left[\rho'' + \frac{d'}{d}\rho_l\right]f_{yh}}{\sqrt{f_c'}} \tag{2-31}$$

$$\varepsilon_{cc} = 0.0024 + 0.005\left[1 - \frac{0.734s}{h}\right]\frac{\rho'' f_{yh}}{\sqrt{f_c'}} \tag{2-32}$$

$$z = \frac{0.5}{\frac{3}{4}\rho_s\sqrt{\frac{h}{s}} + \left[\frac{3 + 0.002 f_c'}{f_c' - 1000}\right] - 0.002} \tag{2-33}$$

where *k* is coefficient of confined strength ratio, *z* is the slope of descending portion, *d* and *d'* are the diameter of longitudinal and transverse reinforcement respectively.

Wang, Shah and Naaman (1978)

Wang et al. (1978) obtained experimentally another stress strain curve describing the behavior of confined reinforced concrete under compression. The concrete tested was normal weight concrete ranging in strength from 3000 to 11000 psi and light weight concrete with strength of 3000-8000 psi. Wang et al. utilized an equation, with four constants, similar to that of Sargin et al.

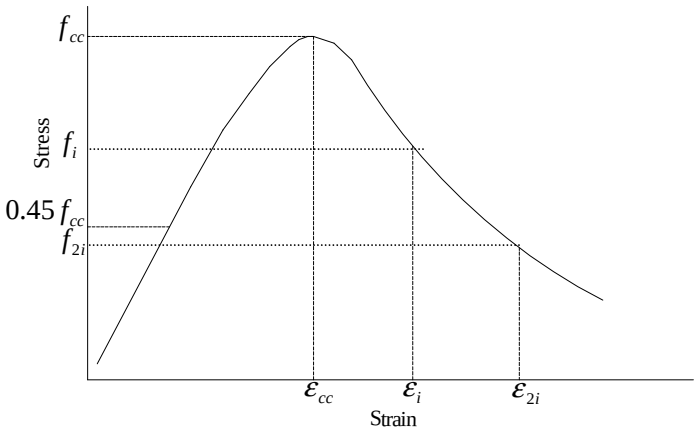

Figure 2-4 Proposed Stress-Strain curve by Wang et al(1978).

$$Y = \frac{AX + BX^2}{1 + CX + DX^2} \tag{2-34}$$

where

$$Y = \frac{f_c}{f_{cc}} \tag{2-35}$$

$$X = \frac{\varepsilon_c}{\varepsilon_{cc}} \tag{2-36}$$

The four constant *A, B, C, D* were evaluated for the ascending part independently of the descending one. The four conditions used to evaluate the constants for the ascending part were

$$\frac{dY}{dX} = \frac{E_{0.45}}{E_{\text{sec}}} \text{ at X=0}$$

$$Y = 0.45 \text{ for } X = \frac{0.45}{\frac{E_{0.45}}{E_{\text{sec}}}}$$

$$Y = 1 \text{ For } X = 1$$

$$\frac{dY}{dX} = 0 \text{ at X=1}$$

whereas for the descending branch:

$$Y = 1 \text{ for } X = 1$$

$$\frac{dy}{dx} = 0 \text{ at X=1}$$

$$Y = \frac{f_i}{f_{cc}} \text{ for } X = \frac{\varepsilon_i}{\varepsilon_{cc}}$$

$$Y = \frac{f_{2i}}{f_{cc}} \text{ for } X = \frac{\varepsilon_{2i}}{\varepsilon_{cc}}$$

where f_i and ε_i are the stress and strain at the inflection point, f_{2i} and ε_i refer to a point such that $\varepsilon_{2i} - \varepsilon_i = \varepsilon_i - \varepsilon_{cc}$.

Scott, Park, Priestly (1982)

Scott et al. (1982) examined specimens by loading at high strain rate to correlate with the seismic loading. They presented the results including the effect of eccentricity loading, strain rate, amount and distribution of longitudinal steel and amount and distribution of transverse steel. For low strain rate Kent and Park equations were modified to fit the experimental data

$$f_c = kf_c^{'}\left[\frac{2\varepsilon_c}{\varepsilon_{co}k} - \left(\frac{\varepsilon_c}{\varepsilon_{co}k}\right)^2\right] \qquad \varepsilon_c \le 0.002k \tag{2-37}$$

$$f_c = kf_c^{'}\left[1 - Z_m(\varepsilon_c - 0.002k)\right] \qquad \varepsilon_c > 0.002k \tag{2-38}$$

where

$$k = 1 + \frac{\rho_s f_{yh}}{f_c^{'}} \tag{2-39}$$

$$Z_m = \frac{0.5}{\frac{3 + 0.29 f_c^{'}}{145 f_c^{'} - 1000} + \frac{3}{4}\rho_s\sqrt{\frac{b}{s} - 0.002k}} \tag{2-40}$$

for the high strain rate, the k and Z_m were adapted to

$$k = 1.25\left(1 + \frac{\rho_s f_{yh}}{f_c^{'}}\right) \tag{2-41}$$

$$Z_m = \frac{0.625}{\frac{3 + 0.29 f_c^{'}}{145 f_c^{'} - 1000} + \frac{3}{4}\rho_s\sqrt{\frac{b}{s} - 0.002k}} \tag{2-42}$$

and the maximum strain was suggested to be:

$$\varepsilon_{cu} = 0.004 + 0.9\rho_s\left(\frac{f_{yh}}{300}\right) \tag{2-43}$$

It was concluded that increasing the spacing while maintaining the same ratio of lateral reinforcement by increasing the diameter of spirals, reduce the efficiency of concrete

confinement. In addition, increasing the number of longitudinal bars will improve the concrete confinement due to decreasing the spacing between the longitudinal bars.

Sheikh and Uzumeri (1982)

Sheikh and Uzumeri (1982) introduced the effectively confined area as a new term in determining the maximum confined strength. In addition to that they, in their experimental work, utilized the volumetric ratio of lateral steel to concrete core, longitudinal steel distribution, strength of plain concrete, and ties strength, configuration and spacing. The stress-strain curve was presented parabolically up to (f_{cc}, ε_{cc}), then it flatens horizontally till $\varepsilon_{cs,}$ and finally it drops linearly passing by ($0.85f_{cc}$, ε_{85}) till $0.3\ f_{cc}$, In that sense, it is conceptually similar to the earlier model of Soliman and Yu (1967).

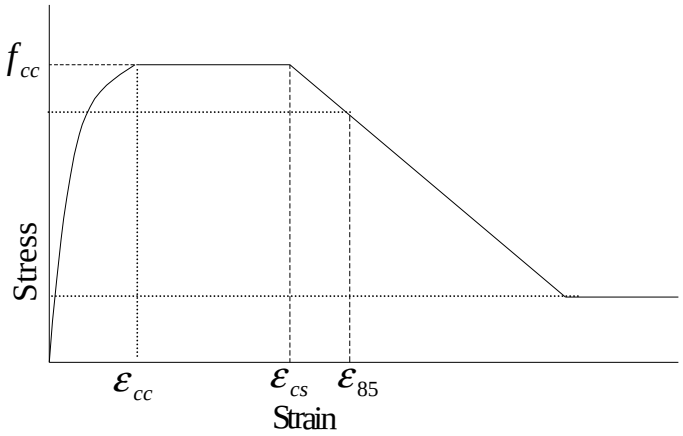

Figure 2-5 Proposed general Stress-Strain curve by Sheikh and Uzumeri .

f_{cc} and ε_{cc} can be determined from the following equations:

$$f_{cc} = k_s f_c^{'} \tag{2-44}$$

$$k_s = 1 + \frac{2.73b^2}{P_{occ}}\left[\left(1 - \frac{nc^2}{5.5b^2}\right)\left(1 - \frac{s}{2b}\right)^2\right]\sqrt{\rho_s f_s^{'}} \quad (2\text{-}45)$$

$$\varepsilon_{cc} = 0.55 k_s f_c^{'} * 10^{-6} \quad (2\text{-}46)$$

$$\varepsilon_{cs} = \varepsilon_{co}\left(1 + \frac{0.81}{c}\left(1 - 5\left(\frac{s}{b}\right)^2\right)\frac{\rho_s f_s^{'}}{\sqrt{f_c^{'}}}\right) \quad (2\text{-}47)$$

Where b is the width of the cross section, f'_s is the stress in the lateral confining bar and c is center-to-center distance between longitudinal bars.

Ahmad and Shah (1982)

Ahmad and Shah (1982) developed a model based on the properties of hoop reinforcement and the constitutive relationship of plain concrete. Normal weight concrete and lightweight concrete were used in tests that were conducted with one rate of loading. No longitudinal reinforcement was provided and the main two parameters varied were spacing and yield strength of transverse reinforcement. Ahmed and Shah observed that the spirals become ineffective when the spacing exceeds 1.25 the diameter of the confined concrete column. They concluded also that the effectiveness of the spiral is inversely proportional with compressive strength of unconfined concrete.

Ahmad and Shah adapted Sargin model counting on the octahedral failure theory, the three stress invariants and the experimental results:

$$Y = \frac{A_i X + (D_i - 1)X^2}{1 + (A_i - 2)X + D_i X^2} \quad (2\text{-}48)$$

$$Y = \frac{f_{pcs}}{f_{pcn}} \quad (2\text{-}49)$$

$$X = \frac{\varepsilon_i}{\varepsilon_{ip}} \tag{2-50}$$

where f_{pcs} is the highest principal compressive stress, f_{pcn} is the highest principal compressive strength, ε_i is the strain in the i-th principal direction and ε_{ip} is the strain at the peak in the i-th direction.

$$A_i = \frac{E_i}{E_{ip}} \qquad E_{ip} = \frac{f_p}{\varepsilon_{ip}}$$

E_i is the initial slope of the stress strain curve, D_i is a parameter that governs the descending branch, and f_p is the highest principal compressive strength. When the axial compression is considered to be the main loading, which is typically the case in concentric confined concrete columns, Equations (2-46), (2-47) and (2-48) become:

$$Y = \frac{AX + BX^2}{1 + CX + DX^2}$$

$$Y = \frac{f_c}{f_{cc}}$$

$$X = \frac{\varepsilon_c}{\varepsilon_{cc}}$$

$$A = \frac{E_c}{E_{\sec}}$$

Martinez, Nilson and Slate (1984)

Experimental investigation was conducted to propose equations to define the stress strain curve for high strength concrete under compressive loading. The main parameters used were compressive strength for concrete, amount of confinement and specimen size. Two types of concrete where used; normal weight concrete with strength to about 12000 psi and light weight concrete with strength to about 9000 psi. Martinez et al. (1984) concluded that the design

specification for low strength concrete might be unsafe if applied to high strength concrete. For normal weight concrete:

$$\left(f_{cc} - f_c^{'}\right) = 4 f_l \left(1 - \frac{s}{d^{'}}\right) \tag{2-51}$$

and for light weight concrete:

$$\left(f_{cc} - f_c^{'}\right) = 1.8 f_l \left(1 - \frac{s}{d^{'}}\right) \tag{2-52}$$

where *d'* is the diameter of the lateral reinforcement.

Fafitis and Shah (1985)

Fafitis and Shah (1985) assumed that the maximum capacity of confined concrete occurs when the cover starts to spall off. The experimental work was done on high strength concrete with varying the confinement pressure and the concrete strength. Two equations are proposed to express the ascending and the descending branches of the model. For the ascending branch:

$$f_c = f_{cc}\left[1 - \left(1 - \frac{\varepsilon_c}{\varepsilon_{cc}}\right)^A\right] \qquad 0 \le \varepsilon_c \le \varepsilon_{cc} \tag{2-53}$$

and for the descending branch:

$$f_c = f_{cc} \exp\left[-k\left(\varepsilon_c - \varepsilon_{cc}\right)^{1.15}\right] \qquad \varepsilon_{cc} \le \varepsilon_c \tag{2-54}$$

The equations for the constant A and k:

$$A = \frac{E_c \varepsilon_{cc}}{f_{cc}^{'}} \tag{2-55}$$

$$k = 0.17 f_{cc} \exp\left(-0.01 \frac{f_l}{\lambda_1}\right) \tag{2-56}$$

$$\lambda_1 = 1 - 25 \frac{f_r}{f_c^{'}}\left[1 - \exp\left(-\frac{f_c^{'}}{6500}\right)^9\right] \tag{2-57}$$

f_{cc} and ε_{cc} can be found using the following equations:

$$f_{cc} = \lambda_2 \left[f_c^{'} + \left(1.15 + \frac{3048}{f_c^{'}} \right) f_r \right] \tag{2-58}$$

$$\varepsilon_{cc} = 1.027 * 10^{-7} f_c^{'} + 0.0296 \lambda_2 \frac{f_l}{f_{cc}} + 0.00195 \tag{2-59}$$

$$\lambda_2 = 1 + 15 \left(\frac{f_r}{f_c^{'}} \right)^3 \tag{2-60}$$

f_l represents the confinement pressure and is given by the following equation:

$$f_l = \frac{2 A_s f_{yh}}{sD} \tag{2-61}$$

D is the core diameter of the column.

Yong, Nour and Nawy (1988)

The model suggested by Yong et al.(1988) was based on experimental work done for rectangular columns with rectangular ties.

$$f_{cc} = K f_c^{'} \tag{2-62}$$

$$\varepsilon_{cc} = 0.00265 + \frac{0.0035 \left(1 - \frac{0.734 s}{h} \right) \left(\rho_s f_{yh} \right)^{2/3}}{\sqrt{f_c^{'}}} \tag{2-63}$$

$$K = 1 + 0.0091 \left(1 - \frac{0.245 s}{h} \right) \left(\rho_s + \frac{m d'}{8 s d} \rho_l \right) \frac{f_{yh}}{\sqrt{f_c^{'}}} \tag{2-64}$$

$$f_l = f_{cc} \left[0.25 \left(\frac{f_c^{'}}{f_{cc}} \right) + 0.4 \right] \tag{2-65}$$

$$\varepsilon_{cu} = K\left[1.4\left(\frac{\varepsilon_{cc}}{K}\right) + 0.0003\right] \tag{2-66}$$

$$f_{cu} = f_c^{'}\left[0.025\left(\frac{f_{cc}}{1000}\right) - 0.065\right] \geq 0.3 f_c^{'} \tag{2-67}$$

Where m is the number of longitudinal bars.

Mander, Priestly and Park (1988)

Using the same concept of effective lateral confinement pressure introduced by Sheikh and Uzumeri, Mander et al. developed a new confined model for circular spiral or rectangular ties. In addition Mander et al. was the second group after Bazant et al.(1972) to investigate the effect of the cyclic load side by side with monotonic one.

$$f_{cc} = f_c^{'}\left(-1.254 + 2.254\sqrt{1 + \frac{7.94 f_l^{'}}{f_c^{'}}} - 2\frac{f_l^{'}}{f_c^{'}}\right) \tag{2-68}$$

$$\varepsilon_{cc} = \varepsilon_{co}\left[1 + 5\left(\frac{f_{cc}^{'}}{f_c^{'}} - 1\right)\right] \tag{2-69}$$

$$f_l^{'} = \frac{1}{2} k_e \rho_s f_{yh} = k_e f_l \tag{2-70}$$

$$f_c = \frac{f_{cc} x r}{r - 1 + x^r} \tag{2-71}$$

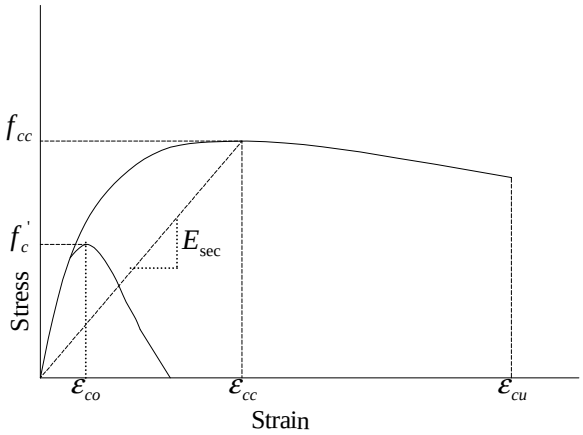

Figure 2-6 Stress- Strain Model proposed by Mander et al.

$$f_c = \frac{f_{cc} x r}{r - 1 + x^r} \tag{2-72}$$

$$r = \frac{E_c}{E_c - E_{\sec}} \tag{2-73}$$

$$x = \frac{\varepsilon_c}{\varepsilon_{cc}} \tag{2-74}$$

Where k_e is the effective lateral confinement coefficient:

$$k_e = \frac{A_e}{A_{cc}} \tag{2-75}$$

A_e is the area of effectively confined concrete, and A_{cc} is area of core within centerlines of perimeter spirals or hoops excluding area of longitudinal steel.

Saatcioglu and Razvi (1992)

Saatcioglu and Razvi (1992). Concluded that the passive lateral pressure generated by laterally expanding concrete and restraining transverse reinforcement is not always uniform. Based on tests on normal and high strength concrete ranging from 30 to 130 MPa, Saatcioglu and Razvi proposed a new model that has exponential relationship between the lateral confinement pressure and the peak confinement strength. They ran tests by varying volumetric ratio, spacing, yield strength, arrangement of transverse reinforcement, concrete strength and section geometry. In addition the significance of imposing the tie arrangement as a parameter in determining the peak confined strength was highlighted.

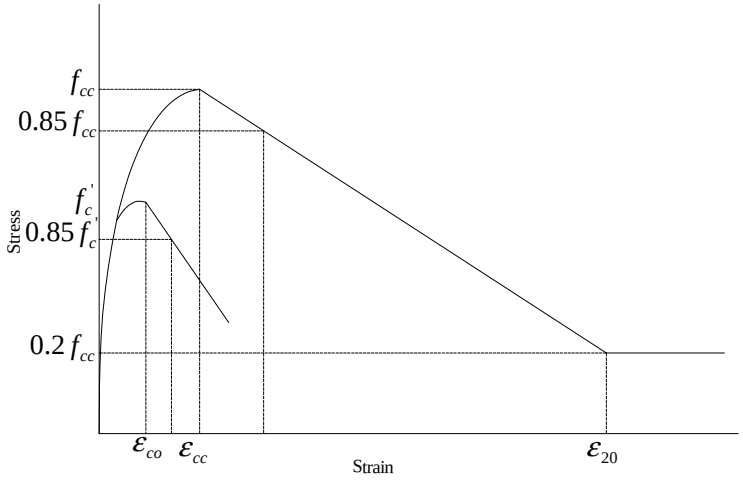

Figure 2-7 Proposed Stress-Strain curve by Saatcioglu and Razvi.

$$f_{cc} = f_c' + k_1 f_l' \tag{2-76}$$

$$k_1 = 6.7(f_l)^{-0.17} \tag{2-77}$$

$$f_l' = k_2 f_l \tag{2-78}$$

$$k_2 = 0.15\sqrt{\left(\frac{h}{s}\right)\left(\frac{h}{c}\right)} \leq 1 \tag{2-79}$$

where c is spacing of longitudinal reinforcement.

Sheikh and Toklucu (1993)

Sheikh and Toklucu(1993) studied the ductility and strength for confined concrete and they concluded that ductility is more sensitive, than the strength, to amount of transverse steel, and the increase in concrete strength due to confinement was observed to be between 2.1 and 4 times the lateral pressure.

Rasheed and Dinno (1994)

Rasheed and Dinno (1994) introduced a fourth degree polynomial to express the stress strain curve of concrete under compression.

$$f_c = a_o + a_1\varepsilon_c + a_2\varepsilon_c^2 + a_3\varepsilon_c^3 + a_4\varepsilon_c^4 \quad (2\text{-}80)$$

They evaluated the constants a_o-a_4 using the boundry conditions of the stress strain curve. Similar to Kent and Park, they assumed no difference between the unconfined and confined peak strength.

$$f_{cc} = k_c f_c^{'} \quad (2\text{-}81)$$

where

$k_c = 1$

They used expression taken from Kent and Park to evaluate the slope of the descending branch starting at 0.003. A flat straight line was proposed when the stress reaches $0.2\ f_{cc}$ up to $C_c\varepsilon_{cc.}$ Where C_c is the ratio of maximum confined compressive strain to $\varepsilon_{cc.}$

El-Dash and Ahmad (1995)

El-Dash and Ahmad (1995) used Sargin et al. model to predict analytically the behavior of normal and high strength concrete in one series of equations. They used the internal force equilibrium, properties of materials, and the geometry of the section to predict the pressure. The parameters imposed in the analytical prediction where plain concrete strength, confining reinforcement diameter and yield strength, the volumetric ratio of confined concrete to the core, the dimension of the column and spacing.

$$Y = \frac{AX + (B-1)X^2}{1 + (A-2)X + BX^2} \quad (2\text{-}82)$$

where

$$Y = \frac{f_c}{f_{cc}} \tag{2-83}$$

$$X = \frac{\varepsilon_c}{\varepsilon_{cc}} \tag{2-84}$$

$$f_{cc} = f_c^{'} + k_1 f_l \tag{2-85}$$

$$\varepsilon_{cc} = \varepsilon_{co} + k_2 \frac{f_l}{f_c^{'}} \tag{2-86}$$

The values of A, B, k_1, k_2 and f_l are defined by the following equations

$$A = \frac{E_c \varepsilon_{cc}}{f_{cc}} \tag{2-87}$$

$$B = \frac{16.5}{\sqrt{f_c^{'}}} \left(\frac{f_l}{\frac{s}{d^{'}}} \right)^{0.33} \tag{2-88}$$

$$k_1 = 5.1 \left(\frac{f_c^{'}}{f_{yh}} \right)^{0.5} \left(\frac{d^{'}}{\rho_s} \right)^{0.25} \tag{2-89}$$

$$k_2 = \frac{0.65}{\left(\frac{s}{d^{'}} \right) f_c^{'1.7}} \tag{2-90}$$

$$f_l = 0.5 \rho_s f_{yh} \left(1 - \sqrt{\frac{s}{1.25 d_s}}\right) \tag{2-91}$$

Cusson and Paultre (1995)

Unlike all the previous work, Cusson and Paultre (1995) built their model based on the actual stress in the stirrups upon failure and they did not consider the yield strength, as the experimental work have shown that the yield strength for the transverse steel is reached in case

of well confined columns. The ascending and the descending branches in the model curve are expressed by two different equations. For the ascending portion

$$f_c = f_{cc}\left(\frac{k\left(\frac{\varepsilon_c}{\varepsilon_{cc}}\right)}{k+1+\left(\frac{\varepsilon_c}{\varepsilon_{cc}}\right)^k}\right) \qquad \varepsilon_c \le \varepsilon_{cc} \tag{2-92}$$

$$k = \frac{E_c}{E_c - \left(\frac{f_{cc}}{\varepsilon_{cc}}\right)} \tag{2-93}$$

For descending one:

$$f_c = f_{cc}\exp\left(k_1\left(\varepsilon_{c50c} - \varepsilon_{cc}\right)^{k_2}\right) \qquad \varepsilon_c \ge \varepsilon_{cc} \tag{2-94}$$

$$k_1 = \frac{\ln 0.5}{\left(\varepsilon_{c50c} - \varepsilon_{cc}\right)^{k_2}} \tag{2-95}$$

$$k_2 = 0.58 + 16\left(\frac{f_l^{'}}{f_c^{'}}\right)^{1.4} \tag{2-96}$$

where ε_{c50c} is axial strain in confined concrete when stress drops to 0.5 f_{cc}.

Following the same methodology of Sheikh and Uzumeri(1982) and Mander et al. (1988) Cusson and Paultre considered the lateral confinement pressure f_l.

$$f_l = \frac{f_{hcc}}{s}\left(\frac{A_{sx} + A_{sy}}{b+h}\right) \tag{2-97}$$

where A_{sx} and A_{sy} are the lateral cross sectional area of the lateral steel perpendicular to x and y axes respectively.

$$k_e = \frac{\left(1 - \frac{\sum w_i^2}{6bh}\right)\left(1 - \frac{s'}{2b}\right)\left(1 - \frac{s'}{2h}\right)}{1 - \rho_{cc}} \tag{2-98}$$

$$f_l^{'} = k_e f_l \tag{2-99}$$

Where $\sum w_i^2$ is the sum of the squares of all the clear spacing between adjacent longitudinal steel bars in a rectangular section. f_{cc} and ε_{cc} can be found by the following equations

$$f_{cc} = f_c^{'}\left[1+2.1\left(\frac{f_l^{'}}{f_c^{'}}\right)^{0.7}\right] \tag{2-100}$$

$$\varepsilon_{cc} = \varepsilon_{co} + 0.21\left(\frac{f_l^{'}}{f_c^{'}}\right)^{1.7} \tag{2-101}$$

$$\varepsilon_{c50c} = 0.004 + 0.15\left(\frac{f_l^{'}}{f_c^{'}}\right)^{1.1} \tag{2-102}$$

Attard and Setunge (1996)

Attard and Setunge (1996) experimentally determined full stress strain-curve for concrete with compressive strength of 60 –130 MPa and with confining pressure of 1-20 MPa. The main parameters used were peak stress; strain at peak stress, secant modulus of elasticity, and the stress and strain at point of inflection. Attard and Setunge followed the same equation used by Wang et al (1978). and Sargin et al (1971):

$$Y = \frac{AX + BX^2}{1 + CX + DX^2} \tag{2-103}$$

where

$$Y = \frac{f_c}{f_{cc}} \tag{2-104}$$

$$X = \frac{\varepsilon_c}{\varepsilon_{cc}} \tag{2-105}$$

For the ascending branch, the four constant were gained by setting four conditions:

1- at $f_c = 0$, $\quad \frac{df_c}{d\varepsilon_c} = E_c$

2- at $f_c = f_{cc}, \frac{df_c}{d\varepsilon_c} = 0$

3- at $f_c = f_{cc}, \varepsilon_c = \varepsilon_{cc}$

4- at $f_c = 0.45 f_{cc}, \varepsilon_c = \frac{f_c}{E_{0.45}}$

The constants are given by:

$$A = \frac{E_c \varepsilon_{cc}}{f_{cc}} \tag{2-106}$$

$$B = \frac{(A-1)^2}{\frac{E_c}{E_{0.45}}\left(1 - \frac{0.45 f_c^{'}}{f_{cc}}\right)} + \frac{A^2 (1 - \frac{E_c}{E_{0.45}})}{\left(\frac{E_c}{E_{0.45}}\right)^2 \frac{0.45 f_c^{'}}{f_{cc}}\left(1 - \frac{0.45 f_c^{'}}{f_{cc}}\right)} - 1 \tag{2-107}$$

$$C = A - 2 \tag{2-108}$$

$$D = B + 1 \tag{2-109}$$

while for the descending curve the four boundary conditions were

1- at $f_c = f_{cc}, \frac{df_c}{d\varepsilon_c} = 0$

2- at $f_c = f_{cc}, \varepsilon_c = \varepsilon_{cc}$

3- at $f_c = f_i, \varepsilon_c = \varepsilon_i$

4- at $f_c = f_{2i}, \varepsilon_c = \varepsilon_{2i}$

where f_i and ε_i refer to the coordinate of the inflection point.

The four constant for the descending curve are

$$A = \left[\frac{\varepsilon_{2i} - \varepsilon_i}{\varepsilon_{cc}}\right]\left[\frac{\varepsilon_{2i} E_i}{(f_{cc} - f_i)} - \frac{4\varepsilon_i E_{2i}}{(f_{cc} - f_{2i})}\right] \tag{2-110}$$

$$B = (\varepsilon_{2i} - \varepsilon_i)\left[\frac{E_i}{(f_{cc} - f_i)} - \frac{E_{2i}}{(f_{cc} - f_{2i})}\right] \tag{2-111}$$

$$C = A - 2 \tag{2-112}$$

$$D = B + 1 \tag{2-113}$$

The f_{cc} came out to be a function of the confining pressure, the compressive and tensile strength of concrete f'_c, f_t, and a parameter k reflects the effectiveness of confinement.

$$\frac{f_{cc}}{f_c'} = \left(\frac{f_t}{f_c'} + 1 \right)^k \tag{2-114}$$

$$k = 1.25\left[1 + 0.062 \frac{f_l}{f_c'} \right] \left(f_c' \right)^{-.0.21} \tag{2-115}$$

$$\frac{\varepsilon_{cc}}{\varepsilon_{co}} = 1 + \left(17 - 0.06 f_c' \right) \left(\frac{f_l}{f_c'} \right) \tag{2-116}$$

Mansur, Chin and Wee (1996)

Mansur et al. (1996) introduced casting direction, if the member is cast in place(vertically) or pre-cast (horizontally), as a new term among the test parameters, for high strength concrete, which were tie diameter and spacing and concrete core area. They concluded that the vertically cast confined fiber concrete has higher strain at peak stress and higher ductility than the horizontally cast specimen. In addition, vertically cast confined non-fiber concrete has larger strain than that of horizontally cast concrete with no enhancement in ductility. Mansur et al. utilized the same equations found by Carreira and Chu for plain concrete with some manipulations, for the ascending branch they used the exact same equation

$$f_c = f_{cc} \left\{ \frac{\beta \left(\frac{\varepsilon}{\varepsilon_{cc}} \right)}{\beta - 1 + \left(\frac{\varepsilon}{\varepsilon_{cc}} \right)^{\beta}} \right\} \tag{2-117}$$

where β is a material parameter depending on the stress strain shape diagram and can be found by :

$$\beta = \frac{1}{1 - \frac{f_{cc}}{\varepsilon_{cc} E_c}} \tag{2-118}$$

k_1 and k_2 are two constants introduced in the equation describing the descending branch:

$$f_c = f_{cc} \left\{ \frac{k_1 \beta \left(\frac{\varepsilon}{\varepsilon_{cc}} \right)}{k_1 \beta - 1 + \left(\frac{\varepsilon}{\varepsilon_{cc}} \right)^{k_2 \beta}} \right\} \tag{2-119}$$

for confined horizontally and vertically cast non fiber concrete:

$$k_1 = 2.77 \left(\frac{\rho_s f_{yh}}{f_c^{'}} \right) \tag{2-120}$$

$$k_2 = 2.19 \left(\frac{\rho_s f_{yh}}{f_c^{'}} \right) + 0.17 \tag{2-121}$$

for horizontally cast confined fiber concrete

$$k_1 = 3.33 \left(\frac{\rho_s f_{yh}}{f_c^{'}} \right) + 0.12 \tag{2-122}$$

$$k_2 = 1.62 \left(\frac{\rho_s f_{yh}}{f_c^{'}} \right) + 0.35 \tag{2-123}$$

and the values of f_{cc} and ε_{cc} can be obtained from the following equations:

for confined non fiber concrete:

$$\frac{f_{cc}}{f_c^{'}} = 1 + 0.6 \left(\frac{\rho_s f_{yh}}{f_c^{'}} \right)^{1.23} \tag{2-124}$$

for confined fiber concrete:

$$\frac{f_{cc}}{f_c^{'}} = 1 + 11.63 \left(\frac{\rho_s f_{yh}}{f_c^{'}} \right)^{1.23} \tag{2-125}$$

for vertically cast fiber concrete

$$\frac{\varepsilon_{cc}}{\varepsilon_{co}} = 1 + 62.2\left(\frac{\rho_s f_{yh}}{f_c^{'}}\right)^2 \quad (2\text{-}126)$$

for horizontally cast fiber concrete and vertically cast non fiber concrete

$$\frac{\varepsilon_{cc}}{\varepsilon_{co}} = 1 + 2.6\left(\frac{\rho_s f_{yh}}{f_c^{'}}\right)^{0.8} \quad (2\text{-}127)$$

and for horizontally cast non fiber concrete

$$\frac{\varepsilon_{cc}}{\varepsilon_{co}} = 1 + 5.9\left(\frac{\rho_s f_{yh}}{f_c^{'}}\right)^{1.5} \quad (2\text{-}128)$$

Hoshikuma, Kawashima, Nagaya and Taylor (1997)

Hoshikuma et al(1997). developed their models to satisfy bridge column section design in Japan. The model was based on series of compression loading tests of reinforced concrete columns specimens that have circular, square and wall type cross sections. The variables that varied in the experimental wok were hoop volumetric ratio, spacing, configuration of the hook in the hoop reinforcement and tie arrangement.

Hoshikuma et al(1997). asserted that the ascending branch represented in second degree parabola is not accurate to satisfy four boundary conditions:

1- Initial condition $f_c = 0$, $\varepsilon_c = 0$.

2- Initial stiffness condition $df_c/d\,\varepsilon_c = E_c$

3- Peak condition $f_c = f_{cc}$

4- Peak stiffness condition $df_c/d\varepsilon_c = 0$

The function that defines the ascending branch is:

$$f_c = E_c \varepsilon_c \left[1 - \frac{1}{n}\left(\frac{\varepsilon_c}{\varepsilon_{cc}}\right)^{n-1}\right] \quad (2\text{-}129)$$

$$n = \frac{E_c \varepsilon_{cc}}{E_c \varepsilon_{cc} - f_{cc}} \tag{2-130}$$

For the descending branch:

$$f_c = f_{cc} - E_{des}(\varepsilon_c - \varepsilon_{cc}) \tag{2-131}$$

where E_{des} is the slope of the descending line and can be found using the following equation

$$E_{des} = \frac{11.2}{\frac{\rho_s f_{yh}}{f_c^{'2}}} \tag{2-132}$$

The peak stress and the corresponding strain for the circular section

$$\frac{f_{cc}}{f_c^{'}} = 1 + 3.83 \frac{\rho_s f_{yh}}{f_c^{'}} \tag{2-133}$$

$$\varepsilon_{cc} = 0.00218 + 0.0332 \frac{\rho_s f_{yh}}{f_c^{'}} \tag{2-134}$$

while for the square section

$$\frac{f_{cc}}{f_c^{'}} = 1 + 0.73 \frac{\rho_s f_{yh}}{f_c^{'}} \tag{2-135}$$

$$\varepsilon_{cc} = 0.00245 + 0.0122 \frac{\rho_s f_{yh}}{f_c^{'}} \tag{2-136}$$

Assa, Nishiyama and Watanabe (2001)

A new model was proposed for concrete confined by spiral reinforcement based on concrete-transverse steel interaction. The two main parameters were concrete strength and lateral stress-lateral strain relationship that represents the response characteristics of the transverse steel to the lateral expansion of concrete. Assa et al. (2001) modeled a confinement mechanism and limited the lateral expansion of the confined concrete with the maximum lateral expansion capacity. Assa et al. reached some relationships expressed in the following equations:

$$\frac{f_{cc}}{f_c^{'}} = 1 + 3.36 \frac{f_l}{f_c^{'}} \tag{2-137}$$

$$\frac{\varepsilon_{cc}}{\varepsilon_{co}} = 1 + 21.5\frac{f_l}{f_c^{'}} \tag{2-138}$$

$$\varepsilon_{lcu} = 0.0021 + 0.016\frac{f_l}{f_c^{'}} \tag{2-139}$$

where ε_{lcu} is the maximum lateral concrete strain. The proposed stress-strain curve has one equation:

$$f_c = f_{cc}\left(\frac{\alpha X + (\beta - 1)X^2}{1 + (\alpha - 2)X + \beta X^2}\right) \tag{2-140}$$

$$X = \frac{\varepsilon_c}{\varepsilon_{cc}} \tag{2-141}$$

where α controls the stiffness of ascending branch and β controls the slope of the descending branch:

$$\alpha = \frac{E_c \varepsilon_{cc}}{f_{cc}} \tag{2-142}$$

$$\beta = \left(\frac{\left(\frac{\varepsilon_{80}}{\varepsilon_{cc}}\right)^2 - (0.2\alpha + 1.6)\frac{\varepsilon_{80}}{\varepsilon_{cc}} + 0.8}{0.2\left(\frac{\varepsilon_{80}}{\varepsilon_{cc}}\right)^2}\right) \tag{2-143}$$

where ε_{80} is the strain at $0.8f_{cc}$

Lokuge, Sanjayan and Setunge (2005)

A simple stress-strain model was proposed based on shear failure. The model was based on the experimental results taken from Candappa 2000. Lokuge et al.(2005) proposed a relationship between axial and lateral strain:

$$\frac{\varepsilon_l}{\varepsilon_{lcc}} = v\left(\frac{\varepsilon}{\varepsilon_{cc}}\right) \qquad \varepsilon \le \varepsilon^{'} \tag{2-144}$$

$$\frac{\varepsilon_l}{\varepsilon_{lcc}} = \left(\frac{\varepsilon}{\varepsilon_{cc}}\right)^a \qquad \varepsilon > \varepsilon^{'} \tag{2-145}$$

where ε' is a strain at a point where axial strain and lateral strain curves deviate. v is the initial Poisson's ratio, and a is a material parameter which depends on the uniaxial concrete strength

$$v = 8*10^{-6}\left(f_c^{'}\right)^2 + 0.0002 f_c^{'} + 0.138 \quad (2\text{-}146)$$

$$a = 0.0177 f_c^{'} + 1.2818 \quad (2\text{-}147)$$

2-3 Classification and comparison of Circular spiral confinement Models

As stated by many researches, like Mander et al 1988, Scott et al 1982, Sheikh and Uzumeri 1980 and Shuhaib and Mallare 1993, the spirals or circular hoops are more efficient than the rectangular hoops. The uniform pressure generated by the circular hoop is one of the reasons of Circular spirals advantage. According to Eid and Dancygier 2005, there are four main approaches for the modeling confined concrete by lateral ties

1- The empirical approach: in which the stress-strain curve generated based on the experimental results. Fafitis and Shah 1985 and Hoshikuma et al. 1997 followed that approach for circular reinforced concrete analysis.

2- Physical engineering model based approach: the lateral pressure, causes the confined behavior of the concrete core, is provided by the arch action between the lateral reinforcement ties. This approach was adopted by Sheikh and Uzumeri 1980, and was followed by Mander et al 1988.

3- The third approach is based either on the first approach or the second one, but it does not assume the lateral ties yielding. Instead, It include computation of the steel stress at concrete peak stress, either by introducing compatibility

conditions, solved by iterative process as Cusson and Paultre 1995 did, or by introducing empirical expressions as Saatcigolu and Razvi 1992 followed.

4- A plasticity model for confined concrete core introduced by Karabinis and Kiousis (1994). The shape of the confined core is based on the arching action.

According to Lokuge et al 2005, the stress strain models can be classified by three categories:

1- Sargin 1971 based models: Martinez et al. 1984, Ahmad and Shah 1982, Eldash and Ahmad 1995 Assa et al. 2001.
2- Kent and Park 1971 based models: Sheikh and Uzumeri 1982, Razvi and Saatcigolu 1992.
3- Popovics 1973 based models: Mander et al. 1988, Cusson and Paultre 1995 and Hoshikuma et al. 1997.

The main circular confined models are Chan 1955, Ahmad and Shah 1982, Martinez et al. 1984, Mander et al. 1988, Fafitis and Shah 1985, El-Dash and Ahmad 1995, Cusson and Paultre 1995, Hoshikuma et al. 1997 and Assa et al. 2001.

Lokuge comparison (2005)

Sargin model was generated empirically from specimens, which did not have longitudinal bars. In addition the section geometry and tie configuration were not considered in generating the model. Dependently Martinez et al. And Ahmad and Shah pursued experimental work with no longitudinal bars and no cover. These conditions are very essential in columns components, as the longitudinal bars are considered to be part of the lateral confinement elements. In addition the work done by Martinez et al. was for

the high strength concrete, which covers portion of the concrete analyzed. El-Dash and Ahmad developed analytically one equation to define the ascending and the descending branch for stress-strain curve. However they relied on Ahmed and Shah and Martinez et al. for defining the lateral confining pressure.

Kent and Park model was based on the unrealistic assumption, which states that the maximum compressive strength for confined and unconfined concrete, are the same. In addition they assume that the failed concrete can sustain load equal to 0.2 f_{cc} up to infinity.

Popovics model was originally for plain concrete. Hoshikuma et al. developed their model empirically. The model proposed has ascending and descending branches, which might represent discontinuity or a lack of smoothness zone. Furthermore, the generated model did not address the arching effect accounted for by the second approach described by Eid and Dancygier 2005. On the contrary, Mander et al. and Cusson and Paultre generated their models according to the effective lateral pressure generated from the arching effect between ties. However, Cusson and Paultre model was utilized based on the high strength concrete, and similar to Hoshikuma, the model has ascending and descending branch, which represents weakness in the modeling concept.

Based on this comparison Mander et al. model was selected among different models for conducting this study. According to Eid and Dancygier (2005) classification, Mander et al. model is among the second approach models. To conform to the first approach and unlike most of the experimental works, fifteen full size reinforced concrete columns, 19.7 in. diameter and 59.1 in. height, were tested concentrically in order to verify the proposed model. Spolestra and Monti 2000 stated that the constant lateral confinement pressure

assumption is correct only when the lateral steel is in the yielding phase, accordingly, Mander model correctly represents the lateral steel behavior, except in the initial phase when steel is elastic. This verification satisfies the third approach in Eid's classification. In addition to that, Mander model uniquely, besides El-Dash and Ahmad Model, is defined by one equation for the ascending and descending branches. Furthermore, O'Shea and Bridge 2001 adapted Mander model to fit the concrete filled steel tubes model, and Spolestra and Monti 2000 adapted the same model to fit concrete wrapped with FRP. So it can be concluded:

1- Mander model is defined by one equation
2- Mander model is adaptable to fit different confinement types like steel tubes and FRP wrapping.
3- Mander model was successfully benchmarked against experimental work done for fully sized columns
4- Mander model is one of the most widely used and known models

2-4 Experimental Studies

Columns under concentric axial loads

Most of the proposed models were compared to experimental work done by the same authors of these models. Experimental work was conducted intensively for columns under concentric axial load. Rectangular cross section was the focus of the most tests, like Scott et al. (1982). The circular cross section was tested as well, by Mander et al. (1988) for example. As illustrated in Table (2-1) Ahmad and Shah 1982 used eight series of specimens, six for normal weight concrete and two for lightweight concrete. The specimens were cylinders with dimensions of 3X6 in and 3X12 in. Martinez et al. (1984) tested ninety-four specimens with

dimension of 4X8,4X16,5X24 and 6X24in cylinders. Mander et al (1988) examined full-size circular reinforced concrete columns with dimension of 19.7X59.1 in. While Cusson and Paultre (1995) examined 11 specimens with core diameter of 5.67 in. Hoshikuma et al. (1997) tested six specimens with diameter of 7.87 in. and 10 columns with diameter of 19.68 in. but the longitudinal steel ratio was around 1 % and less according to Japanese codes. Finally Razvi and Saatcigolu 1999 tested 16 specimens with core diameter ranging from 8.6 in. to 8.8 in.

Table 2-1 Experimental work conducted for concentrically loaded columns and cylinders

Name	Dimensions (in.)	Columns/cylinders Number
Ahmad and Shah 1982	3*6 and 3*12	8 series cylinders
Martinez et al. 1984	4*8,4*16,5*24 and 6*24	94 cylinders
Mander et al. 1988	19.7*59.1	15 columns
Cusson and Paultre 1995	5.67	11 cylinders
Hoshikuma et al. 1997	7.87 and 19.68	6 cylinders and 10 columns
Razvi and Saatcigolu 1999	8.6 -8.8	16 cylinders

Columns under combined axial load and bending moment.

University of Illinois (1930) was one of the pioneers to test circular specimen concentrically as well as eccentrically. Chan 1955 examined eccentrically loaded specimens with very small eccentricity. Sargin 1971 conducted experimental work for eccentric loading besides concentric one. However no full information was documented for verification. Fafitis and Shah 1985 examined four 23.65 in. diameter octagonal columns with circular spirals. Dodd and Cooke conducted experimental work for specimens with a diameter of 7.87 in. Esmaeily and Xiao examined 16 in diameter columns with a height of 100 in.

2-5 Eccentricity consideration

Unlike concentric loading, the eccentric loading generates bending moment in addition to axial loading. Columns subjected to eccentric loading behave differently from those concentrically loaded, as the shape of the stress strain curve for fully confined reinforced concrete (concentric loading) shows higher peak strength and more ductility than the unconfined one (infinite eccentricity). Most of the previous studies were based on the uniform distribution of compressive strain across the column section. According to Saatcigolu et al. 1995, there is no difference between the stress strain curves for concentric and eccentric columns for plain concrete. Soliman and Yu 1967 reported, by testing small-scale specimens, that the confinement pressure provided by transverse reinforcement would be different under a strain gradient than under uniform compression. Sargin 1971 showed relationship between location of the neutral axis and improvement in the strength and ductility. Samra et al. 1996 adapted ACI expression for spiral steel by multiplying it by a function of eccentricity to column diameter ratio.

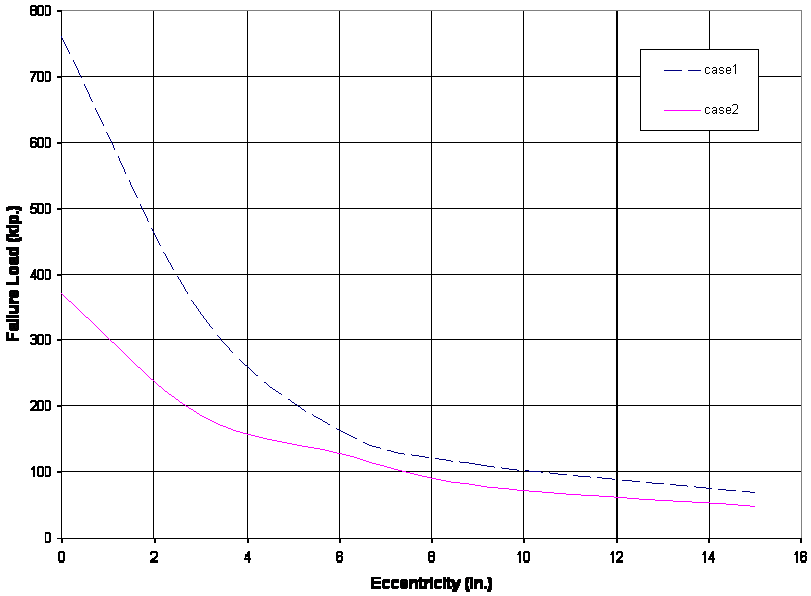

Figure 2-8 Eccentricity and maximum force relationship

Figure 2-8 shows the decrease in maximum applied force with eccentricity increasing for two different cases, which are taken from Hogenstad 1930. Table 2-2 shows different parameter values for the two cases.

Table 2-2 Parameter details for the two cases taken from Hogenstad 1930

Parameter	Case 1	Case 2
Diameter in.	12	12
Cover in.	1	1
f_y ksi.	43.5	43.5
f_{yh} ksi.	32	32
Spacing in.	1.5	1.5
Longitudinal steel	8#7	8#7
Spiral Steel Diameter in.	0.283	0.2625
f'_c k.	5.15	3.37

Fafitis and Shah 1985 examined four full size columns subjected to eccentric loads, and generated computer program, as mentioned earlier, for moment curvature prediction. Sheikh and Yeh 1990 stated that none of the confinement models available represents the behavior of eccentrically loaded columns. Saatcigolu et al. 1995 tested twelve rectangular cross section columns loaded eccentrically. The parameter tested were the arrangement, spacing and volumetric ratios of transverse steel. They concluded that the concentrically loaded confined concrete stress strain curve could represent the eccentrically loaded confined concrete by incorporating the relevant parameters of concentric confinement in their model.

Esmaeily and Lucio 2004 stated that the depth of compression zone does not play any role in any model in terms of strength and ductility. Figure (2-9) illustrates three different sections under concentric load, pure bending moment and combination of axial load and bending moment, The highlighted fiber in the three cases has the same strain, and any current confinement model will yield the same stress for these three fibers. So it is more realistic to relate the strength and ductility in a new model to the level of confinement utilization.

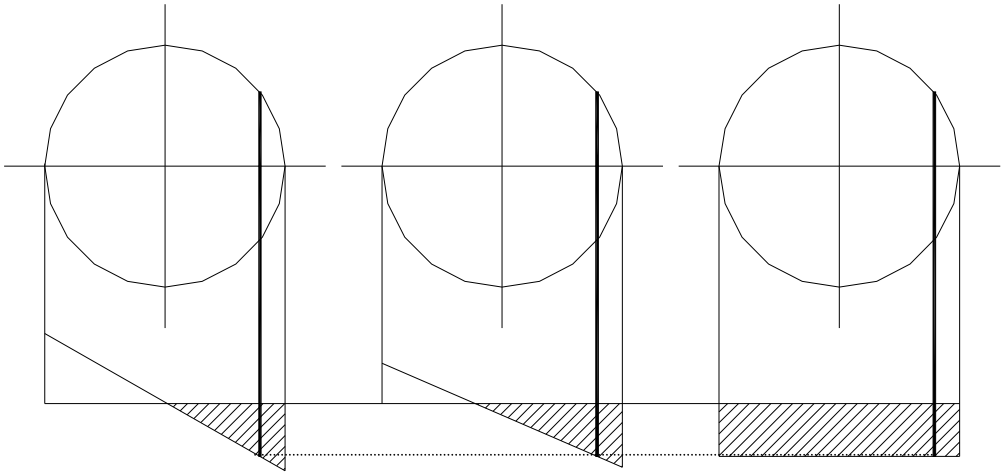

Figure 2-9 Effect of compression zone depth on concrete strength

Fam et al. 2003 was the first to develop eccentricity based model for concrete filled FRP tubes, they utilized Fam and Rizkalla 2001 model as an upper bound (bi-linear curve) as well as Popovics model for unconfined concrete as a lower bound (non linear curve). For the concentric loading case, the failure strain proposed was the strain corresponding to the peak strength. Then it increases based on the eccentricity till maximum strain for unconfined concrete. A shape parameter was introduced to allow for smooth transition between the upper linear curve and the lower non-linear curve.

2-6 Numerical and Mathematical Analysis

Numerical and Mathematical analysis varies according to the geometry of the section. Rectangular cross section analysis has been investigated by many researchers like Medland and Taylor (1971), Lazaro and Richards (1973), Kronke et al. (1973), Gunnin and Furlong (1977), Rasheed and Dinno (1994). The main focus was on the unconfined cross section, since this was the first priority of different codes. On the other hand, the circular cross section analysis was conducted by adapting some concepts of the rectangular cross section or by considering some approximations. The numerical analysis procedures for unconfined and confined circular cross section are summarized chronologically below.

Unconfined Concrete

Everand and Cohen (1964, 1997)

Everand and Cohen (1964) developed equations for generating the interaction diagram for square and circular cross sections with longitudinal steel bars arranged in a circle. The computer program produced was used by ACI committee 340-design handbook. According to Everand (1997), the equations generated are adaptable to any cross section enclosed by a square with an area D^2 by imposing an area factor λ ($\pi/4$ for circles, 0.866 for hexagonal cross section and 0.8284 for octagonal cross section). In addition the equations were generated for reinforcement ratio between 0.01 and 0.08. However, they can be used for a ratio less than 0.01.

As shown in Figure (2-8) Everand and Cohen replaced longitudinal bars arrangements with a thin steel ring equivalent to steel total area:

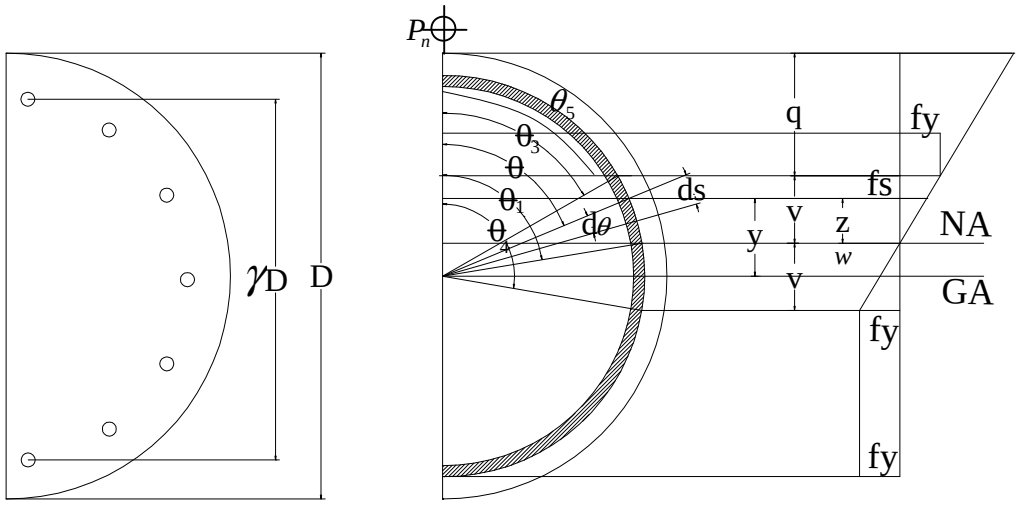

Figure 2-10 One half real and substitute cross-section

$$\psi = \frac{\varepsilon_y}{\varepsilon_u} \tag{2-148}$$

$$q = c(1-\psi) \tag{2-149}$$

$$v = c(\psi) \tag{2-150}$$

$$w = \frac{D}{2}\left(1-2\frac{c}{D}\right) \tag{2-151}$$

$$y = \frac{\gamma D}{2}\cos\theta \tag{2-152}$$

$$z = \frac{\gamma D}{2}(\cos\theta_1 - \cos\theta) \tag{2-153}$$

$$\theta_1 = \arccos\left[\frac{1}{\gamma}\left(1-2\frac{c}{D}\right)\right] \le \pi \tag{2-154}$$

$$\theta_3 = \arccos\left[\frac{1}{\gamma}\left(1-2\frac{c}{D}(1-\psi)\right)\right] \le \pi \tag{2-155}$$

$$\theta_4 = \arccos\left[\frac{1}{\gamma}\left(1-2\frac{c}{D}(1+\psi)\right)\right] \le \pi \tag{2-156}$$

$$h = \frac{\rho_s \lambda D}{\pi\gamma} \tag{2-157}$$

$$ds = \lambda\frac{D}{2}d\theta \tag{2-158}$$

where h is the ring thickness. The dimensionless expression for the nominal axial force $k_{n:}$

$$k_n = \frac{P_n}{f_c^{'} A_g} = k_s + k_c - k_f \tag{2-159}$$

where k_s represents the reinforcement force, k_f is a correction factor for concrete displaced by steel and k_c represents the concrete force:

$$k_s = \frac{\rho_s f_y}{f_c^{'} \lambda \pi}\left[\theta_3 + \theta_4 - \pi + \left(\frac{\gamma}{2\psi \frac{c}{D}}\right)\left(\sin\theta_4 - \sin\theta_3 - (\theta_4 - \theta_3)\cos\theta_1\right)\right] \tag{2-160}$$

$$k_f = \left[\frac{0.85\rho_s \theta_5}{\pi}\right] \tag{2-161}$$

$$k_c = \left[\frac{0.85}{4\lambda}\right](\theta_2 - \sin\theta_2 \cos\theta_2) \tag{2-162}$$

The dimensionless expression for the nominal moment $R_{n:}$

$$R_n = k_n \frac{e}{D} = \frac{M_n}{f_c^{'} A_g D} = R_s + R_c - R_f \tag{2-163}$$

where R_s represents the reinforcement moment, R_f is a correction factor for concrete displaced by steel and R_c represents the concrete moment:

$$R_s = \frac{\rho_s f_y \gamma}{2 f_c^{'} \lambda \pi}\left[\sin\theta_3 + \sin\theta_4 + \left(\frac{\gamma}{2\psi \frac{c}{D}}\right)\left(\frac{\sin\theta_4 \cos\theta_4 - \sin\theta_3 \cos\theta_3}{2} + \left(\frac{\theta_4}{2} - \frac{\theta_3}{2}\right) - (\cos\theta_1(\sin\theta_4 - \sin\theta_3))\right)\right] \tag{2-164}$$

$$R_f = \left[\frac{0.85\rho_s \gamma}{2\pi}\right]\sin\theta_5 \tag{2-165}$$

$$R_c = \left[\frac{0.85}{12\lambda}\right]\sin^3\theta_2 \tag{2-166}$$

According to Everand 1997, The closed form solution for the nominal force and nominal moment can not be adaptable to any other cross section different than the circle. In addition The development of equations was based on the assumption that the entire steel area is lumped into equivalent steel ring. Although this assumption simplify the calculations, it affects the results and does not account for vertical bars location with respect to the neutral axis.

Davalth and Madugula (1988)

Davalth and Madugula (1988) developed a numerical procedure for analysis and design of reinforced concrete circular sections subjected to axial load and bending moment, using the strength theory of ACI 318-83. Davalth and Madugula argued that the equations of equilibrium are complex because of the cross section type and the discrete position of bars. Instead a trial and error procedure was followed using computer programming.

1- Strain in reinforcement and concrete is assumed directly proportional to the distance from the neutral axis.

2- Maximum strain in extreme concrete compression fiber is 0.003

3- The stress-strain curve for reinforcement is elastic-perfectly plastic.

4- Tensile strength of concrete is negligible.

5- The relationship between concrete compressive stress distribution and concrete strain is assumed to be rectangular satisfying the ACI 318-83.

6- Design strength is developed either when compressive strain in concrete reaches 0.003,or the maximum tensile strain in the reinforcement is equal to the limiting value specified by the designer.

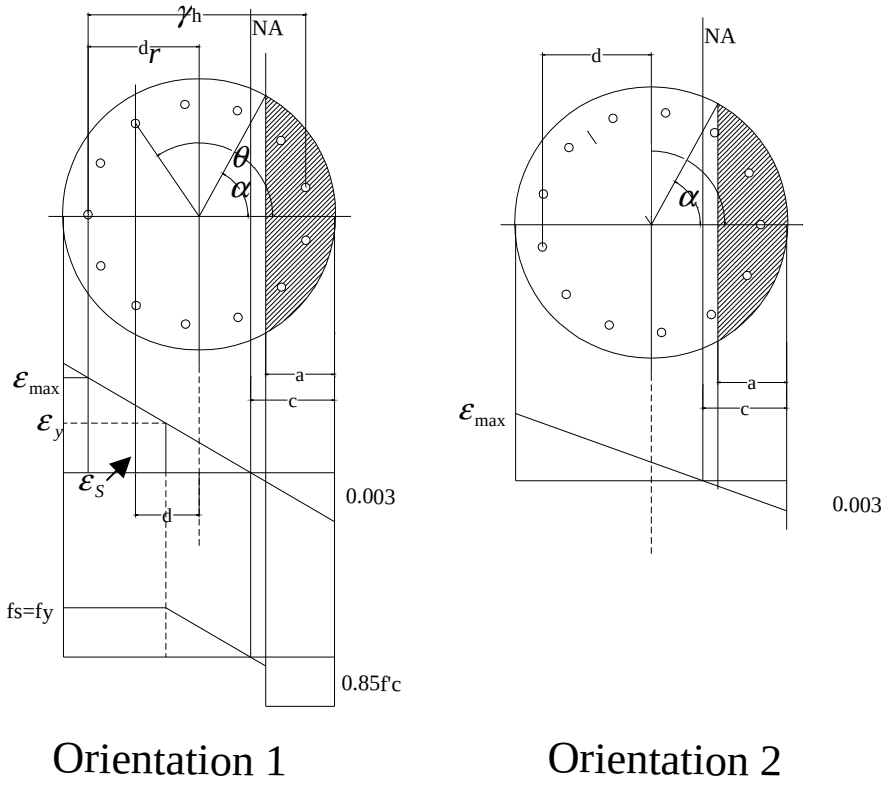

Figure 2-11 Two different cases for circular cross section according to Davalth and Madugula analysis

The equilibrium of force equation:

$$P_n = P_c + P_s \tag{2-167}$$

where P_n is the nominal axial load strength of cross section, P_c is the nominal compression strength of concrete and P_s is the nominal axial load strength of steel.

$$P_c = 0.85 f_c^{'} \left[\frac{h^2}{8} (2\alpha - \sin 2\alpha) - \sum_1^{n_c} A_b n_b \right] \tag{2-168}$$

$$P_s = \sum_1^{n_r} f_s A_b n_b \tag{2-169}$$

where h is the diameter of the circular cross section, α is one half of the angle subtended at the center of the cross section by the concrete compression stress block, A_b is the cross sectional area of each reinforcing bar, n_b is the number of reinforcing bars in each row parallel to moment axis, and n_c is the number of rows of reinforcing bars in the zone of concrete compression stress block. The nominal flexural strength M_n is equal to the nominal flexural strength due to concrete M_c and the nominal flexural strength due to M_s.

$$M_n = M_c + M_s \tag{2-170}$$

$$M_c = 0.85 f_c^{'} \left[\frac{h^2}{12} \sin^3 \alpha - \sum_1^{n_c} A_b n_b \frac{\gamma h}{2} \cos\theta \right] \tag{2-171}$$

$$M_s = \sum_1^{n_r} (f_s A_b n_b) \frac{\gamma h}{2} \cos\theta \tag{2-172}$$

where θ is the angle between the radial line through the reinforcing bar and the line perpendicular to the moment axis, and γh is the diameter of reinforcing bar circle. As orientation 1 Figure (2-9) illustrates, the strain ε_s and the stress f_s in any bar when the maximum strain in concrete is equal to 0.003:

$$\varepsilon_s = \frac{0.003(d + 0.5h - c)}{c} \tag{2-173}$$

$$f_s = \frac{87(d + 0.5h - c)}{c} \qquad f_s < f_y \tag{2-174}$$

where d is the distance of reinforcing bar from the moment axis.

The strain and the stress in any bar when the maximum strain in reinforcing bar is equal to the limiting value specified by the designer, and the maximum strain in concrete is less than 0.003:

$$\varepsilon_s = \frac{\varepsilon_{\max}\left(d + 0.5h - c\right)}{\left(d_r + 0.5h - c\right)} \tag{2-175}$$

$$f_s = \frac{29000\varepsilon_{\max}\left(d + 0.5h - c\right)}{\left(d_r + 0.5h - c\right)} \qquad f_s < f_y \tag{2-176}$$

As shown in orientation 2 Figure (2-9). The maximum tensile strain in bars is given by:

$$\varepsilon_m = \frac{0.003\left(d_r + 0.5h - c\right)}{c} \tag{2-177}$$

where d_r is the distance from the farthest reinforcing bar on the tension side to the moment axis.

and the angle α is given by:

$$\alpha = \cos^{-1}\left[1 - \frac{0.003\beta_1\left(d_r + 0.5h\right)}{0.5h\left(\varepsilon_{\max} + 0.003\right)}\right] \tag{2-178}$$

where β_1 is a factor defined in section 10.2.7.3 of ACI 318-83.

Since the angle α is unknown and it depends on the factored axial load P_u or eccentricity *e*, a trial and error process is followed , till a convergence is obtained between computed and desired values.

The procedure developed by Davalth and Madugula was based on ACI specification, which consider the concrete stress distribution to be rectangular. This assumption is approximate for the circular cross section. Dependently, the analysis is not very accurate.

Tayem and Najmi (1996)

Tayem and Najmi (1996) developed a closed form solution for circular short columns based on transforming the components, steel and concrete, to elastic material to which the classical bending theory is applicable. The analysis was based on the following assumptions:

1- Plane sections at right angles to the column axis remain plane

2- Reinforcing steel is elastic perfectly plastic

3- Stress-strain curve of concrete is modeled by Whitney's block.

4- Tensile strength of concrete is ignored

5- Vertical bars have the same diameter and grade

6- Vertical bars are equally spaced on the perimeter inside the lateral reinforcement.

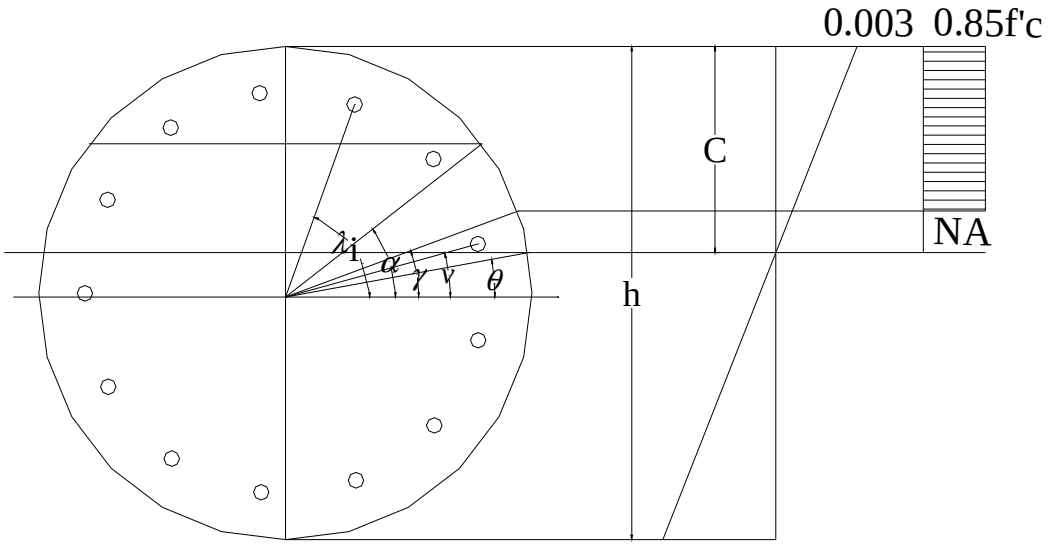

Figure 2-12 Geometric configuration of Tayem and Najmi. Analysis

The transformed concrete area is determined by:

$$A_c = \frac{h^2\sqrt{f_c^{'}}}{405}(1-\sin\theta)z \tag{2-179}$$

$$z = -\cos\gamma + \left[\gamma - \left(\frac{\pi}{2}\right)\right]\sin\theta + \cos\theta\left[\log\frac{\left(1-\tan\frac{\theta}{2}\tan\frac{\lambda}{2}\right)}{\left(\tan\frac{\gamma}{2}-\tan\frac{\theta}{2}\right)}\right] \tag{2-180}$$

and the first moment of area Q_c:

$$Q_c = \frac{h^3\sqrt{f_c^{'}}}{810}(1-\sin\theta)\left(\frac{\pi}{4}-\frac{\gamma}{2}-\frac{\sin 2\gamma}{4}+z\sin\theta\right) \tag{2-181}$$

and the centroid of the transformed area is located at distance C_c from the x-axis:

$$c_c = \frac{Q_c}{A_c} \tag{2-182}$$

and the moment of inertia of the transformed section I_c:

$$I_c = \frac{h^4\sqrt{f_c^{'}}}{1621}(1-\sin\theta)\left[\frac{\cos^3\gamma}{3}+\sin\theta\left(\frac{\pi}{4}-\frac{\gamma}{2}-\frac{\sin 2\gamma}{4}+z\sin\theta\right)\right] \tag{2-183}$$

The transformed steel area A_{st}

$$A_{st} = \frac{As}{57400\sqrt{f_c^{'}}}\sum_{i=1}^{n}\left(E_{si}-E_{dci}\right) \tag{2-184}$$

where A_s is the bar area, and E_{dci} is the secant modulus of concrete displaced by steel bar. And the first moment of the transformed steel area with respect to x-axis Q_s:

$$Q_s = \frac{A_s\left(h-2\bar{d}\right)}{114800\sqrt{f_c^{'}}}\sum_{i=1}^{n}\left(E_{si}-E_{dci}\right)\sin\lambda_1 \tag{2-185}$$

where $\bar{d}$ is the radial distance from perimeter of column to the centroid of vertical reinforcement bars, and the totally transformed area of the cross section A_t:

$$A_t = A_c + A_s \tag{2-186}$$

the centroid of the totally transformed area c_t:

$$c_t = \frac{Q_c + Q_s}{A_t} \tag{2-187}$$

The moment of inertia I_{xt} of the composite section about an axis parallel to the neutral axis through the centroid of the transformed section:

$$I_{xt} = I_c + A_c c_t (c_t - 2c_c) + \frac{A_s}{57400\sqrt{f_c'}} \sum_{i=1}^{n} (E_{si} - E_{dci}) \left[\left(\frac{h}{2} - \bar{d} \right) \sin \lambda_1 - c_t \right] \quad (2\text{-}188)$$

The elastic section modulus S_{xc} with respect to the concrete compression side:

$$S_{xc} = \frac{2I_{xt}}{h - 2c_t} \quad (2\text{-}189)$$

and the position of neutral axis must satisfy:

$$2I_{xt1} - A_t e_s (2c_t - h \sin \theta) = 0 \quad (2\text{-}190)$$

where e_s is the pertinent structure eccentricity:

$$e_s = e - c_t \quad (2\text{-}191)$$

Similar to Davalth and Madugula ,the approximate use of Whitney's block, although certified by ACI, is not very accurate since the circular cross section differs from the rectangular one. Consequently the analysis considered not to be very accurate since it was built on this assumptions.

Confined Concrete

Fafitis and Shah 1985

. Fafitis and Shah 1985 developed a computer program to calculate the moment-curvature relationship. They found the moment for the given load by dividing the cross section into strips, and assuming constant stress all over each strip including core, cover and reinforcement. However, no details were provided describing the iterative process for calculating the depth of the neutral axis.

Samra, Deeb and Madi 1996

Based on theoretical study using Mander model, for concrete subjected to uniaxial compressive loading and confined by transverse steel, Samra et al. derived theoretical analysis for generating moment curvature characteristics. The main factors account for:

1- Level of eccentricity of axial load on column e.

2- Longitudinal steel content ρ_{ls}

3- Value of curvature ductility factor required to be achieved ϕ_u/ϕ_y.

4- Material strength *f'c* and *fy*.

Where ϕ_u is ultimate curvature, and ϕ_y is yielding curvature.

The assumptions used in this analysis are:

1- Plane section remains plain after flexural deformation.

2- Mander et al. model was used for spirally confined concrete.

3- The tensile strength of concrete is ignored.

4- Steel is linearly elastic till yield then, strain hardening was considered.

The analysis is summarized in the following steps:

1- Calculating the spalling cover strain and maximum strain based on Mander model

2- For strain compatibility profile has extreme fiber compressive strain ε_{cm} and depth of compression zone *c:*

Using similar triangle in strain diagram to find the strain in each longitudinal bar, then calculating the stress f_{si} and force for each bar .

Dividing the compressed concrete into two parts; confined part and unconfined part, dividing the section into small rectangular layers, and calculating the concrete force

for each layer, then summing the forces up to have the concrete force *Cc* and the moment arm X_c.

3- The force *P* and moment *M* equilibrium equations:

$$P = C_c + \sum_{i=1}^{n} f_{si} A_{si} \tag{2-192}$$

$$M = C_c \left(\frac{D}{2} - X_c \right) + \sum_{i=1}^{n} f_{si} A_{si} \left(\frac{D}{2} - d_i \right) \tag{2-193}$$

The curvature ϕ:

$$\phi = \frac{\varepsilon_{cm}}{c} \tag{2-194}$$

where *D* is column diameter, A_{si} is the area of each bar and d_i represents the location of each bar.

4- For a given eccentricity and by incrementing the extreme fiber compressive strain, finding the neutral axis depth based on:

$M = P * e$

The sequenced loading is used in this analysis for determining the depth of neutral axis. In plasticity, radial loading gives the same results as non-linear elasticity, whereas sequenced loading gives different results compared to nonlinear elasticity.

CHAPTER 3 - New Confinement Model

As earlier stated, Mander Model was selected to be the base of the new eccentricity-based model, This chapter views mander model in details. Then, the new model is discussed.

3-1 Mander Model

The Mander model (1988) was developed based on the effective lateral confinement pressure and the confinement effective coefficient, the same concept found by Sheikh and Uzumeri (1982). The advantage of this procedure is its applicability to any cross section since it defines the lateral pressure based on the section geometry. Mander et al (1988) showed the adaptability of their model for circular or rectangular sections, under static or dynamic loading, either monotonically or cyclically applied. In order to develop a full stress-strain curve and to assess ductility, an energy balance approach is used to predict the maximum longitudinal compressive strain in the concrete.

Mander derived the longitudinal compressive concrete stress-strain equation from Popovics model that was originally developed for unconfined concrete (1973):

$$f_c = \frac{f_{cc} x r}{r - 1 + x^r} \tag{3-1}$$

where:

$$x = \frac{\varepsilon_c}{\varepsilon_{cc}} \tag{3-2}$$

$$r = \frac{E_c}{E_c - E_{\sec}} \tag{3-3}$$

$$E_c = 5000\sqrt{f'_{co}} \quad \text{in MPA} \tag{3-4}$$

$$E_{\sec} = \frac{f_{cc}}{\varepsilon_{cc}} \tag{3-5}$$

and as suggested by Richart et al. (1928) the strain corresponding to the peak compressive strength:

$$\varepsilon_{cc} = \varepsilon_{co}\left[1+5\left(\frac{f_{cc}}{f_c^{'}}-1\right)\right] \tag{3-6}$$

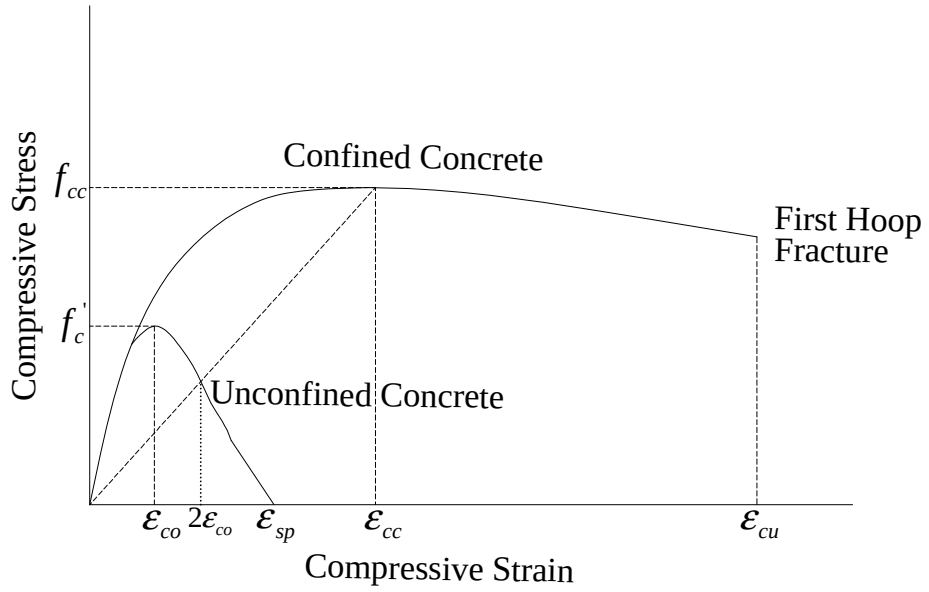

Figure 3-1 Stress-Strain Model proposed by Mander et al. for monotonic loading

As shown in Figure 3-1, Mander et al. (1988) model has two curves; one for unconfined concrete (lower curve) and the other for confined concrete (upper one). The upper one refers to the behavior of confined concrete with concentric loading (no eccentricity). It can be shown from the Figure that it has ascending branch with varying slope starting from E_c decreasing till it reaches the peak confined strength at (f_{cc}, ε_{cc}). Then the slope becomes negative in the descending branch representing ductility till point ε_{cu} where first hoop fracture occurs. The lower curve expresses the unconfined concrete behavior. It has the same ascending branch as the confined concrete curve till it peaks at (f'_c, ε_{co}). Then, the falling branch comes next till 1.5-2ε_{co}. A straight line is assumed after that till zero stress at spalling strain ε_{sp}.

Mander et al. (1988) utilized an approach similar to that of Sheik and Uzumeri (1982) to determine effective lateral confinement pressure. It was assumed that the area of confined concrete is the area within the centerlines of perimeter of spiral or hoop A_{cc} as illustrated in

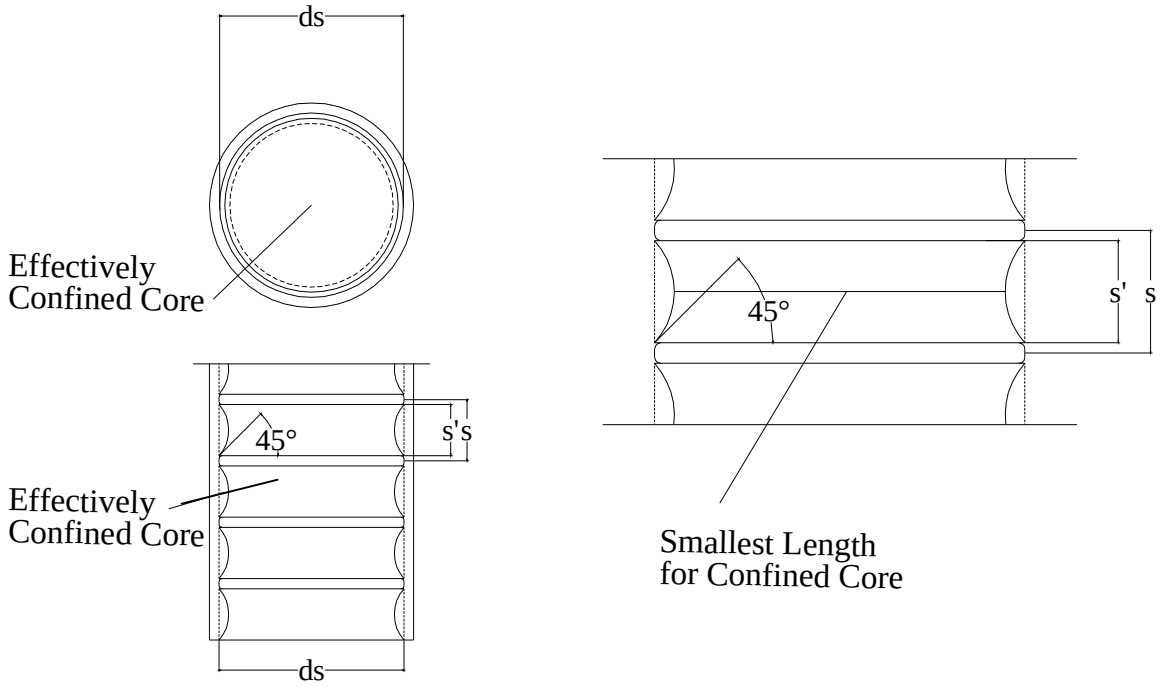

Figure (3-2)

Figure 3-2 Effectively confined core for circular hoop reinforcement

Figure (3-2) shows that effectively confined concrete core A_e is smaller than A_{cc}, and to satisfy that condition the effective lateral confinement pressure f'_l should be a percentage of the lateral pressure f_l:

$$f_l^{'} = k_e f_l \tag{3-7}$$

and the confinement effectiveness coefficient k_e is defined as the ratio of effective confined area to the area enclosed by centerlines of spiral or hoop:

$$k_e = \frac{A_e}{A_{cc}} \tag{3-8}$$

$$A_{cc} = A_c - A_{ls} \tag{3-9}$$

$$\frac{A_{cc}}{A_c} = 1 - \frac{A_{ls}}{A_c} \tag{3-10}$$

$$A_{cc} = A_c\left(1 - \rho_{cc}\right) \tag{3-11}$$

where A_c is the area of the section core enclosed by spiral, A_{ls} is the area of longitudinal steel and ρ_{cc} is the ratio of longitudinal steel to the area of the core. For hoop case the effective lateral confinement core:

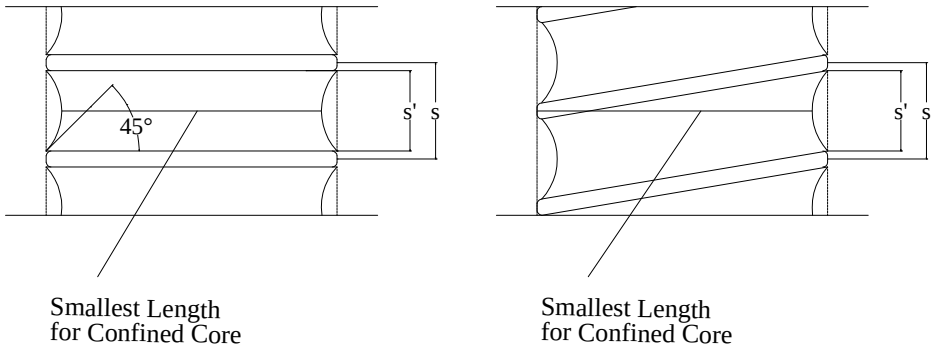

Figure 3-3 Effective lateral confined core for hoop and spiral reinforcement

$$A_e = \frac{\pi}{4} d_s^2 \left(1 - \frac{s'}{2d_s}\right)^2 \tag{3-12}$$

$$k_e = \frac{\left(1 - \frac{s'}{2d_s}\right)^2}{1 - \rho_{cc}} \tag{3-13}$$

while for spiral case it can be shown from Figure (3-3) that

$$A_e = \frac{\pi}{4} d_s^2 \left(1 - \frac{s'}{4d_s}\right)^2 = \frac{\pi}{4} d_s^2 \left(1 - \frac{2s'}{4d_s} + \frac{s'^2}{16 d_s^2}\right) \tag{3-14}$$

and the last term can be neglected and the value of k_e can be found from the following equation:

$$k_e = \frac{1 - \frac{s'}{2d_s}}{1 - \rho_{cc}} \tag{3-15}$$

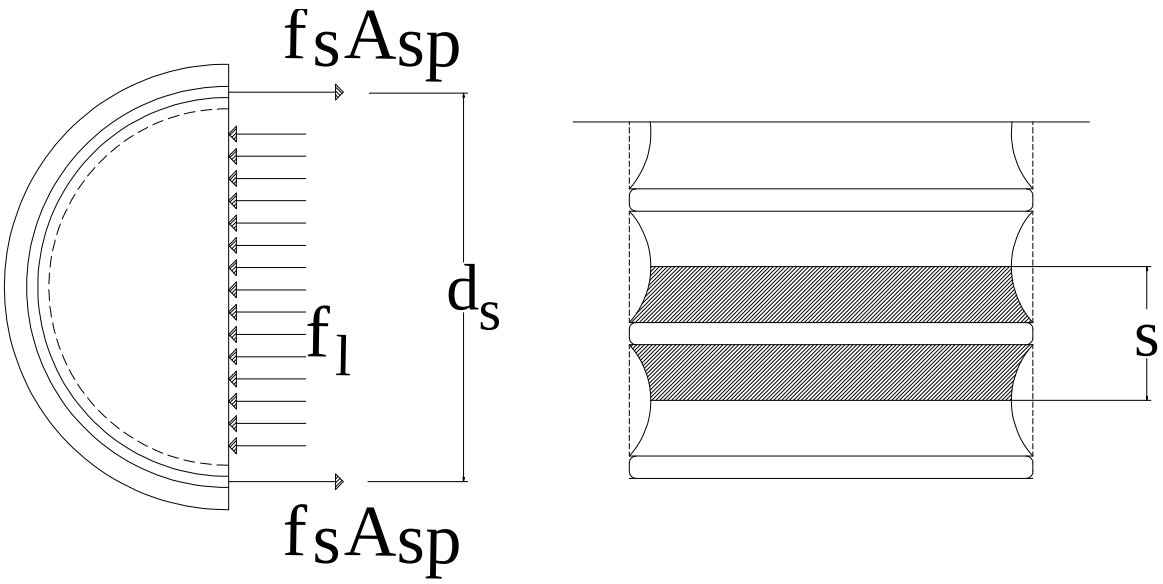

Figure 3-4 Confinement forces on concrete from circular hoop reinforcement

Figure (3-4) illustrates force equilibrium on a half turn of a circular hoop. The uniform hoop tension at yield generated in the transverse steel should be balanced by the uniform lateral stress on the concrete core:

$$2 f_{yh} A_{sp} = f_l s d_s \tag{3-16}$$

$$f_l = \frac{2 f_{yh} A_{sp}}{s d_s} \tag{3-17}$$

but ρ_s can be expressed as

$$\rho_s = \frac{A_{sp}\pi d_s}{\frac{\pi}{4} s d_s^2} = \frac{4A_{sp}}{s d_s} \tag{3-18}$$

hence

$$f_l = \frac{1}{2}\rho_s f_{yh} \tag{3-19}$$

and from equation (3-7) f'_l can be found:

$$f_l^{'} = \frac{1}{2} k_e \rho_s f_{yh} \tag{3-20}$$

The maximum confined compressive strength can be described as a function of the peak unconfined strength and the uniform effective lateral confinement pressure:

$$f_{cc} = f_c^{'}\left(-1.254 + 2.254\sqrt{1 + \frac{7.94 f_l^{'}}{f_c^{'}}} - 2\frac{f_l^{'}}{f_c^{'}}\right) \tag{3-21}$$

Mander et al. (1988) proposed an energy balancing theory to predict the ultimate confined strain, which is determined at the first hoop fracture. They presumed that the additional ductility for confined concrete results from the additional strain energy stored in the hoops U_{sh}. Therefore from equilibrium:

$$U_{sh} = U_g - U_{co} \tag{3-22}$$

where U_g is the external work done in the concrete to fracture the hoop, and U_{co} is the work done to cause failure to the unconfined concrete. U_{sh} can be represented by the area under the tension stress strain curve for the transverse steel between zero and fracture strain ε_{sf}.

$$U_{sh} = \rho_s A_{cc} \int_0^{\varepsilon_{sf}} f_s d\varepsilon \tag{3-23}$$

while *Ug* is equal to the area under the confined stress strain curve plus the area under the longitudinal steel stress strain curve:

$$u_g = \int_0^{\varepsilon_{scu}} f_c A_{cc} d\varepsilon + \int_0^{\varepsilon_{scu}} f_s A_{ls} d\varepsilon \qquad (3\text{-}24)$$

similarly, it was proven experimentally that U_{co} is equal to:

$$u_{co} = A_{cc} \int_0^{\varepsilon_{spall}} f_c d\varepsilon = A_{cc} 0.017\sqrt{f_c'} \quad \text{in MPa} \qquad (3\text{-}25)$$

and

$$U_{ssh} = \rho_s A_{cc} \int_0^{\varepsilon_{sf}} f_s d\varepsilon = 110\rho_s A_{cc} \qquad (3\text{-}26)$$

Substituting equations (3-24), (3-25) and (3-26) into equation (3-22):

$$110\rho_s = \int_0^{\varepsilon_{cu}} f_c d\varepsilon + \int_0^{\varepsilon_{cu}} f_{sl} d\varepsilon - 0.017\sqrt{f_c'} \qquad (3\text{-}27)$$

where f_{sl} is a function of longitudinal strain.

3-2 Eccentricity based confined Model

In previous studies, various models were implemented to assess the ultimate confined capacity of columns under concentric axial load. On the other hand the effect of partial confinement in case of eccentric load (combined axial load and bending moments) is not investigated in any proposed model above. Therefore, it is pertinent to relate the strength and ductility of reinforced concrete to the degree of confinement utilization in a new model.

The two curves of fully confined and unconfined concrete in Mander model are used in the eccentricity-based model as upper and lower boundaries. The upper curve refers to

concentrically loaded confined concrete (zero eccentricity), while the lower one refers to pure bending applied on concrete (infinite eccentricity). In between the two boundaries, infinite numbers of stress-strain curves can be generated based on the eccentricity. The higher the eccentricity the smaller the confined concrete region in compression. Accordingly, the ultimate confined strength is gradually reduced from the fully confined value f_{cc} to the unconfined value f'_c as a function of eccentricity to diameter ratio. In addition the Ultimate strain is reduced from the ultimate strain ε_{cu} for confined concrete to the ultimate strain for unconfined concrete $1.5\varepsilon_{co}$. The equation that defines the peak strength according to the eccentricity is:

$$\overline{f_{cc}} = \frac{1}{1+\frac{e}{H}} f_{cc} + \frac{1}{1+\frac{H}{e}} f_c' \tag{3-28}$$

where e is the eccentricity, H is the column diameter and $\overline{f_{cc}}$ is the peak strength at eccentricity e. and the corresponding strain $\overline{\varepsilon_{cc}}$ is given by

$$\overline{\varepsilon_{cc}} = \varepsilon_{co}\left[1+5\left(\frac{\overline{f_{cc}}}{f_c'}-1\right)\right] \tag{3-29}$$

and the maximum strain corresponding to the required eccentricity will be a function of stress corresponding to maximum strain for confined concrete f_{cu} and unconfined concrete f_{cuo}:

$$\overline{\varepsilon_{cu}} = \overline{\varepsilon_{cc}}\left[\frac{\frac{\overline{E_{\sec}}}{E_{\sec,u}}\bar{r}}{\frac{c}{\overline{\varepsilon_{cu}}}+1} - \bar{r} + 1\right]^{\frac{1}{r}} \qquad E_{\sec,u} = \frac{f_{cu}-f_{cuo}}{\varepsilon_{cu}-0.003} \tag{3-30}$$

In order to verify the accuracy of the model at the extreme cases, the eccentricity is first set to be zero. The coefficient of f_{co} will be zero and equation (3-28) and (3-30) will reduce to be:

$$\overline{f_{cc}} = f_{cc} \tag{3-31}$$

$$\overline{\varepsilon_{cu}} = \varepsilon_{cu} \tag{3-32}$$

on the other hand, if the eccentricity is set to be infinity the other coefficient will be zero, and the strength and ductility equations will be:

$$\overline{f_{cc}} = f_{cc}^{'} \tag{3-33}$$

$$\overline{\varepsilon_{cu}} = 0.003 \tag{3-34}$$

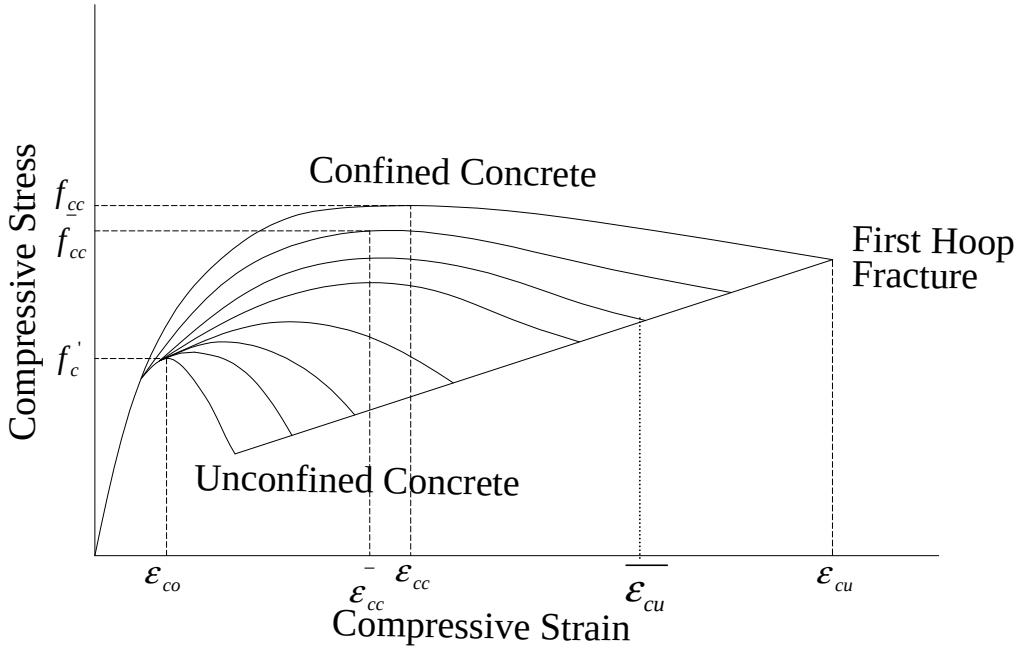

Figure 3-5 Eccentricity based confinement model

Any point on the generated curves can be calculated using the following equation:

$$f_c = \frac{\overline{f_{cc}} xr}{r - 1 + x^r} \tag{3-35}$$

where:

$$x = \frac{\varepsilon_c}{\overline{\varepsilon_{cc}}} \tag{3-36}$$

$$r = \frac{E_c}{E_c - E_{\sec}} \tag{3-37}$$

$$E_{\sec} = \frac{\overline{f_{cc}}}{\overline{\varepsilon_{cc}}} \tag{3-38}$$

CHAPTER 4 - Analysis of Columns

4-1 Unconfined Concrete Columns

Analysis of unconfined concrete is based on the finite layer procedure accounting for concrete and reinforcing steel separately then using the concept of superposition to get the overall behavior of the section.

The following assumptions are made in the analysis:

1- There is perfect bond between the longitudinal steel bars and the concrete.

2- Strains along the depth of the column are assumed to be distributed linearly.

3- Concrete stress in tension is neglected after cracking.

4- The maximum stress for concentric axially loaded confined concrete and corresponding strain is given by using Mander model.

5- The steel stress-strain relation is elastic-perfectly plastic as shown in fig (4-1)

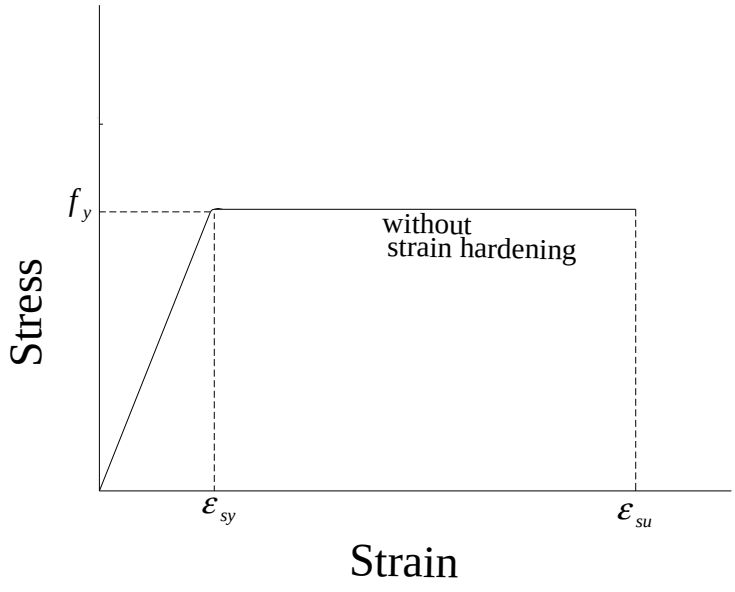

Figure 4-1 Stress-strain relationship of reinforcing steel

- Concrete analysis

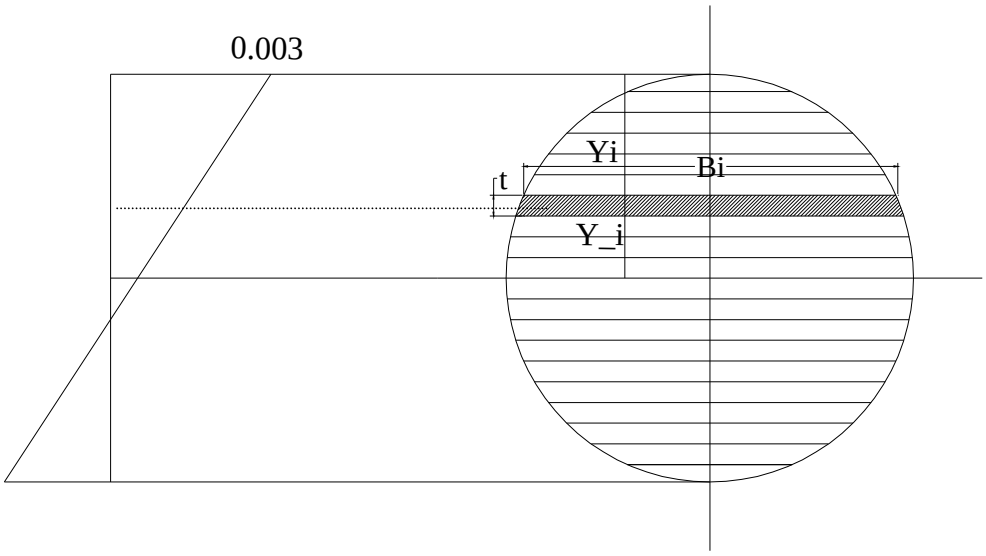

Figure 4-2 Unconfined Concrete section -concrete analysis-

Figure (4-2) depicts the procedure utilized in the calculation of concrete force and moment, which can be summarized in the following steps:

1- Breaking down the section into a finite number of thin layers that have equal thickness.

2- Getting the geometric properties of each layer:

Bi: Layer width.

t: Layer thickness.

Yi: Vertical distance from the layer centerline to the extreme compression fiber.

Y_i: Vertical distance from the layer centerline to the section geometric centroid.(mid-height)

3- Using the pre assumed strain profile and the layer location found from the previous step to get the strain ε (assuming that strain is constant through out the layer).

4- Calculating the stress f_c from the strain using Hognestad's parabola.

$$f_c = f_c^{'}\left(\frac{\varepsilon_c}{\varepsilon_{co}} - 2\left(\frac{\varepsilon_c}{\varepsilon_{co}}\right)^2\right) \tag{4-1}$$

5- Getting the area of the layer A.

6- Finding the force p, and moment m of the layer.

$$p = f_c * A \tag{4-2}$$

$$m = p * Y\_i \tag{4-3}$$

7- Summing up the forces and moments to have the concrete forces *Pc* and moment *Mc*.

$$Pc = \sum p \tag{4-4}$$

$$Mc = \sum m \tag{4-5}$$

The tensile stress is negligible beyond $7.5\sqrt{f_c^{'}}$ in psi.

- <u>Reinforcing steel bars analysis</u>

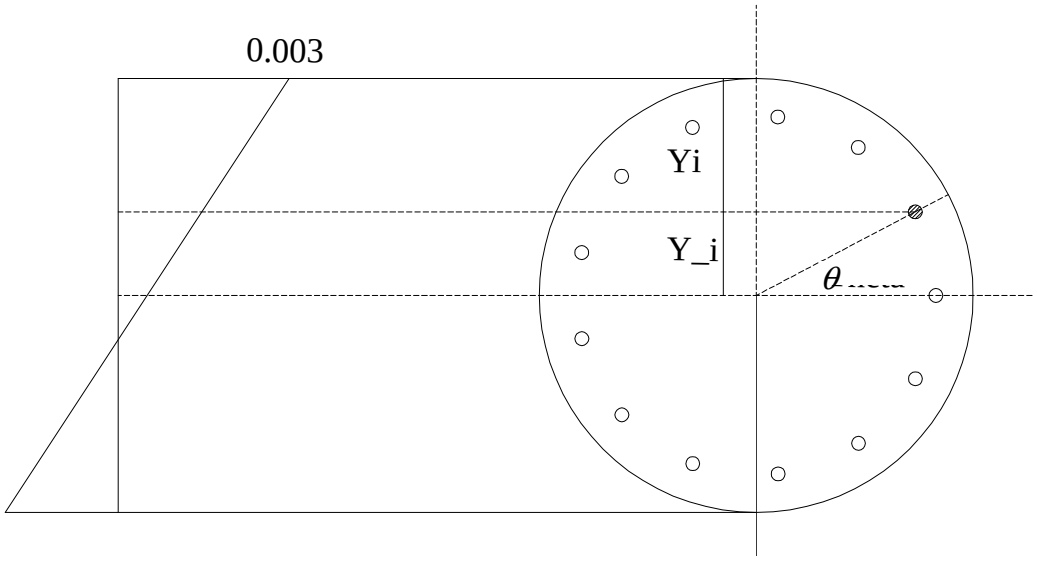

Figure 4-3 Unconfined Concrete section -steel analysis-

As illustrated in Figure (4-3), similar procedure is approached to determine the steel force and moment

For each bar:

1- Getting the geometric properties:

   Yi: Vertical distance from the bar centerline to the extreme compression fiber.

   Y_I: Vertical distance from the bar centerline to the section center.

   θ: The angle between the radius of the bar location and the positive direction of X-axis.

2- Using the pre assumed strain profile and the bar location found from the previous step to get the strain ε_s

3- Calculating the stress f_s from the strain.

4- Getting the area of the bar A_s.

5- Finding the force $\underline{p_s}$, and moment m_s.

$$p_s = f_s * A_s \tag{4-2}$$

$$m_s = p_s * Y\_i \tag{4-3}$$

6- Summing up the forces and moments to have the steel forces P_s and moment M_s.

$$Ps = \sum p_s \tag{4-4}$$

$$Ms = \sum m_s \tag{4-5}$$

After getting the concrete and steel forces and moments, the section force and moment are given using the following equations:

$$P = Pc + Ps \tag{4-6}$$

$$M = Mc + Ms \tag{4-7}$$

These two values represent a point coordinate on the interaction diagram (*M*,*P*) for unconfined concrete. The full-unconfined concrete interaction diagram can be plotted by repeating this method for different strain compatibility profiles.

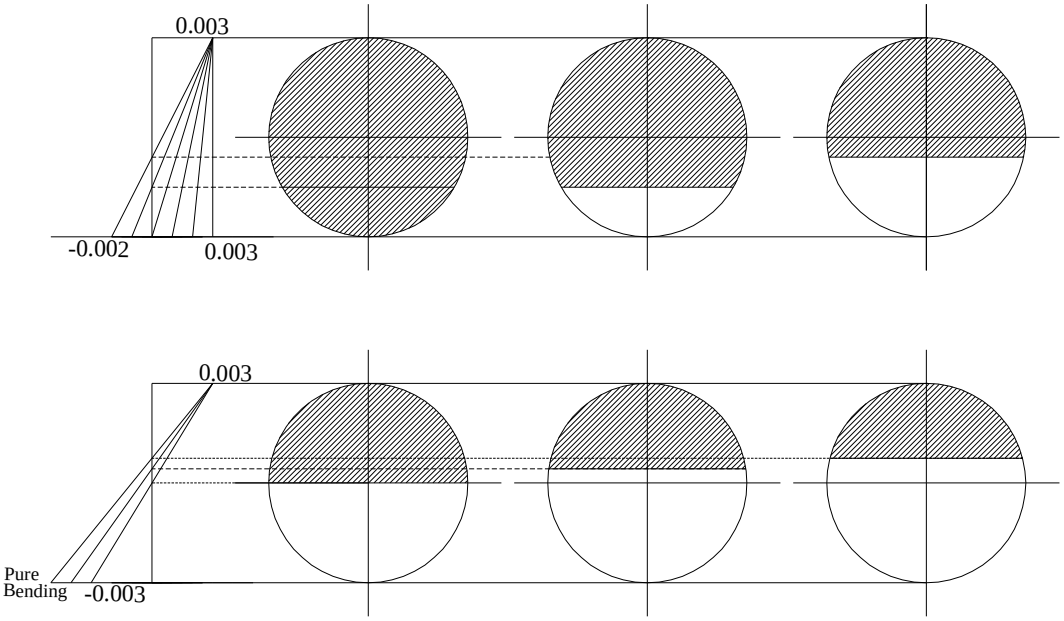

Figure 4-4 Different strain profile cases used in generating the Interaction Diagram

Figure (4-4) shows six different strain profiles. Point 0.003 was selected as a value for the extreme compression fiber as proven experimentally. While for the other extreme fiber, the values were 0.003 (Pure axial compression), 0.002,0.001, zero, -0.001,-0.002,-0.003, -0.004 and a point were the pure bending occurs.

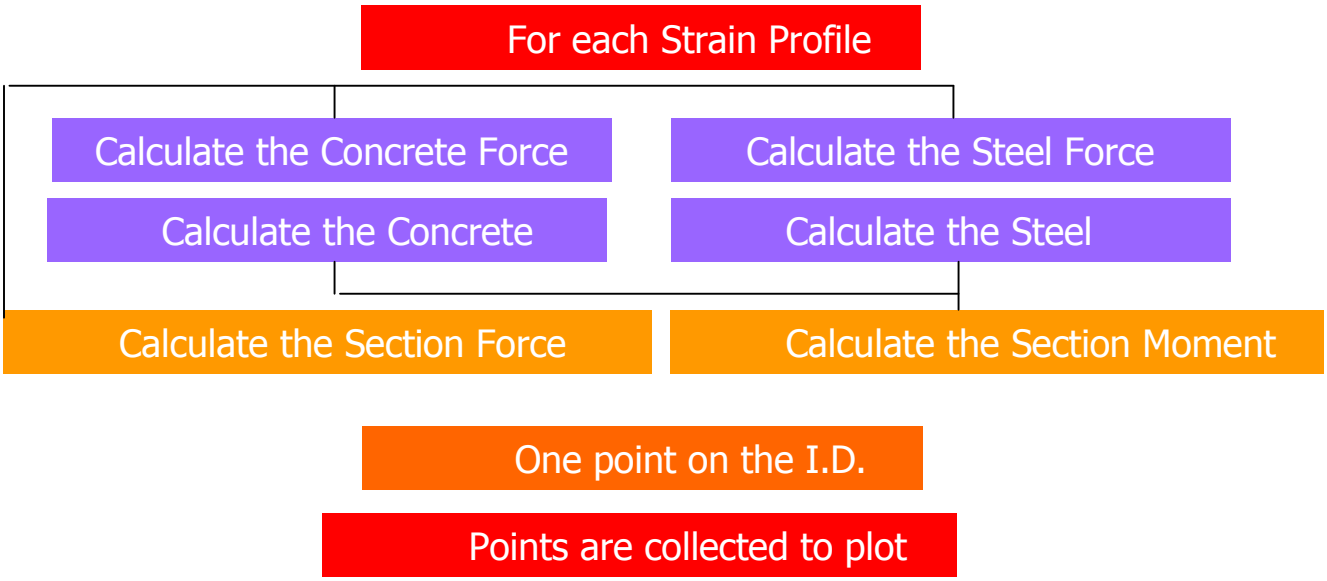

Figure 4-5 Unconfined Concrete analysis for plotting the Interaction Diagram

As shown in Figure (4-5) the smoothness of the curve can increase by running the analysis for more strain profiles and imposing many intermediate points in the Interaction diagram. The inner curve represents the design curve after applying the factor of safety based on AASHTO-code provisions.

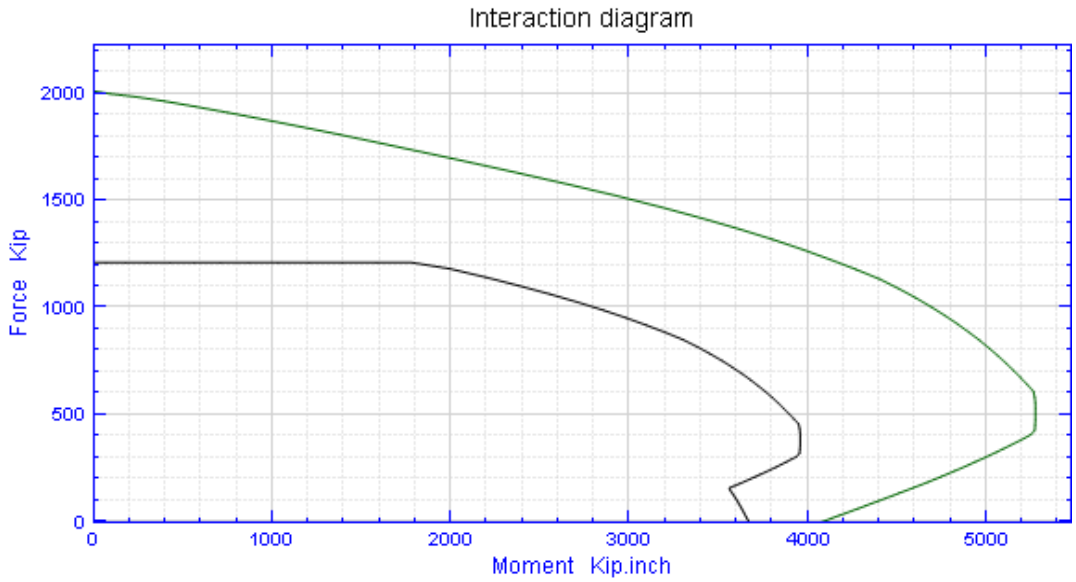

Figure 4-6 Unconfined and design interaction diagram according to AASHTO-code

4-2 Confined Concrete Columns

Analysis of confined concrete is approached using numerical non-linear finite layer procedure. As Figure (4-6) shows radial loading with constant eccentricity is conducted in the non-linear moment of area concept to achieve equilibrium points along the loading line up to failure.

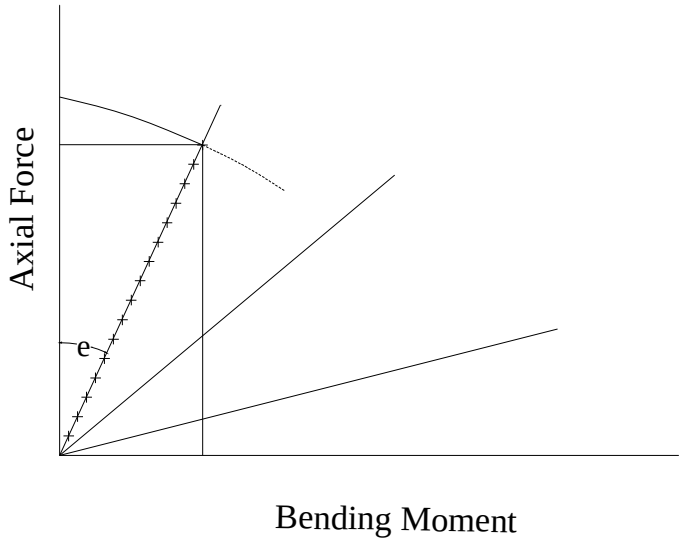

Figure 4-7 Radial loading with constant eccentricity up to failure

The following assumptions are made in the analysis:

1- There is perfect bond between the longitudinal steel bars and the concrete.

2- Strains along the depth of the column are assumed to be distributed linearly.

3- Concrete stress in tension is neglected after cracking.

4- The maximum stress for concentric axially loaded confined concrete and corresponding strain are given by using Mander model.

5- The steel stress-strain relation is elastic-perfectly plastic. However strain hardening is also allowed for longitudinal steel by assuming bilinear model as shown as shown in Figure (4-8)

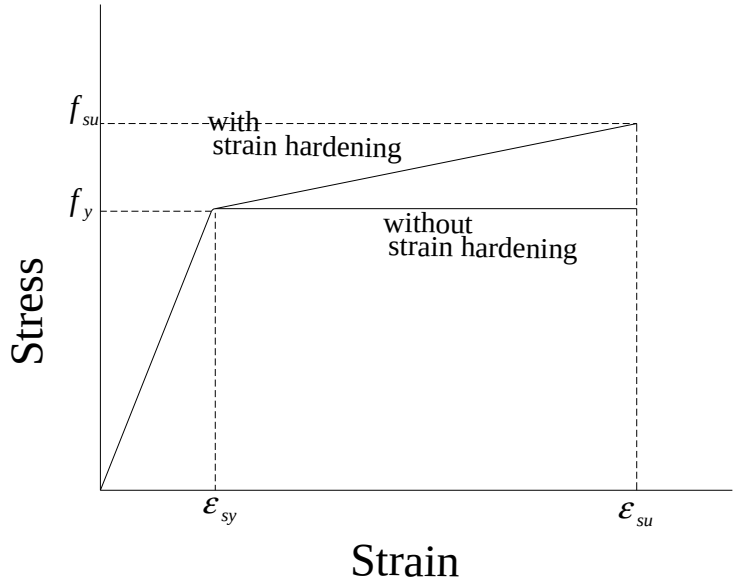

Figure 4-8 Stress-strain relationship of reinforcing steel

The procedure used to analyze the confined concrete section is described in the following steps as shown in Figure (4-8):

1- Calculating the section initial properties:

Elastic axial rigidity *EA*:

$$EA = \sum_i E_c B_i t + \sum_i (E_s - E_c) A_{si} \tag{4-8}$$

Elastic flexural rigidity about the elastic centroid *EI*:

$$EI = \sum_i E_c B_i t (H - Y_i - Y_c)^2 + \sum_i (E_s - E_c) A_{si} (H - Y_{si} - Y_c)^2 \tag{4-9}$$

The depth of the inelastic centroid position from the bottom fiber of the section Y_c:

$$Y_c = \frac{\sum_i E_c B_i t (H - Y_i) + \sum_i (E_s - E_c) A_{si} (H - Y_{si})}{EA} \tag{4-10}$$

The depth of the geometric section centroid position from the bottom fiber of the section Y_G:

$$Y_G = \frac{H}{2} \tag{4-14}$$

2- Inputting eccentricity *e*.

3- Defining loading step ΔGP, and computing the axial force at the geometric centroid.

$$GP = GP + \Delta GP \tag{4-15}$$

4- Calculating moment *GM* about the geometric centroid.

$$e = \frac{GM}{GP} \qquad GM = e * GP \tag{4-16}$$

5- Transferring moment to the inelastic centroid and calculating the new transferred moment *TM*:

$$TM = GM + GP(Y_G - Y_c) \tag{4-17}$$

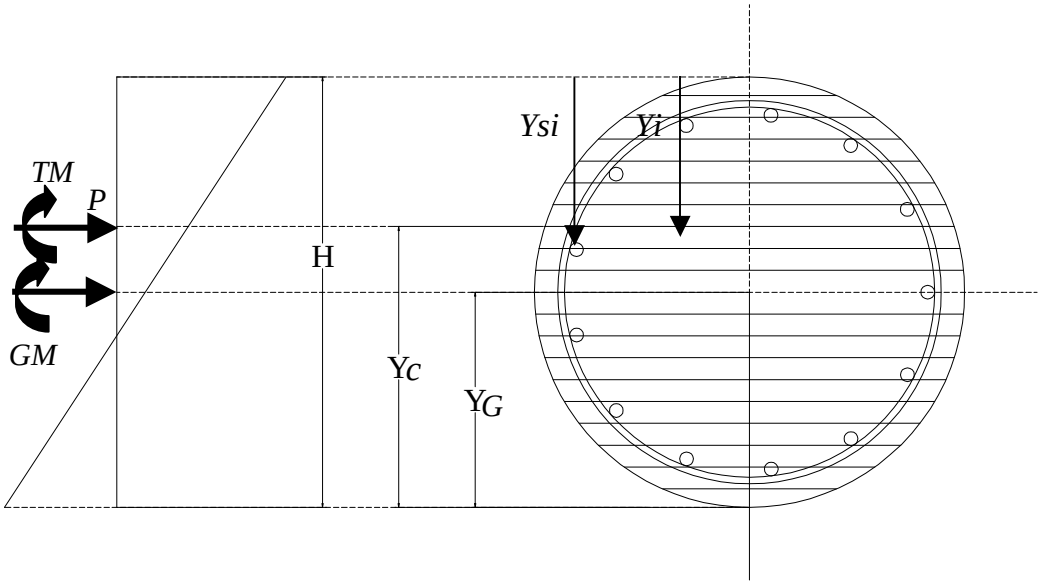

Figure 4-9 Idealized section, strain distribution and applied forces

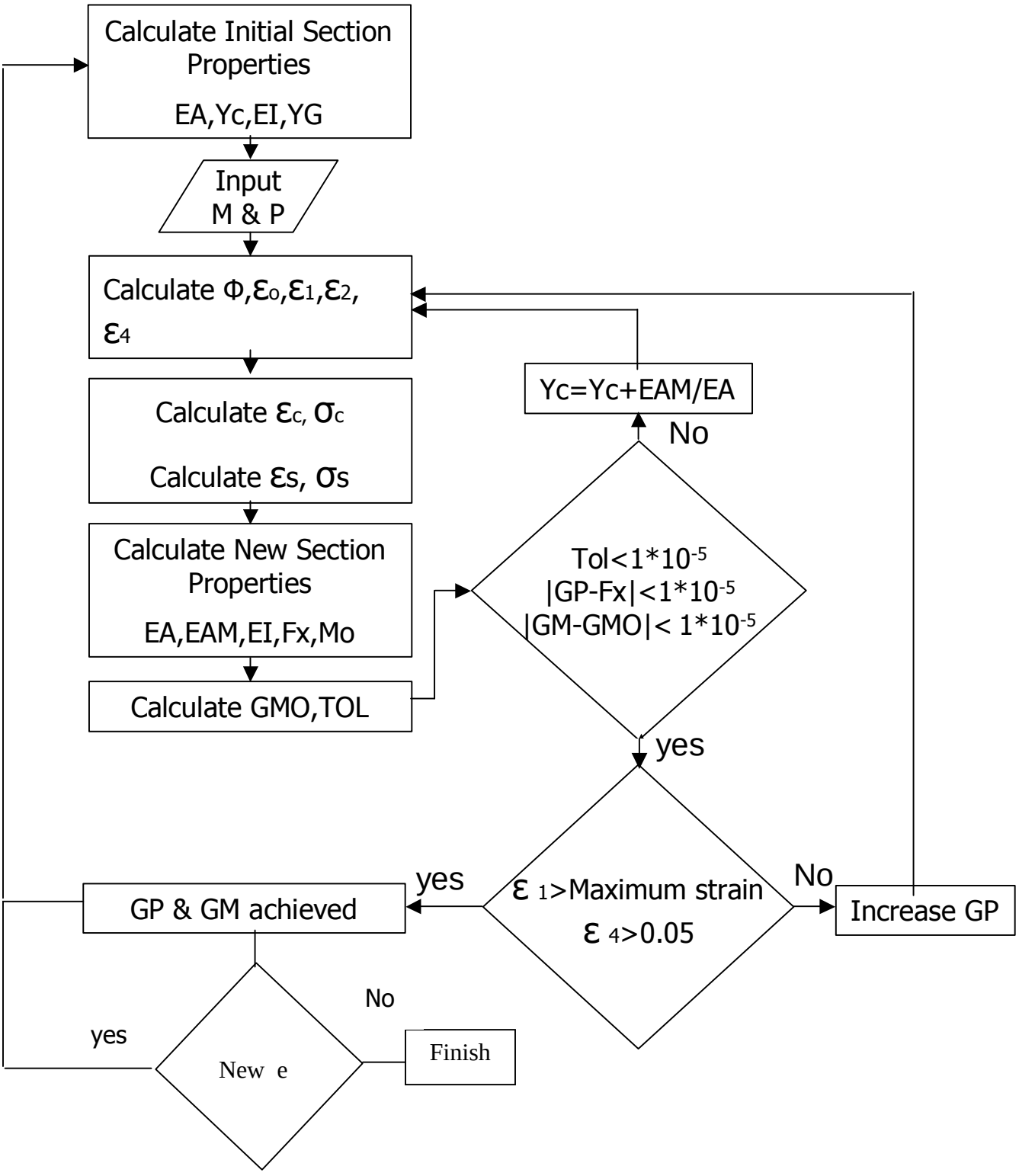

Figure 4-10 Confined concrete analysis flowchart

6- Finding:

Curvature ϕ

$$\phi = \frac{TM}{EI} \tag{4-18}$$

Strain at the inelastic centroid ε_o, the extreme compression fiber strain ε_1, the other extreme fiber ε_2, and at the extreme level of steel strain in tension ε_4:

$$\varepsilon_o = \frac{GP}{EA} \tag{4-19}$$

$$\varepsilon_1 = \varepsilon_o + \phi(H - Y_c) \tag{4-20}$$

$$\varepsilon_2 = \varepsilon_o - \phi Y_c \tag{4-21}$$

$$\varepsilon_4 = \varepsilon_o - \phi(Y_c - Cover) \tag{4-22}$$

7- Calculating strain ε_c and corresponding stress f_c in each layer of concrete section by using the eccentricity based model

$$\varepsilon_c = \varepsilon_1 - \phi Y_i$$

8- Calculating strain ε_s and corresponding stress in each bar in the given section by using the stress-strain relationship curves shown in Figure (4-8).

9- Calculating the new section properties EA, EI, moment of axial rigidity about inelastic centroid EAM, internal axial force F_x, internal bending moment about the inelastic centroid M_o:

$$EI = \sum_i E_{ci} B_i t (H - Y_c - Y_{ci})^2 + \sum_i (E_{si} - E_{ci}) A_{si} (H - Y_c - Y_{si})^2 \tag{4-23}$$

$$EAM = \sum_i E_{ci} B_i t (H - Y_c - Y_{ci}) + \sum_i (E_{si} - E_{ci}) A_{si} (H - Y_c - Y_{si}) \tag{4-24}$$

$$F_x = \sum f_{ci} B_i t + \sum (f_{si} - f_{ci}) A_{si} \tag{4-25}$$

$$M_o = \sum f_{ci} B_i t (H - Y_c - Y_i) + \sum (f_{si} - f_{ci}) A_{si} (H - Y_c - Y_{si}) \tag{4-26}$$

10- Transferring back the internal moment about the geometric centroid:

$$GM_o = M_o - GP(Y_G - Y_c) \tag{4-27}$$

11- Checking the convergence of the inelastic centroid :

$$TOL = EAM / EA / Y_c \tag{4-28}$$

12- Comparing the internal force to applied force, internal moment to applied moment, and the change of the new inelastic centroid to the previous location:

$$GP - F_x \le 1*10^{-5} \tag{4-29}$$

$$GM - GM_o \le 1*10^{-5} \tag{4-30}$$

$$Tol \le 1*10^{-5} \tag{4-31}$$

13- If equations (4-27), (4-28) and (4-29) are satisfied, equilibrium is attained.

Checking for the ultimate point by comparing the strain in the extreme compression fiber to the maximum strain as defined in equation (3-30), or comparing the strain at the level of steel at maximum tension to 0.05 as proven experimentally:

$$\varepsilon_1 \ge \max imum - strain \tag{4-32}$$

$$\varepsilon_4 \ge 0.05 \tag{4-33}$$

If equations (4-30) and (4-31) are satisfied, a point on the interaction diagram is found for the eccentricity value used in step 2. Otherwise increase GP by ΔGP as in step 3.

If equations (4-27), (4-28) and (4-29) are not satisfied:

$Y_c = Y_c + \dfrac{EAM}{EA}$ and go back to step 5

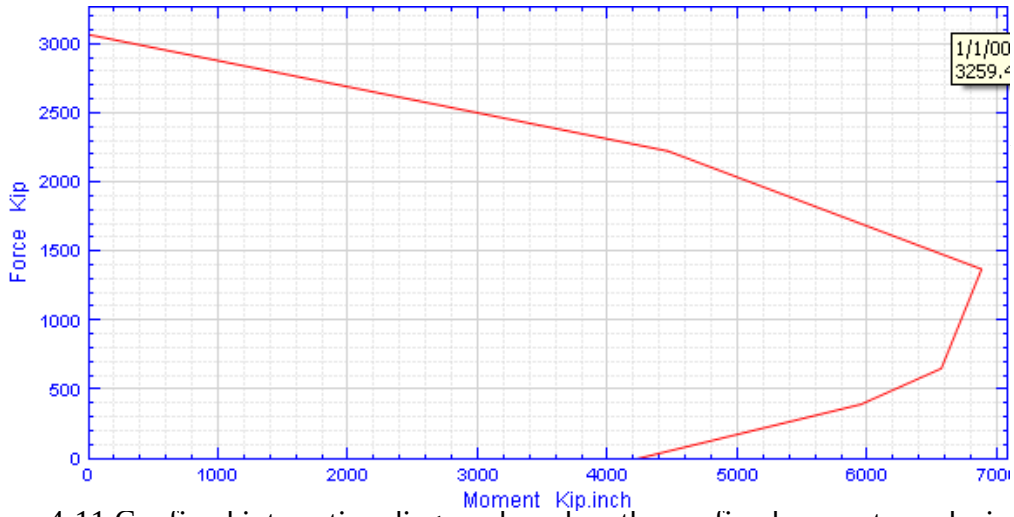

Figure 4-11 Confined interaction diagram based on the confined concrete analysis

CHAPTER 5 - Results and Discussions

The generated results are compared with experimental data. They are also compared with well-established software. They are further compared with Mander's concentric model. Discussions are also reported on comparisons between extreme confinement cases. The confinement analysis are is benchmarked against the extreme case of zero yield strength of spiral hoops. Finally, different behavior parameters are generated and studied.

5-1 Comparison with experimental results

This section compares the results obtained from using the present analysis and some experimental data gathered from five papers. Twelve cases are examined and discussed. The interaction diagram is generated in four different ways for the sake of comparison:

1- Cover removal when the strain exceeds the unconfined peak strain 0.003, without accounting for strain hardening (Reduced area curve)
2- No cover removal with no strain hardening considered. (Full area curve)
3- Cover removal when the strain exceeds the unconfined peak strain 0.003, with strain hardening considered
4- No cover removal with strain hardening

Strain hardening is modeled by assuming the hardening modulus to be 5% of the elastic modulus. Figure (5-1) illustrates the Geometric form for the cross section and the input data required for each case

.

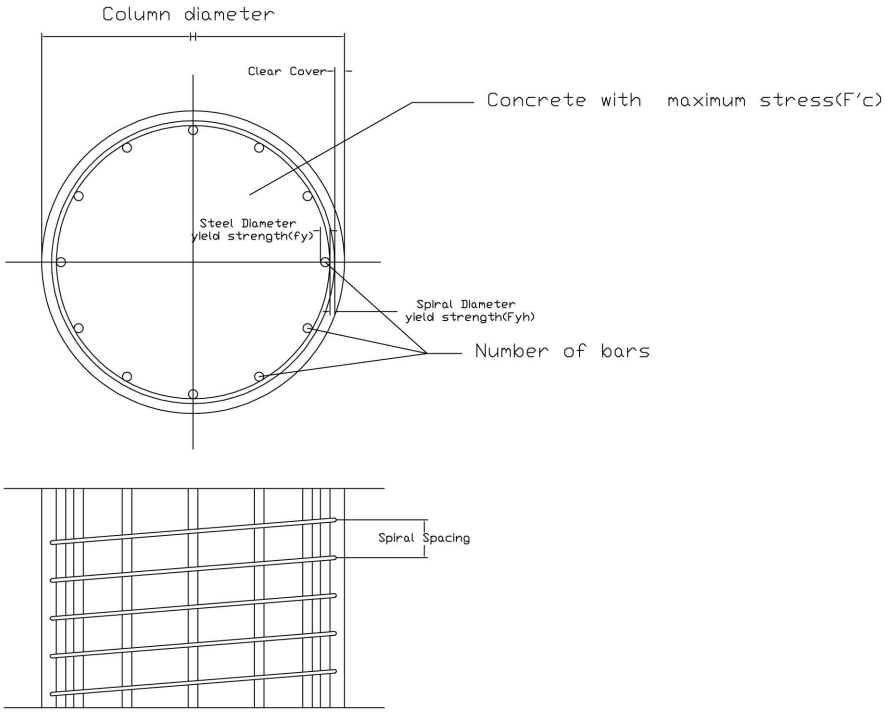

Figure 5-1 Cross section and sectional elevation for reinforced concrete column

Case 1:

This is the first octagonal column with spiral reinforcement tested by Fafitis and Shah 1985. The column has the following properties:

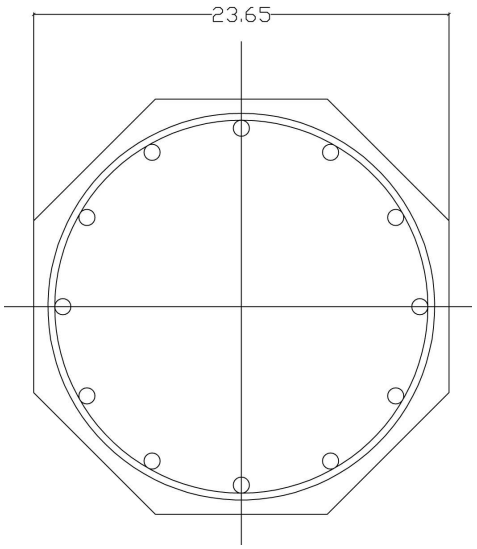

Column Diameter (H) : 23.65 in

Clear Cover : 0.8 in

Longitudinal Reinforcement: 16#8

f'_c : 4.118 ksi

f_y : 43.5 ksi

f_{yh} : 43.5 ksi

Transverse Reinforcement

Spiral Diameter : 0.394 in

Spiral Spacing : 2.95 in

Figure 5-2: Cross section for the column used in case 1

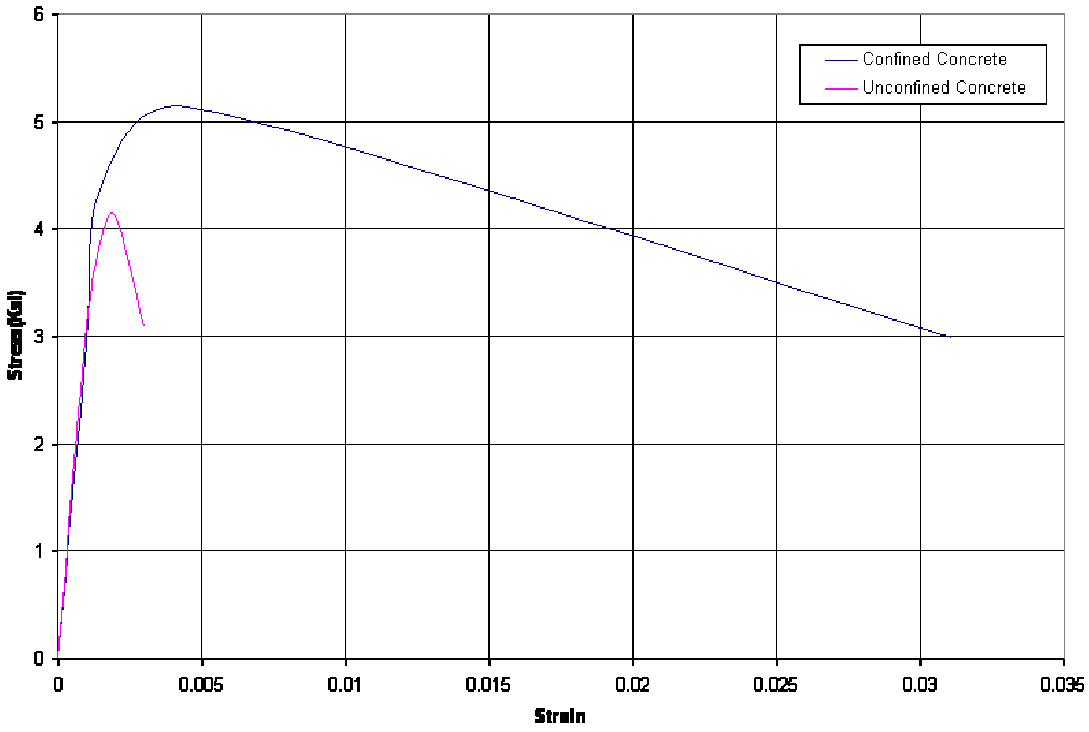

Figure 5-3 Stress strain curves for case 1 column

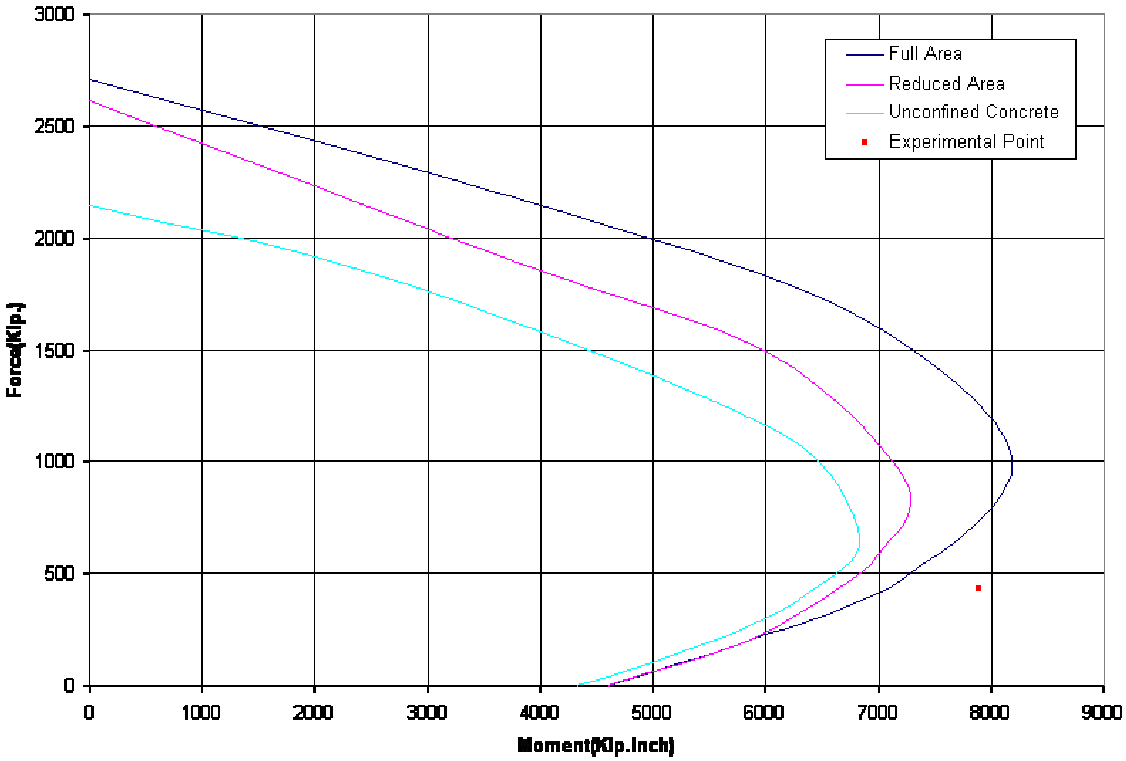

Figure 5-4: Interaction diagrams for case 1 colum(without strain hardening)

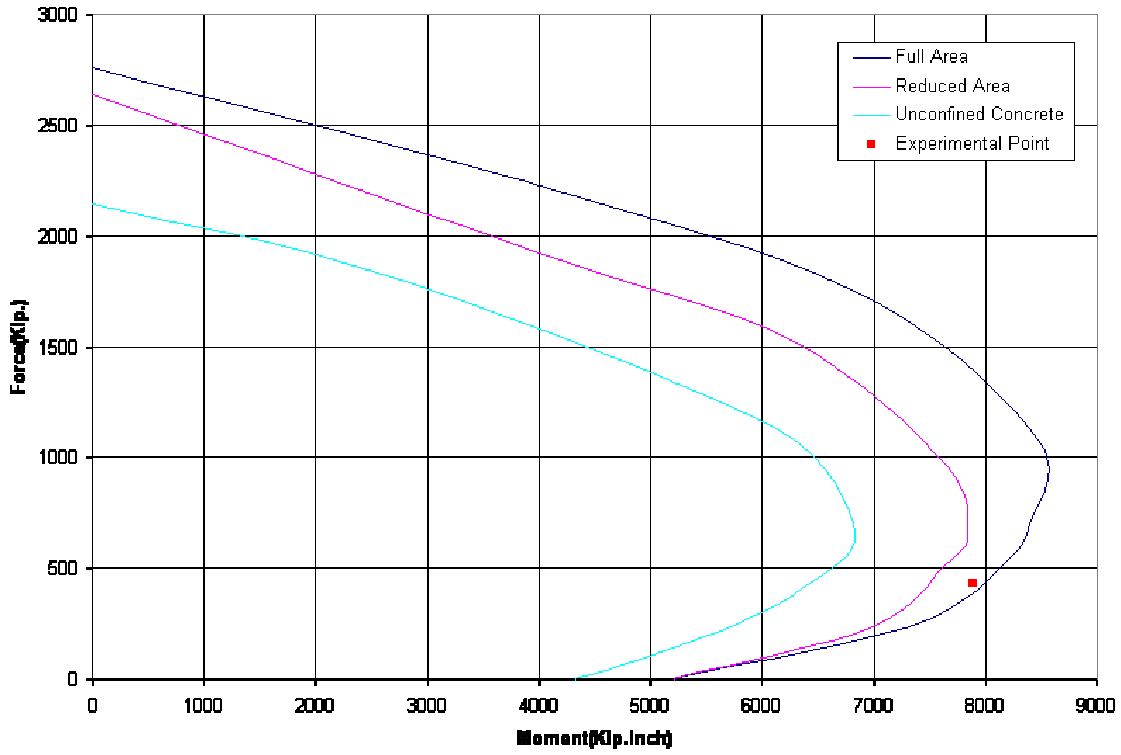

Figure 5-5: Interaction diagrams for case 1 column(with 5% strain hardening)

Figure (5-3) shows that all three curves are conservative compared to the experimental tension-controlled data point. The full area curve is just accurate even though it is slightly less conservative than the more realistic reduced area curve. Figure (5-4) shows the reduced area curve to be in excellent correlation with the experimental point, while the full area curve becomes non conservative although it is closer to that experimental point once strain hardening of the steel is accounted for.

Case 2:

This is the second octagonal column with spiral reinforcement tested by Fafitis and. Shah (1985). This case has the same parameters as case 1 except smaller spiral spacing and slightly lower concrete strength. The column has the following parameters:

Column Diameter (H) : 23.65 in

Clear Cover : 0.8 in

Longitudinal Reinforcement: 16#8

f'_c : 3.857 ksi

f_y : 43.5 ksi

f_{yh} : 43.5 ksi

Transverse Reinforcement

Spiral Diameter : 0.394 in

Spiral Spacing : 1.97 in

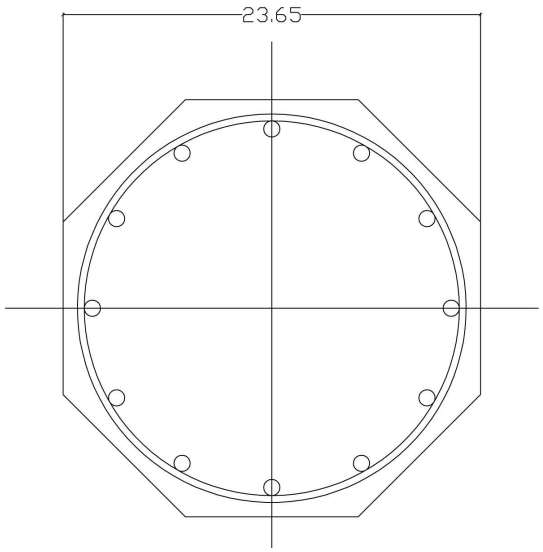

Figure 5-6 : Cross section for the column used in Case 2

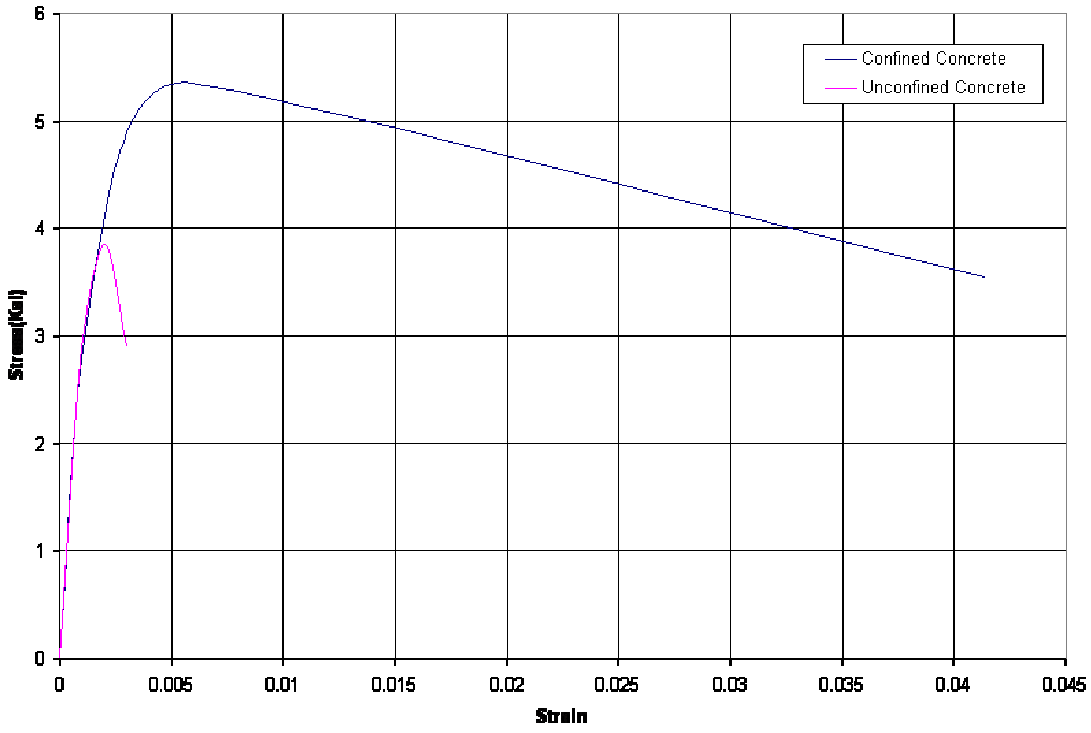

Figure 5-7 Stress strain curves for case 2 column

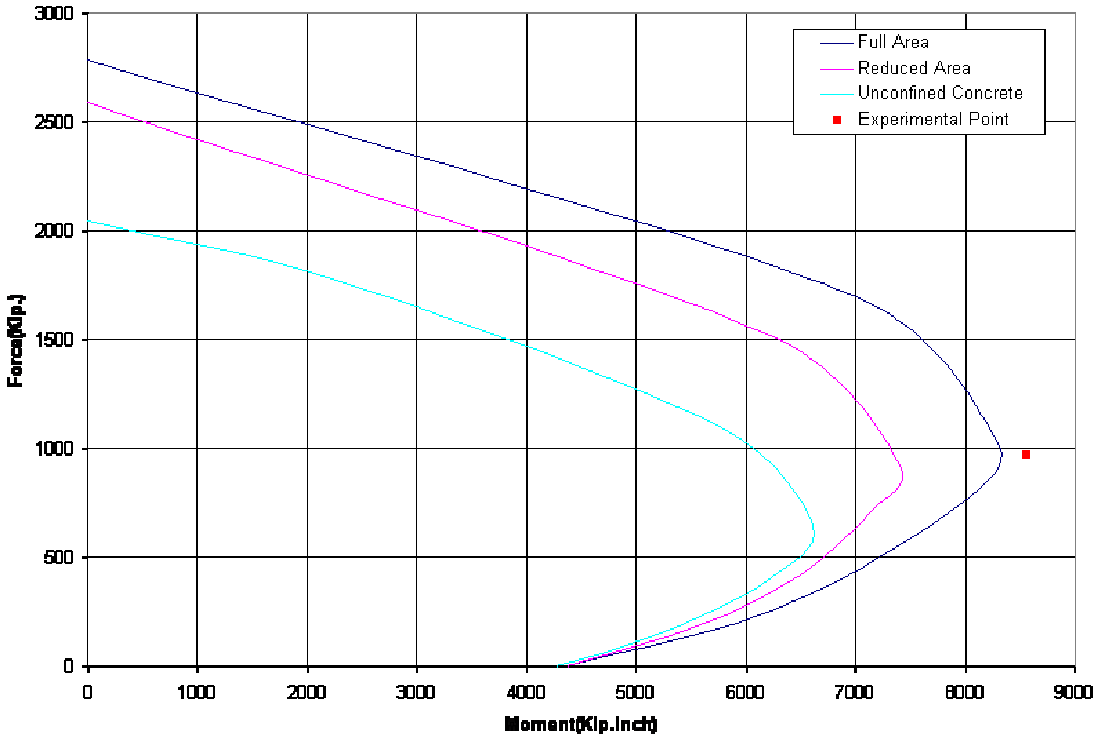

Figure 5-8 : Interaction diagrams for case 2 column (without strain hardening)

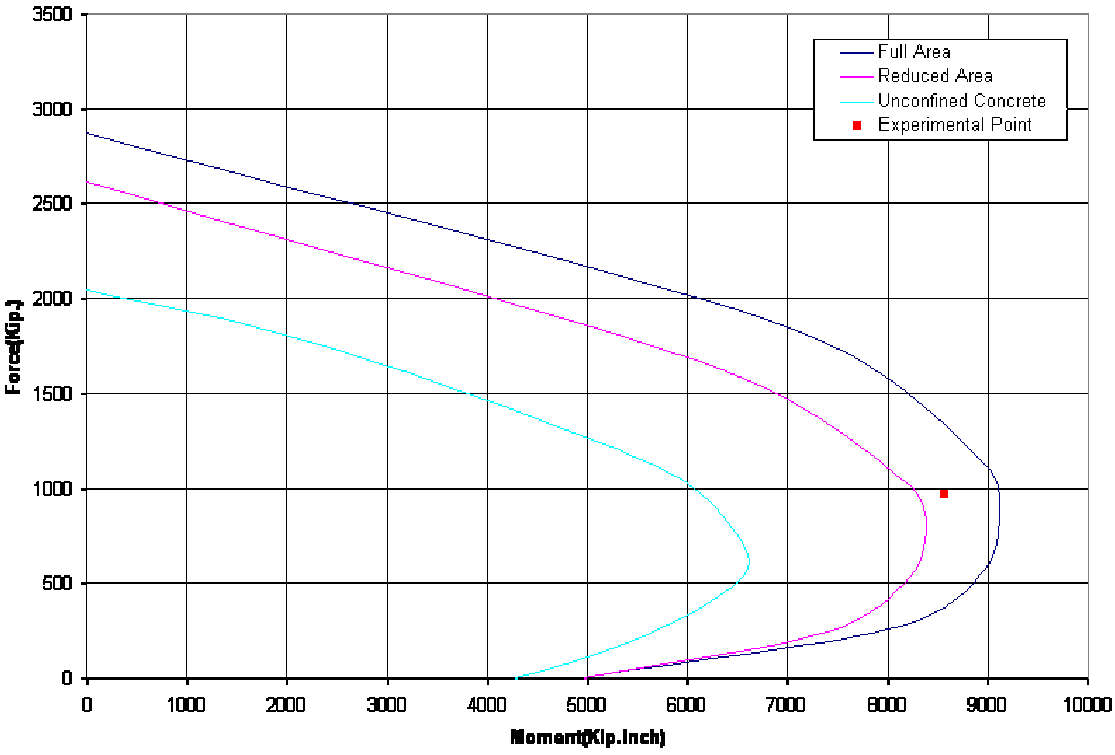

Figure 5-9 : Interaction diagrams for case 2 column (with 5% strain hardening)

Similar to case 1, all the three curves in Figure (5-8) are conservative compared to the experimental point. The full area curve has an excellent correlation to the experimental result at the balanced point although it is appreciably less conservative than the reduced area curve. When the 5% strain hardening is considered the cover removal(reduced area curve) correlates extremely well to the experimental point, as shown in Figure (5-8). It is also evident that the confinement improvement over the unconfined curve is noticeably more in case 2 (Figure 5-9) than case 1 (Figure 5-5) due to the smaller spiral spacing.

Case 3:

This is the third octagonal column with spiral reinforcement tested by Fafitis and Shah (1985). This case has the very same parameters as case 1 except slightly smaller spiral spacing and significantly higher spiral yield strength. The column has the following properties:

Column Diameter (H) : 23.65 in
Clear Cover : 0.8 in
Longitudinal Reinforcement: 16#8
f'_c : 3.857 ksi
f_y : 43.5 ksi
f_{yh} : 61.3 ksi
Transverse Reinforcement
Spiral Diameter : 0.394 in
Spiral Spacing : 2.76 in

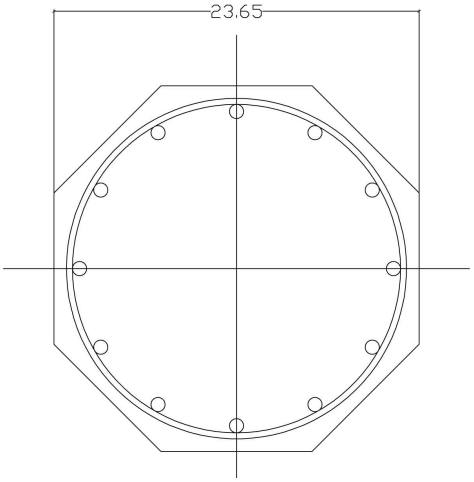

Figure 5-10 Cross section for the column used in Case 3

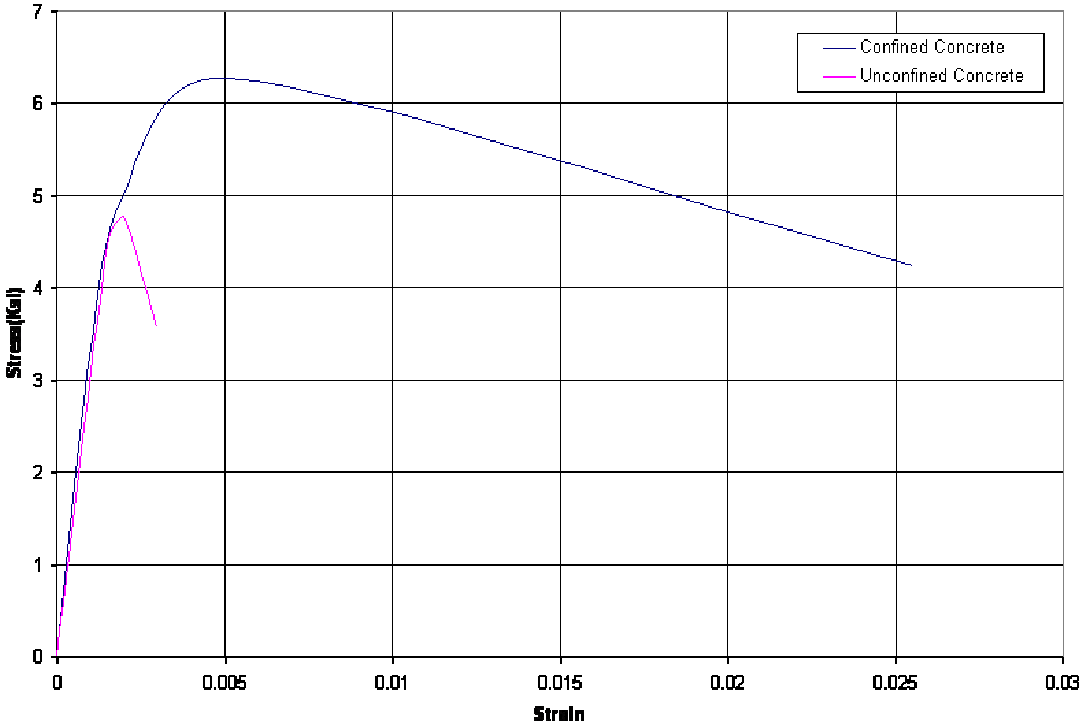

Figure 5-11 Stress strain curves for case 3 column

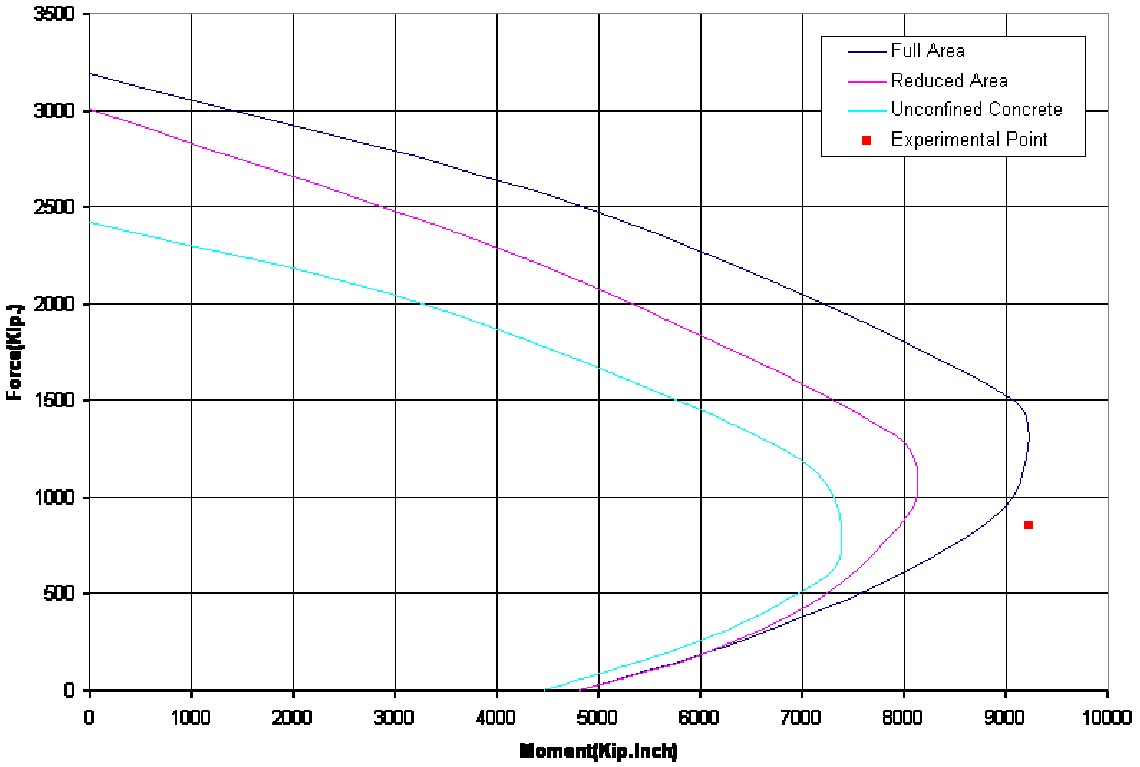

Figure 5-12: Interaction diagram for case 3 column(without strain hardening)

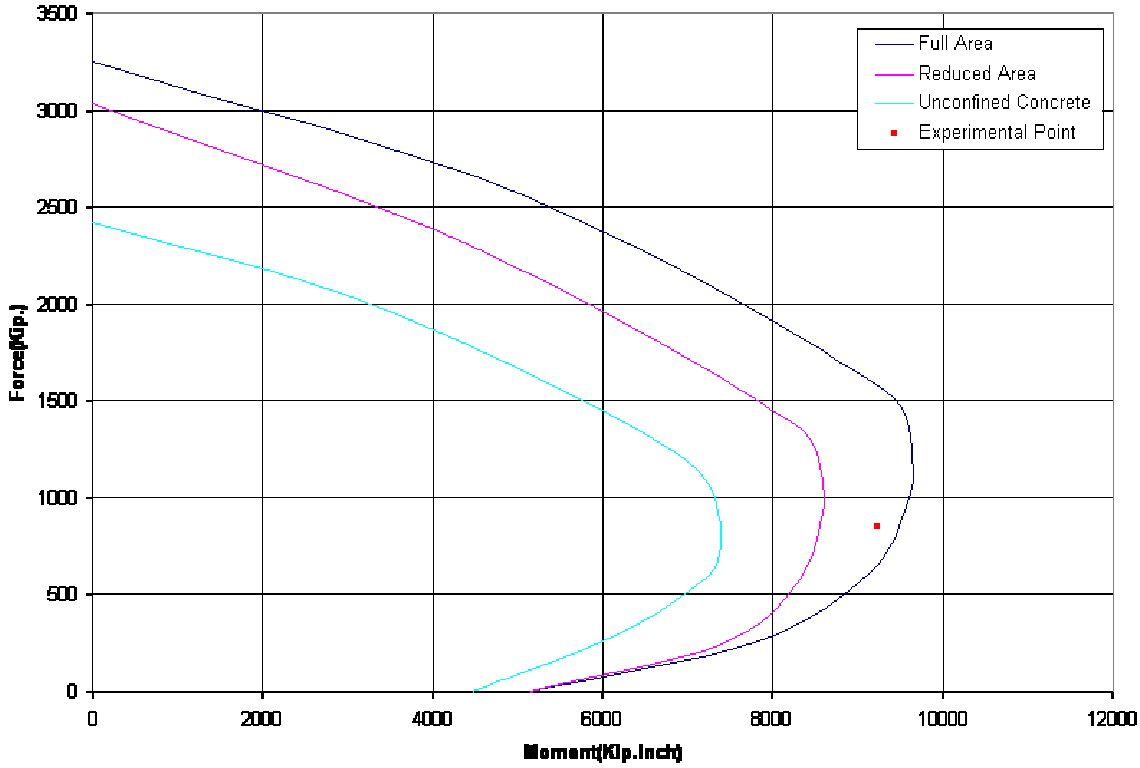

Figure 5-13: Interaction diagram for case 3 column (with 5% strain hardening)

In this case, the full area curve is very close to the experimental tension-controlled data point while the full area curve is considerably farther away from the reduced area curve Figure (5-13). However, the reduced area curve becomes accurate enough and conservative compared to the experimental point and the gap between the two confined curves reduces.

Case 4:

This is the fourth octagonal column with spiral reinforcement tested by Fafitis and Shah (1985). This case is similar to case 1 except for a slightly higher concrete strength and slightly lower yield strength of spiral. The diameter of the spiral is around 3 times higher and the spiral spacing is lower. So the confinement effect is expected to be much higher than case 1. The column has the following properties:

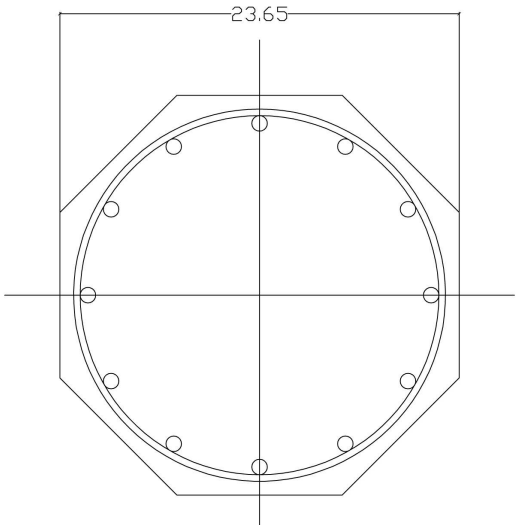

Column Diameter (H) : 23.65 in

Clear Cover : 0.8 in

Longitudinal Reinforcement: 16#8

f'_c : 4.71 ksi

f_y : 43.5 ksi

f_{yh} : 40.6 ksi

Transverse Reinforcement

Spiral Diameter : 0.63 in

Spiral Spacing : 2.17 in

Figure 5-14 : Cross section for the column used in Case 3

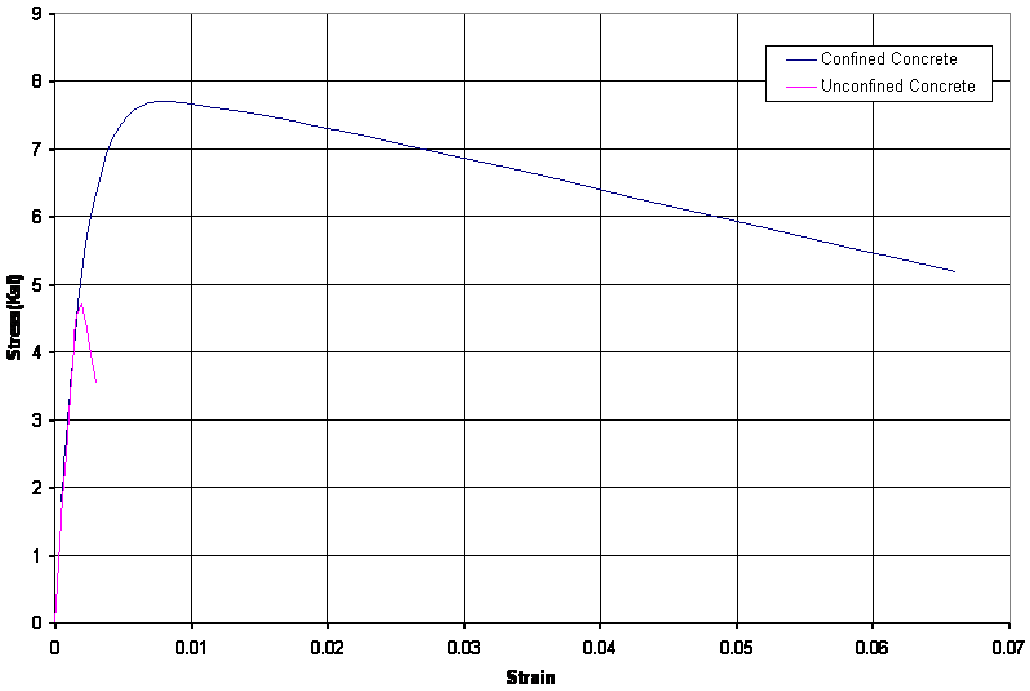

Figure 5-15 Stress strain curves for case 4 column

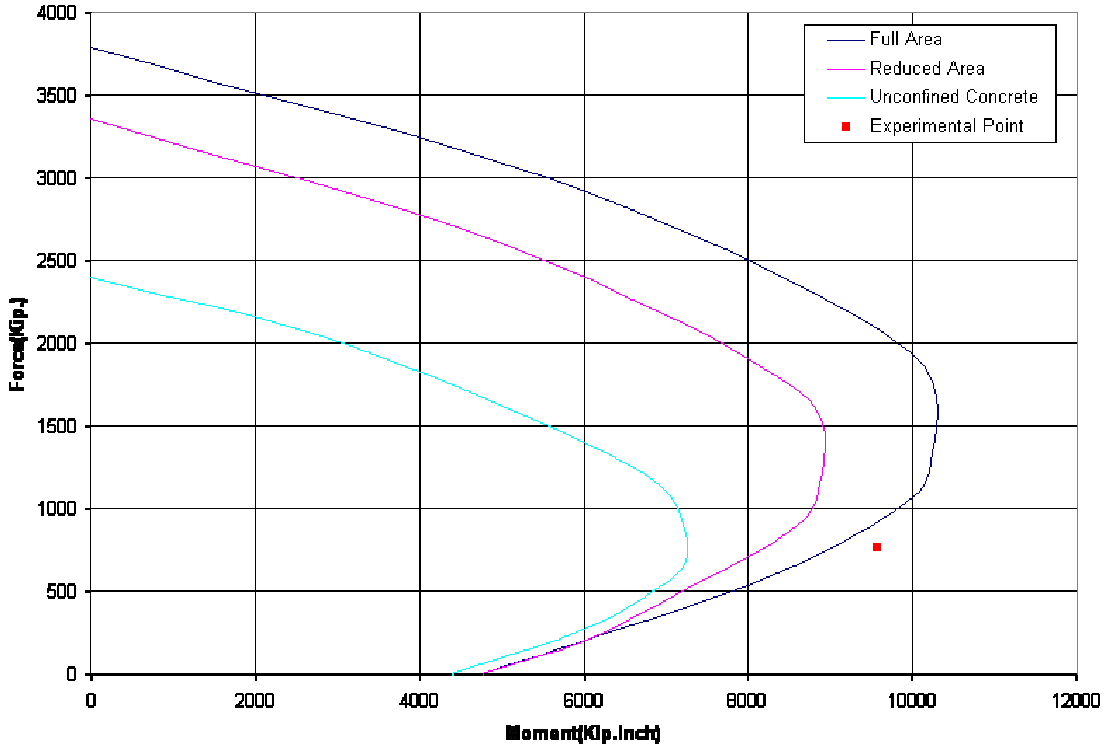

Figure 5-16: Interaction diagram for case 4 column (without strain hardening)

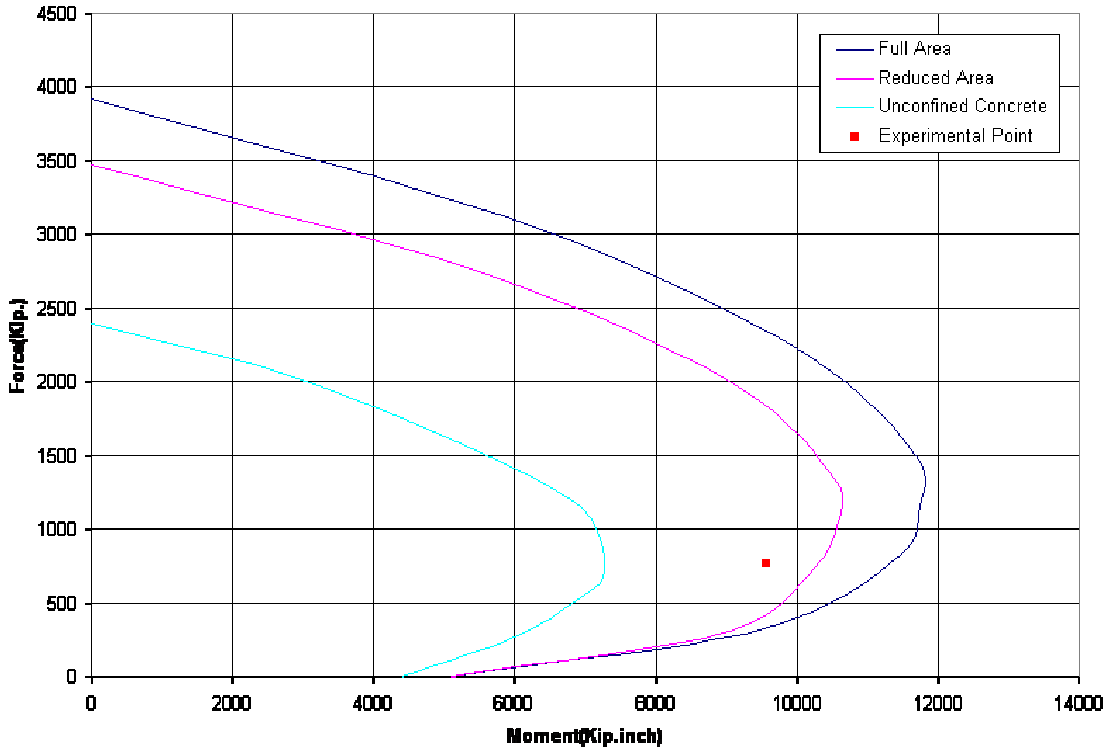

Figure 5-17: Interaction diagram for case 4 (with 5% strain hardening)

The effect of confinement is clearly reflected in Figure (5-16) and Figure (5-17). The gap between the unconfined and confined curves is the largest among the four cases analyzed.The full area and reduced area curves compare well to the experimental point as shown in Figure (5-16), on the other hand, by using 5% strain hardenenig both curves become nonconservative compared with the experimental point. The fyh in this case is the lowest 40.6 ksi so the hardening modulus is expected to be far less than 5% of the elastic modulus (mild steel).

Case 5:

This is one of the concentric columns tested by J. B. Mander, M. J. Priestley, and R. Park. The full scale column has a relatively large spacing of spiral. Accordingly, the confinement has a limited effect on the interaction diagram; Figure (5-20). The column has the following properties:

Column Diameter (H) : 19.68 in
Clear Cover : 0.98 in
Longitudinal Reinforcement: 12#5
f'_c : 4.06 ksi
f_y : 42.78 ksi
f_{yh} : 46.4 ksi
Transverse Reinforcement
Spiral Diameter : 0.393 in
Spiral Spacing : 4.68 in

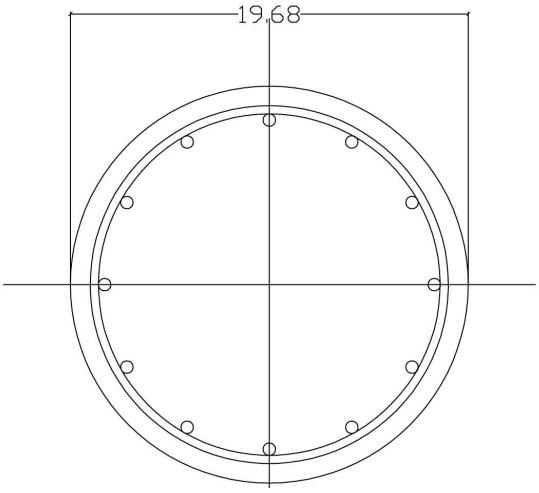

Figure 5-18: Cross section for the column used in Case 5

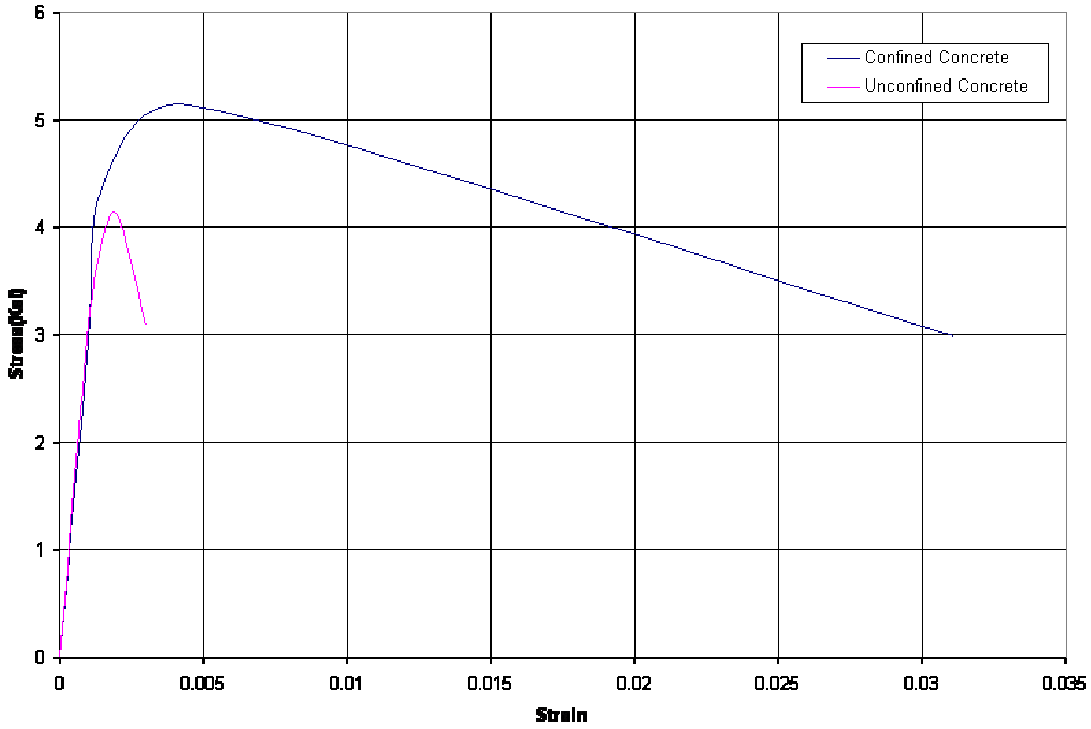

Figure 5-19 Stress strain curves for case 5 column

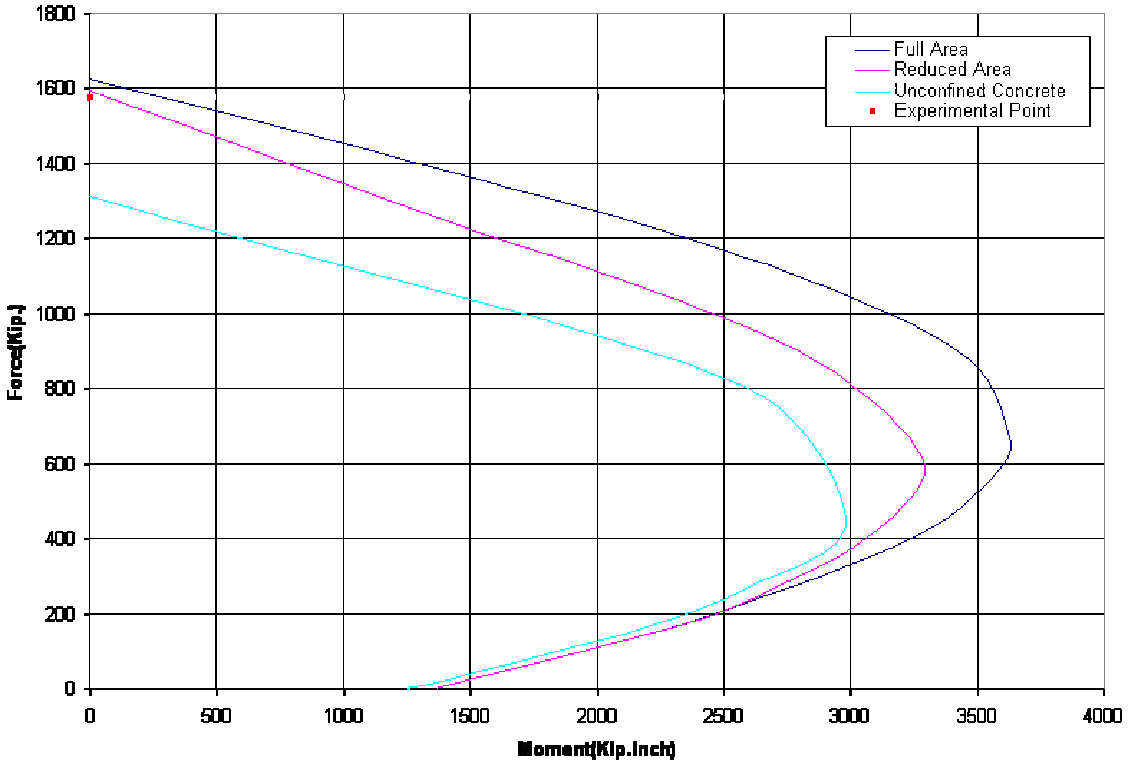

Figure 5-20: Interaction diagrams for case 5 column (without strain hardening)

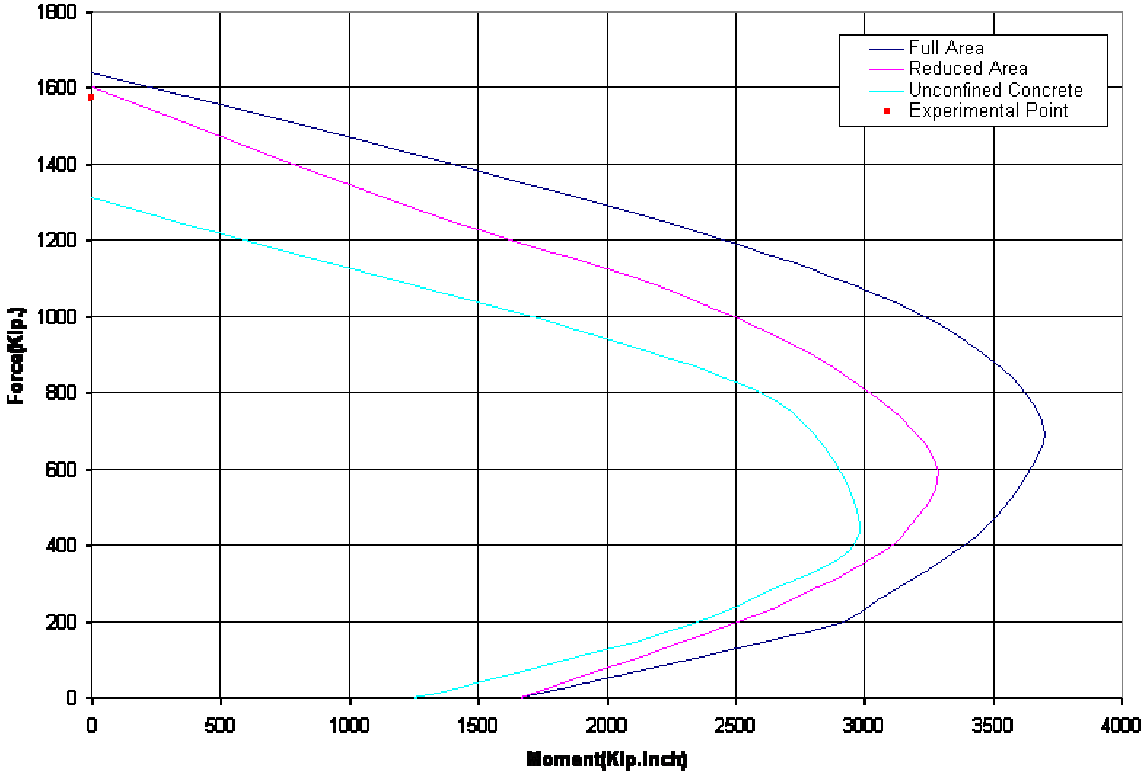

Figure 5-21: Interaction diagram for case 5 column(with 5% strain hardening)

Case 5 represents a point in the pure axial compression. The reduced area curve shown in Figure (5-20) and (5-121) compare well with the experimental point with and without strain hardening. This is attributed to the fact that once the cover spalls off at 0.003 train, the section reaches its ultimate capacity with limited contribution from strain hardening at such a low strain (.003). The full area curve is also reasonably close to the experimental data point at concentric compression.

Case6:

This is another one of the concentric columns tested by: J. B. Mander, M. J. Priestley, and R. Park. The full scale column has smaller spiral spacing. Accordingly, the confinement has a significant effect on the interaction diagram; Figure (5-24). The column has the following properties:

Column Diameter (H) : 19.68 in
Clear Cover : 0.98 in
Longitudinal Reinforcement: 12#5
f'_c : 4.06 ksi
f_y : 42.9 ksi
f_{yh} : 49.3 ksi
Transverse Reinforcement
Spiral Diameter : 0.472 in
Spiral Spacing : 2.04 in

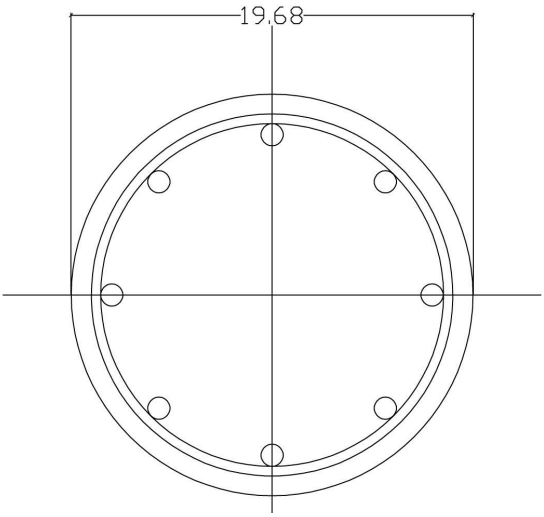

Figure 5-22 : Cross section for the column used in Case 6

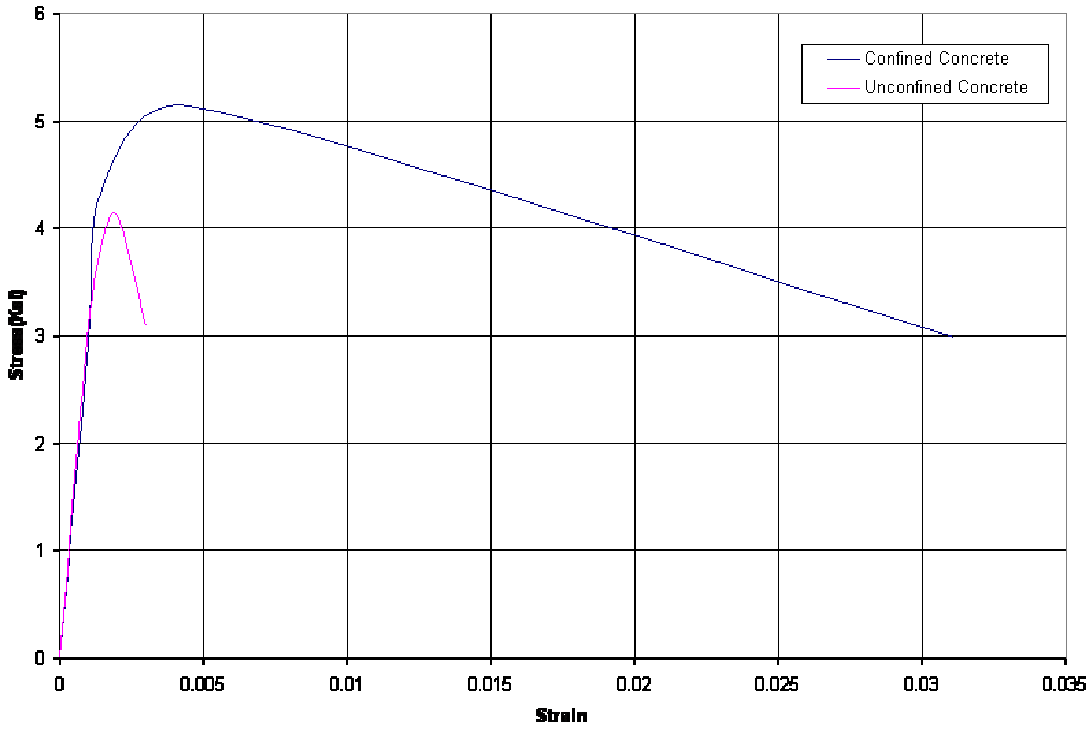

Figure 5-23 Stress strain curves for case 6 column

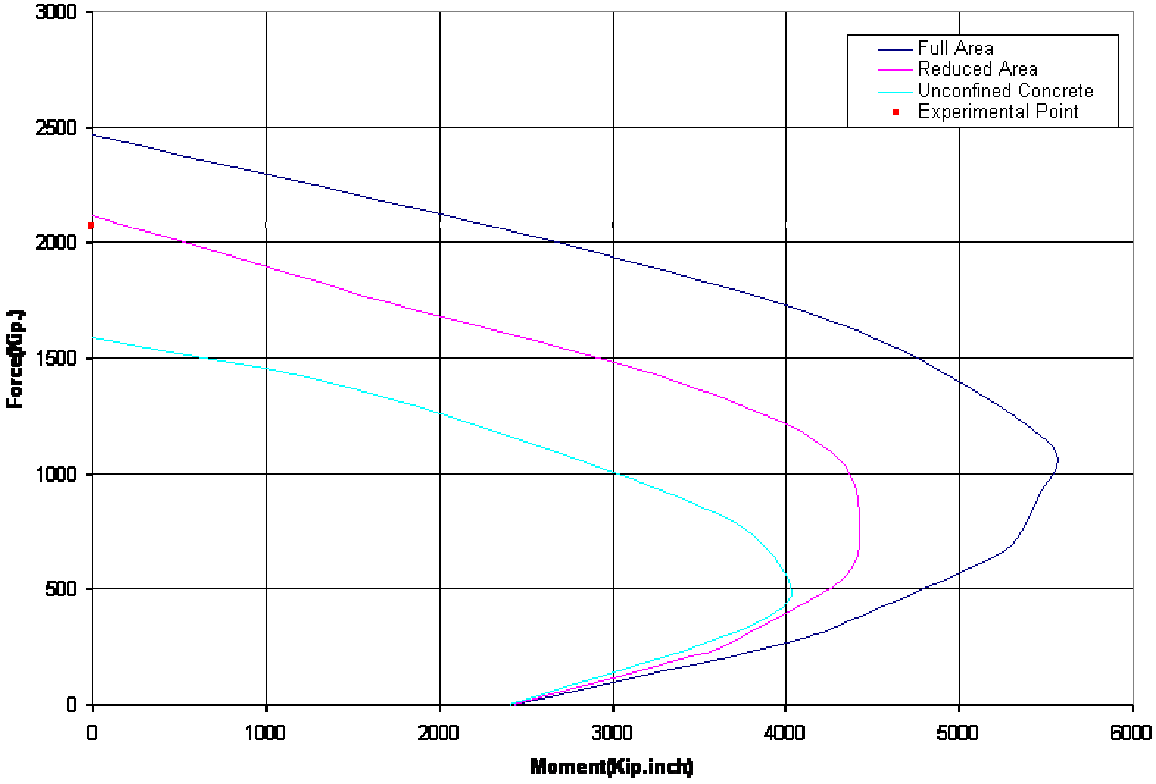

Figure 5-24: Interaction diagrams for case 6 column (without strain hardening)

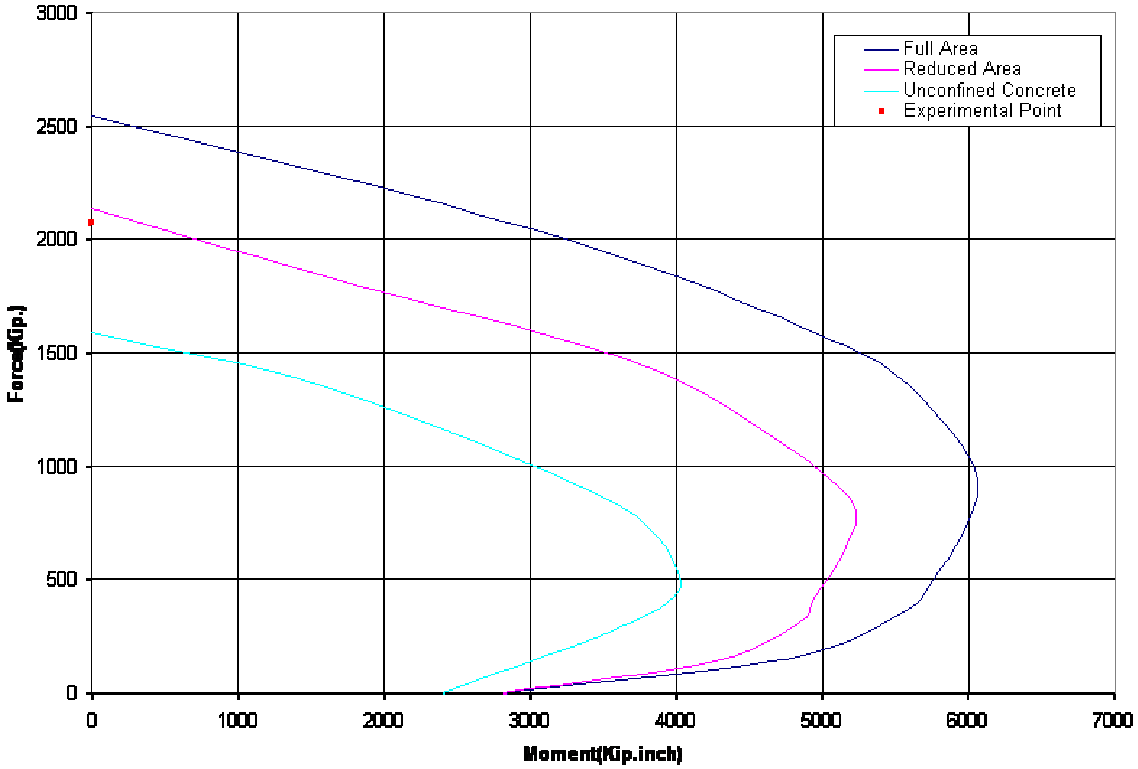

Figure 5-25: Interaction diagrams for case 6 column(with 5% strain hardening)

Similar to the previous case, case 6 show that the curves developed with cover removal consideration correlate very well to the experimental point with and without considering strain hardening, Figure (5-24) and Figure (5-25). On the other hand, the full area curve significantly overestimates the axial compression capacity indicating the importance of accounting for cover spalling in compression-controlled columns.

Case 7:

This small scale column was tested byResource: Dodd and Cooke 2000. It has a small spiral diameter and tight spacing of spiral. The column has the following properties:

Column Diameter (H) : 7.87 in

Clear Cover : 0.43 in

Longitudinal Reinforcement: 18#0.236 in

f'_c : 5.07 ksi

f_y : 65.2 ksi

f_{yh} : 36.25 ksi

Transverse Reinforcement

Spiral Diameter : 0.157 in

Spiral Spacing : 1.1 in

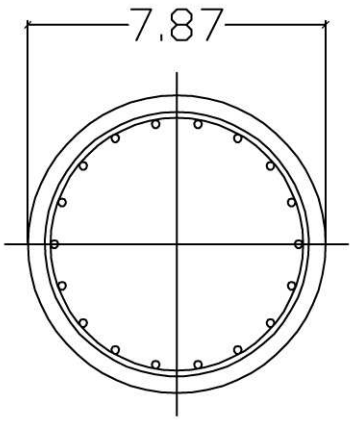

Figure 5-26: Cross section for the column used in Case 7

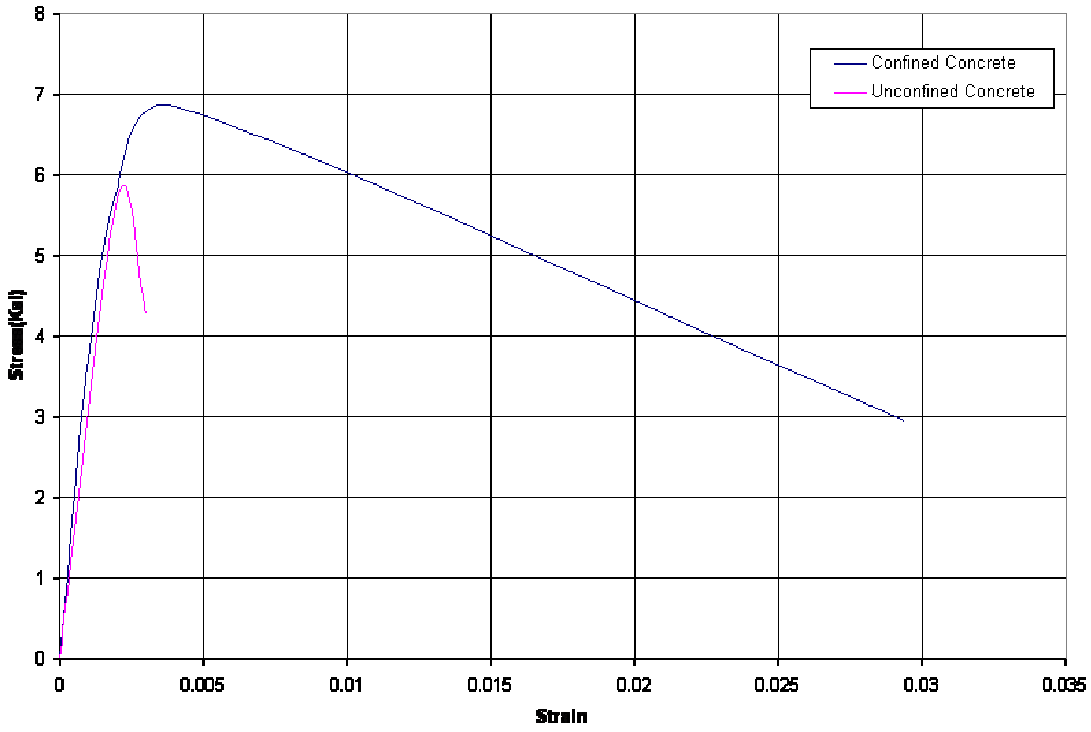

Figure 5-27 Stress strain curves for case 6 column

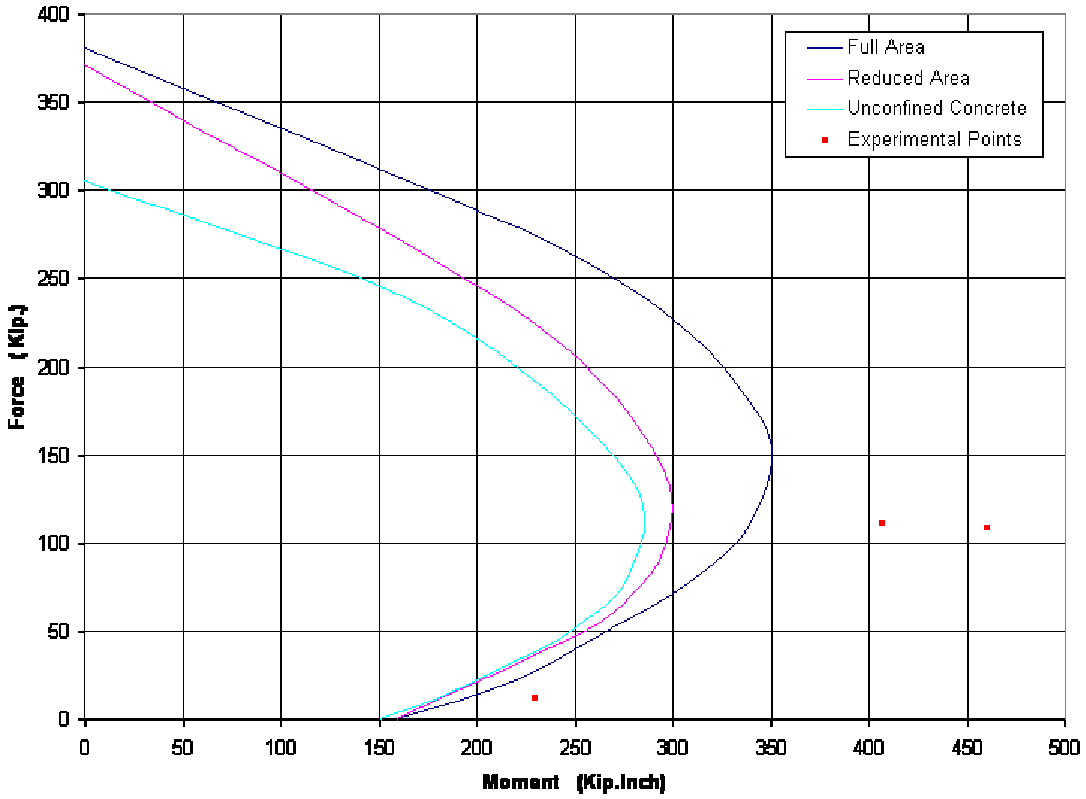

Figure 5-28: Interaction diagrams for case 7 column(without strain hardening)

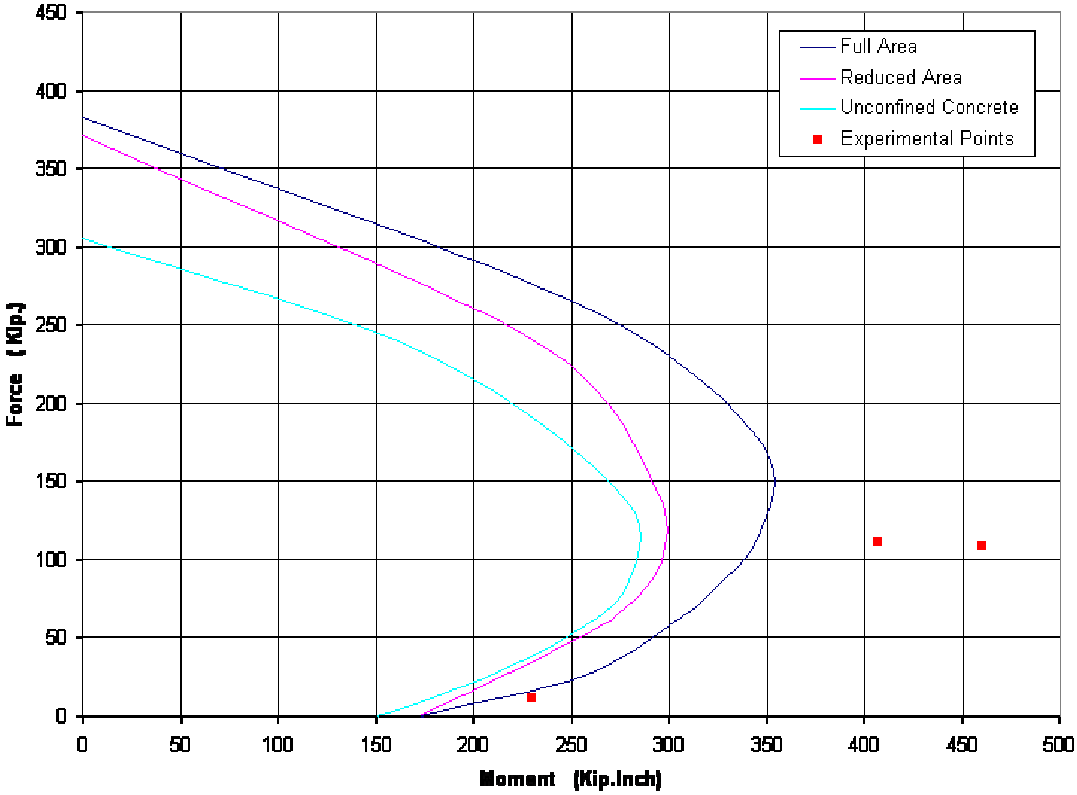

Figure 5-29: Interaction diagram for case 7 column (with 5% strain hardening)

It is evident from Figure (5-28) that Mander model under estimates the confinement of the small diameter spiral, Nevertheless, this seems to be an acceptable conservative result when comparing the scatter of the two tension controlled points. It is also evident that the pure bending point is in excellent agreement with the confinement interaction diagam.The three experimental points are within the bending zone. In case of strain hardening included, the lower point compare very well with the full area curve as shown in Figure (5-22). While the two curves are still conservative in comparisson with the upper tension controlled two points.

Case 8:

This full scale column was tested by Esmaily and Xiao (2004). The diameter of the spiral is #2 which is realistic. The spiral spacing is tight inviting a significant amount of confinement. The column has the following properties:

Column Diameter (H) : 16 in
Clear Cover : 0.512 in
Longitudinal Reinforcement: 12#4 in
f'_c : 7.29 ksi
f_y : 71 ksi
f_{yh} : 68 ksi
Transverse Reinforcement
Spiral Diameter : 0.25 in
Spiral Spacing : 1.26 in

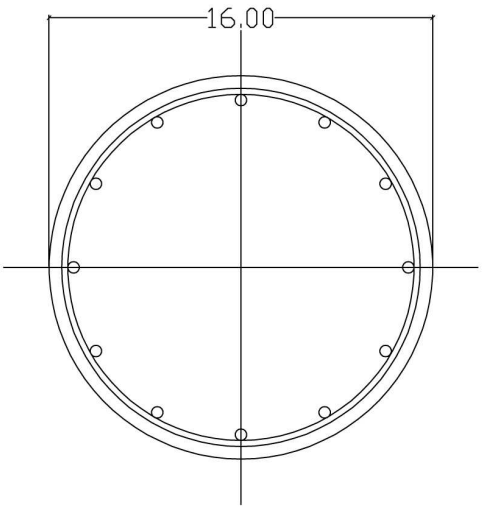

Figure 5-30: Cross section for the column used in Case 8

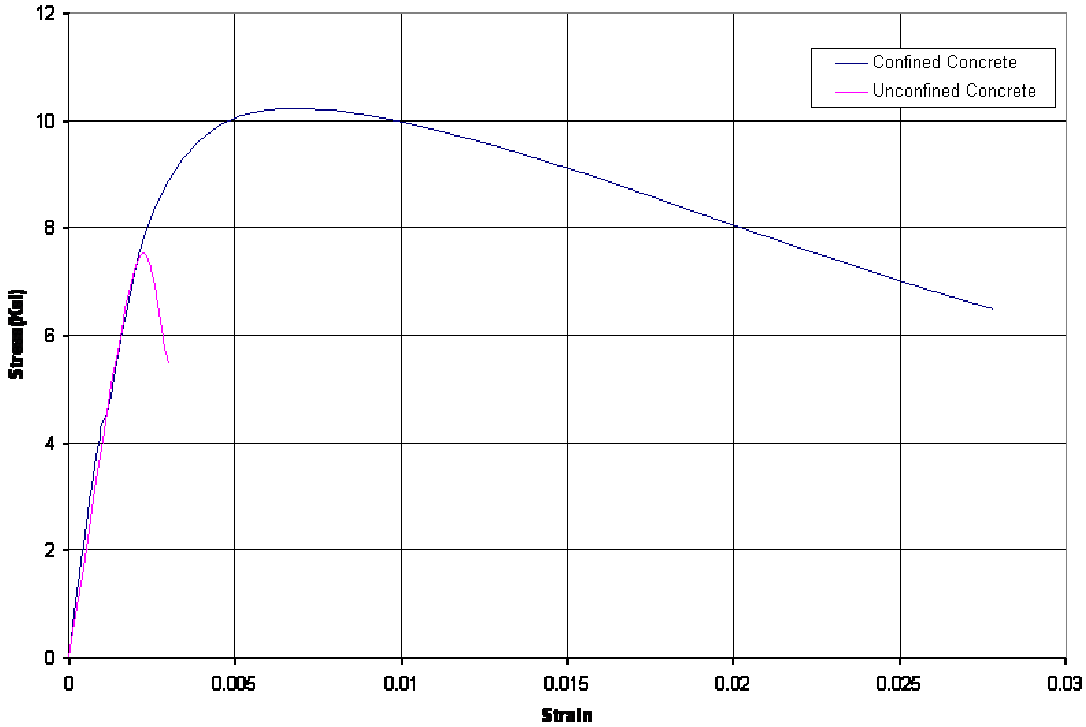

Figure 5-31 Stress strain curves for case 8 column

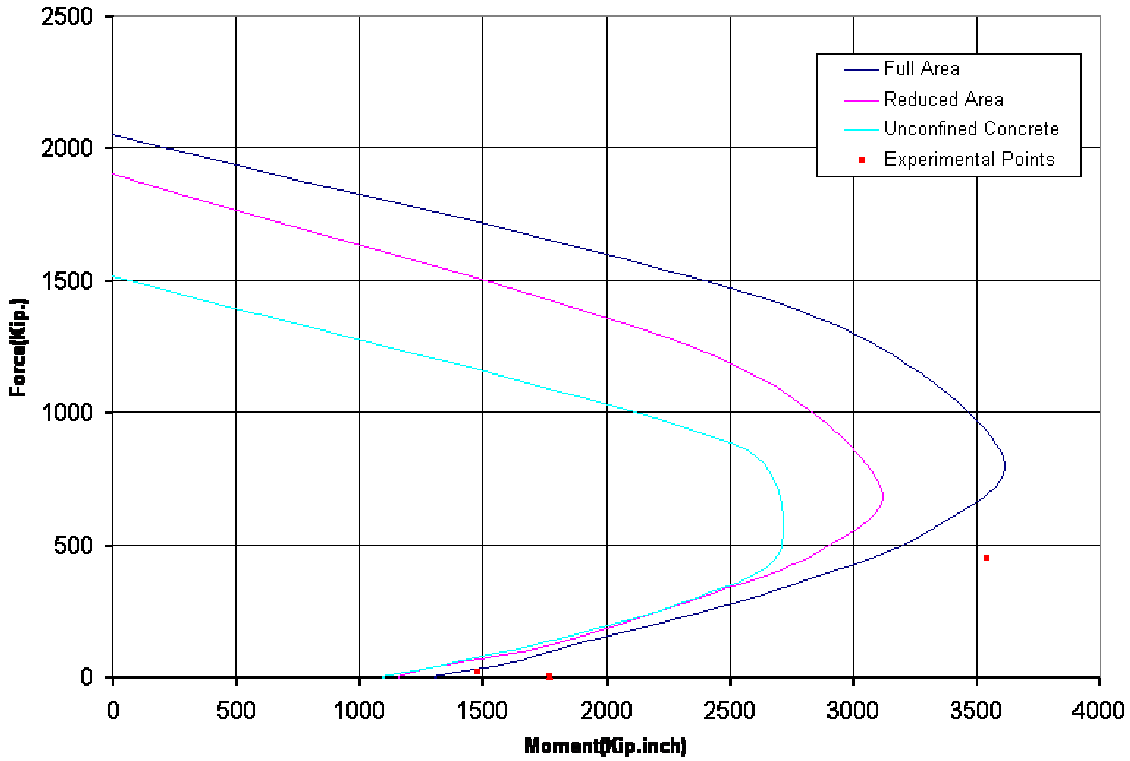

Figure 5-32: Interaction diagrams for case 8 column(without strain hardening)

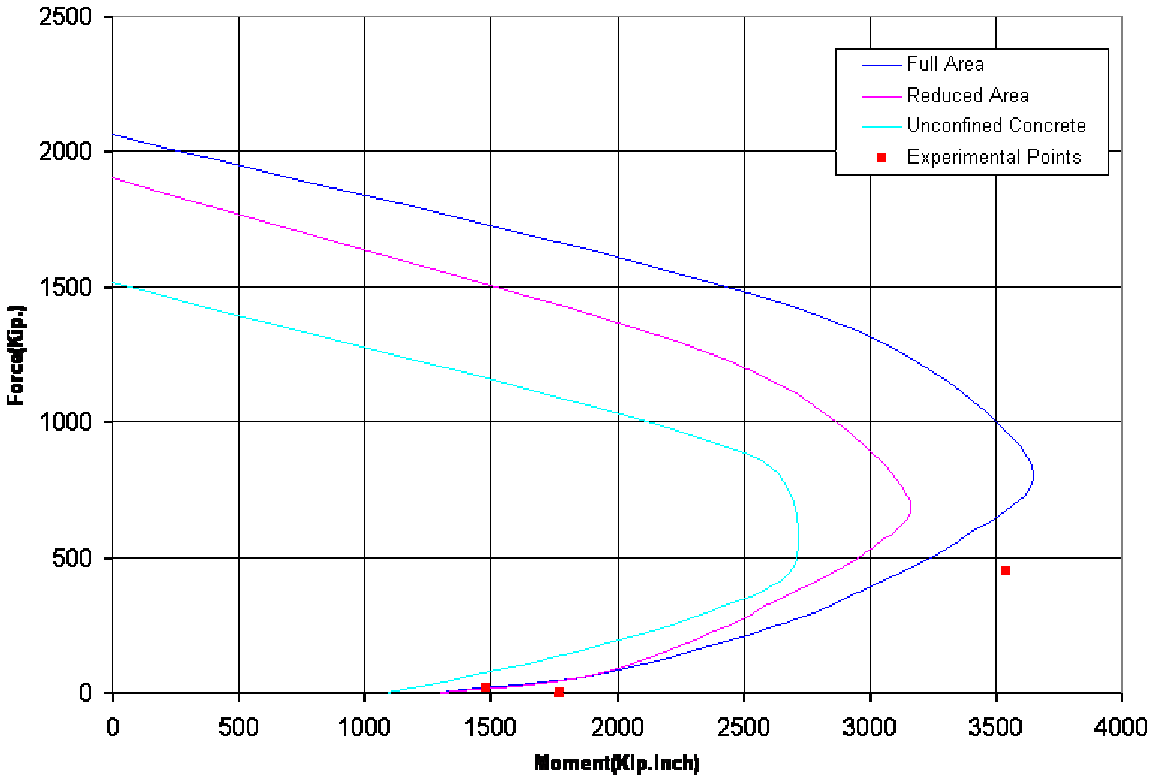

Figure 5-33: Interaction diagram for case 8 column(with 5% strain hardening)

It can be seen from Figure (5-32) that the contribution of confinement is very limited near the pure bending case where two experimental points compare well with the ful area curve. The fullarea curve compare very well with the third experimental point and is on the conservative side.Accordingly, all of the experimental points correlate well to the full area curve in Figure (5-33), When the strain hardening is implemented, all the three points become closer to the full area curve, and the two lower pure bending points match very well the reduced area curve as well.

Case 9:

A series of full scale columns is tested by the University of Illinois, Engineering Experiment Station in 1930. The column has the following parameters:

Column Specifications:

Column Diameter (H) : 12 in

Clear Cover : 1 in

Longitudinal Reinforcement: 8#7

f'_c : 5.15 ksi

f_y : 43.5 ksi

f_{yh} : 32 ksi

Transverse Reinforcement

Spiral Diameter : 0.283 in

Spiral Spacing : 1.5 in

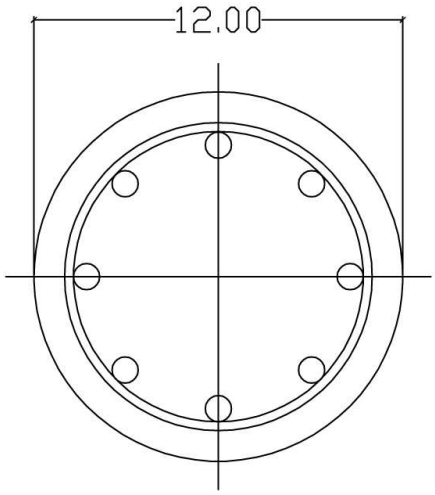

Figure 5-34 : Cross section for the column used in Case 9

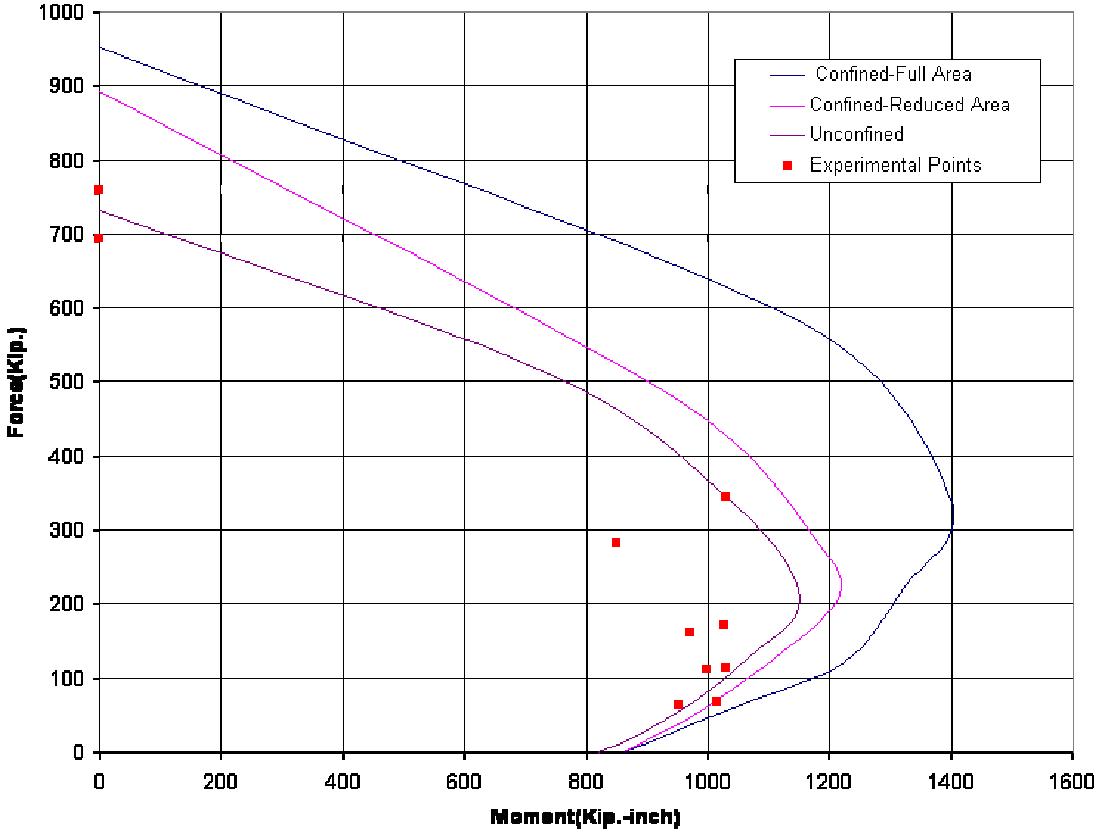

Figure 5-35: Interaction diagrams for case 9 column(without strain hardening)

The transverse reinforcement has a realistic spiral diameter between #2 and #3 sizes with tight spiral spacing. However the spiral yield strength is low with no strain hardening expected.

It is evident from Figure (5-5) that all the tension-controlled experimental points scatter around the unconfined interaction diagram slightly o the un-conservative side except for three point, one of which matches the reduced area curve and two match the unconfined curve.

It is clear that the confinement played no role in this set of experiments. This may be attributed to the fact the test was old.

Case 10:

Another series of full scale columns was tested by the University of Illinois, Engineering Experiment Station in 1930. The column has the following parameters:

Column Specifications:

Column Diameter (H) : 12 in

Clear Cover : 1 in

Longitudinal Reinforcement: 8#7

f'_c : 3.37 ksi

f_y : 43.5 ksi

f_{yh} : 32 ksi

Transverse Reinforcement

Spiral Diameter : 0.2625 in

Spiral Spacing : 1.5 in

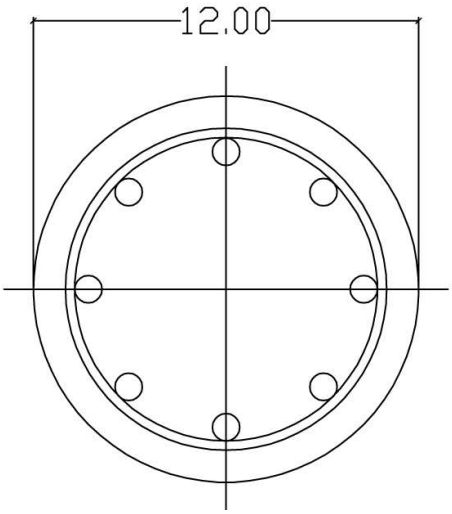

Figure 5-36 : Cross section for the column used in Case 10

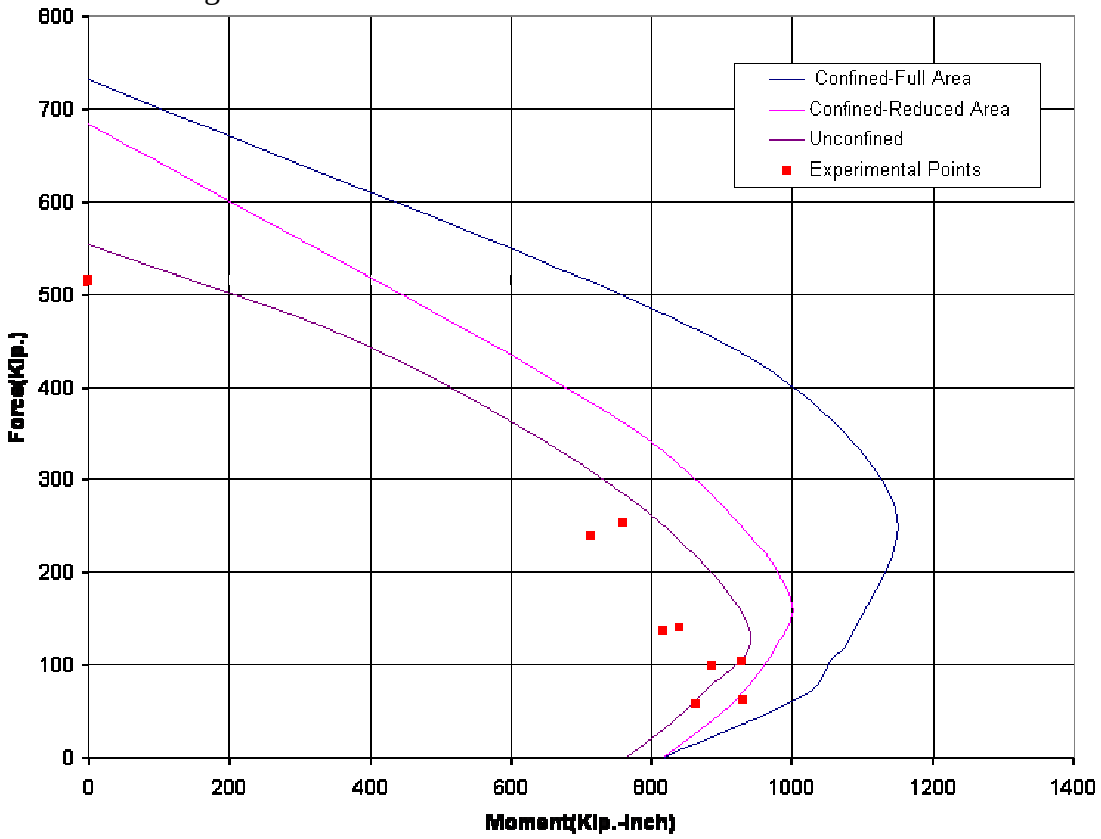

Figure 5-37: Interaction diagrams for case 10 column (without strain hardening)

The transverse reinforcement has the same spacing as that of case 9 and almost the same spiral diameter (slightly smaller here). The concrete strength is less here too. Nevertheless, the results are much improved. Even though they compared very well to the unconfined curve, one point is just outside the reduced area curve, Figure (5-37).

Case 11:

A third series of full scale columns was tested by the University of Illinois, Engineering Experiment Station in 1930. The column has the following parameters:

Column Specifications:

Column Diameter (H) : 12 in

Clear Cover : 1 in

Longitudinal Reinforcement: 8#7

f'_c : 1.58 ksi

f_y : 43.5 ksi

f_{yh} : 32 ksi

Transverse Reinforcement

Spiral Diameter : 0.177 in

Spiral Spacing : 1.5 in

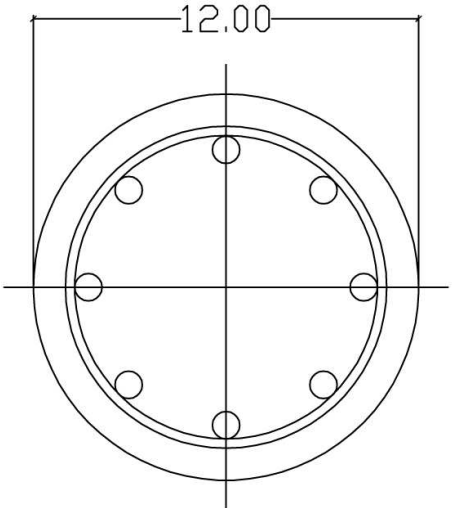

Figure 5-38 : Cross section for the column used in Case 11

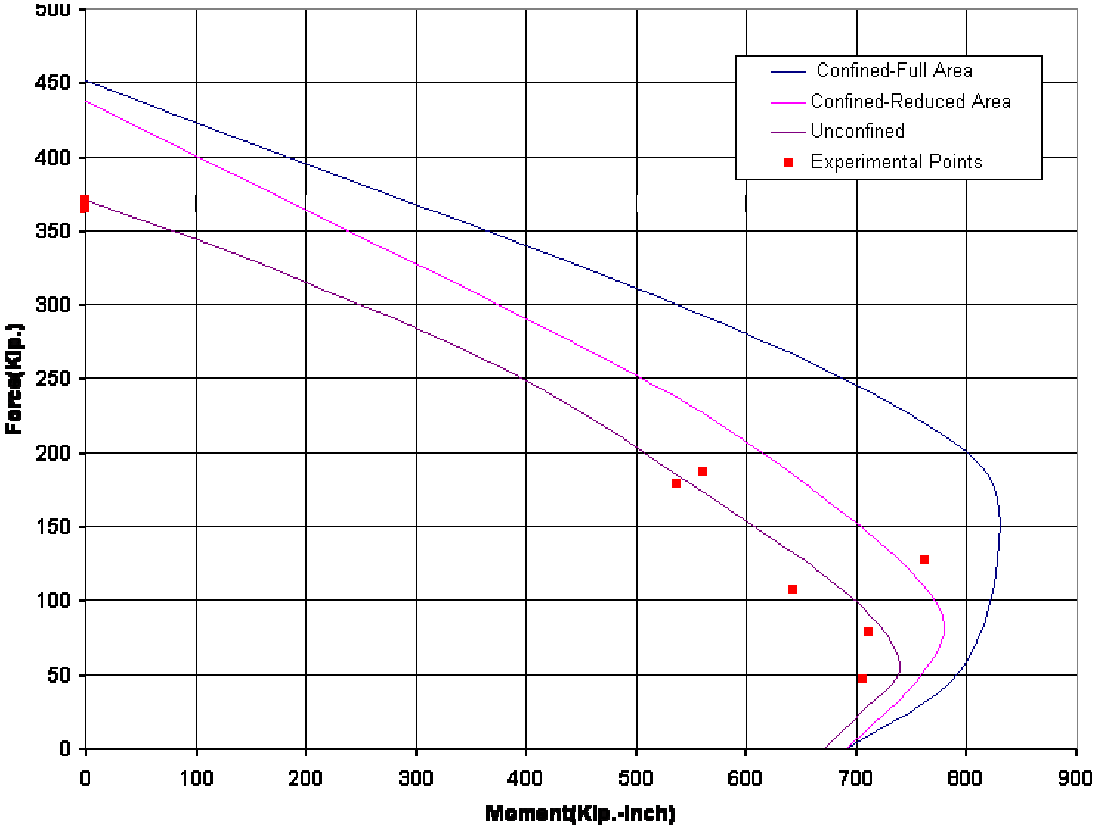

Figure 5-39 Interaction diagrams for case 11 column (without strain hardening)

The transverse reinforcement here has the same spacing as in case 9 but the spiral diameter is much smaller. The concrete strength is very smaller as well. However, the results are similar to these of case 9, Figure (5-39).

In case 9, 10 and 11, almost all of the experimental points lay around the unconfined interaction diagram, although these points were taken from confined cases. This may be attributed to the fact that the test was performed long time ago.

Figure (5-40) shows an experimental point to correlate well to the reduced area interaction diagram without steel strain hardening. Strain hardening is not realistic to implement here because the f_{yh} = 32 ksi indicates that the spiral is truly mild steel.

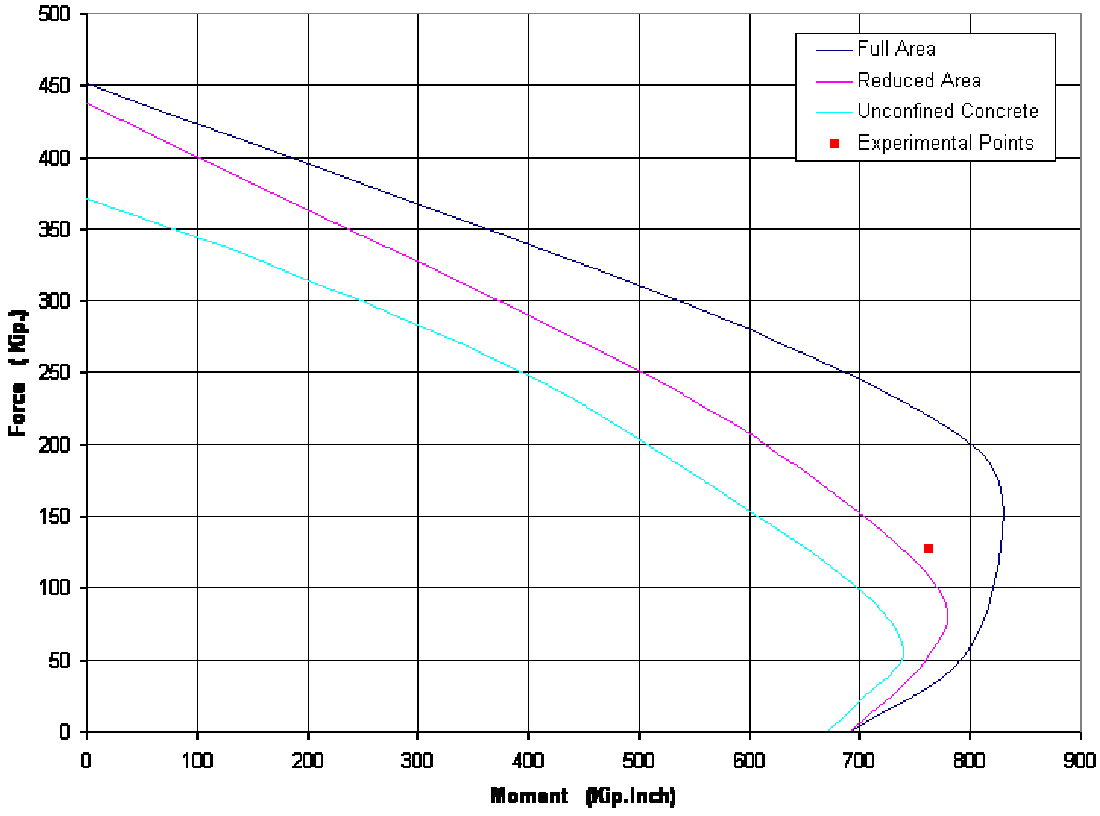

Figure 5-40 Interaction diagram for case 11 column (with strain hardening)

5-2 Comparison with CSI-Section builder software

Three different cases for unconfined concrete columns are compared to CSI-Section builder software of computers and structures Inc. The parameters of these three columns are as follow:

Case 12:

Diameter (H):	36	in
Clear Cover:	1.5	in
Longitudinal Steel:	13#11	
Spiral Diameter:	#5	
f'_c:	4	ksi
f_y:	60	ksi

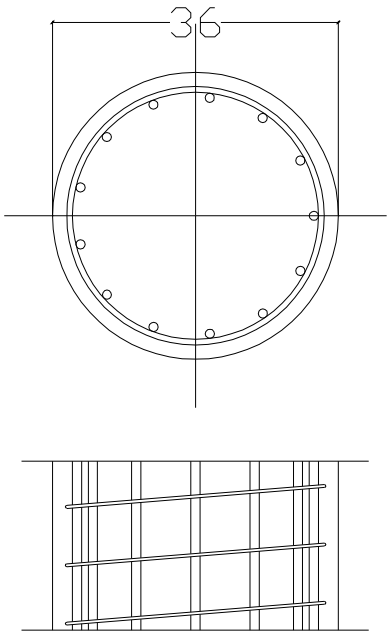

Figure 5-41 Cross section for the column used in Case 12

Case 13:

Diameter (H):	25	in
Clear Cover:	1	in
Longitudinal Steel:	12#10	
Spiral Diameter:	#4	
f'_c:	4	ksi
f_y:	60	ksi

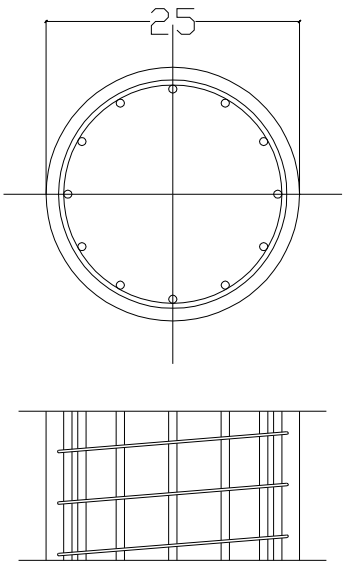

Figure 5-42 Cross section for the column used in Case 13

Case 14:

Diameter (H): 20 in

Clear Cover: 1 in

Longitudinal Steel: 10#8

Spiral Diameter: #4

f'_c: 4 ksi

f_y: 60 ksi

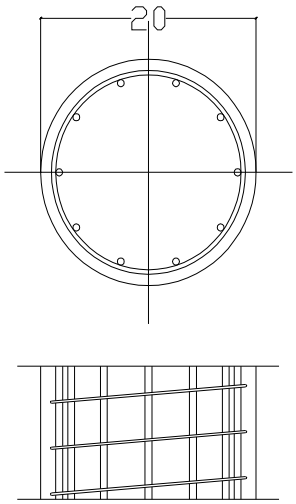

Figure 5-43 Cross section for the column used in Case 14

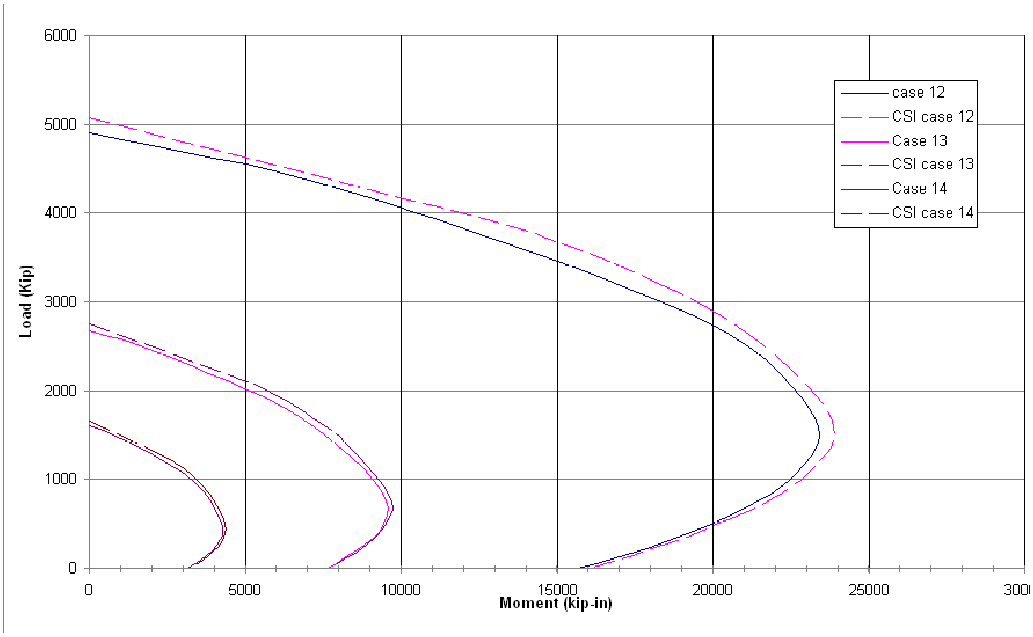

Figure 5-44 Unconfined Interaction diagrams using the present software and CSI Section Builder

Figure (5-44) shows the excellent match between the curves plotted using CSI-Section Builder and the present software (KCE). It can be noticed that the KCE curves are slightly more conservative

5-3 Comparison with Mander concentric compression model

To compare the predications of the present analysis against the well-known and widely used Mander model, the complete interaction diagram is generated using the Mander model, which is known to be valid for pure axial compression only, relative to the eccentricity based model. The parameters of the column examined are as follow:

Column Diameter (H) : 23.65 in
Clear Cover : 0.8 in
Longitudinal Reinforcement: 16#8
f'_c : 3.857 ksi
f_y : 43.5 ksi
f_{yh} : 43.5 ksi
Transverse Reinforcement
Spiral Diameter : 0.394 in
Spiral Spacing : 1.97 in

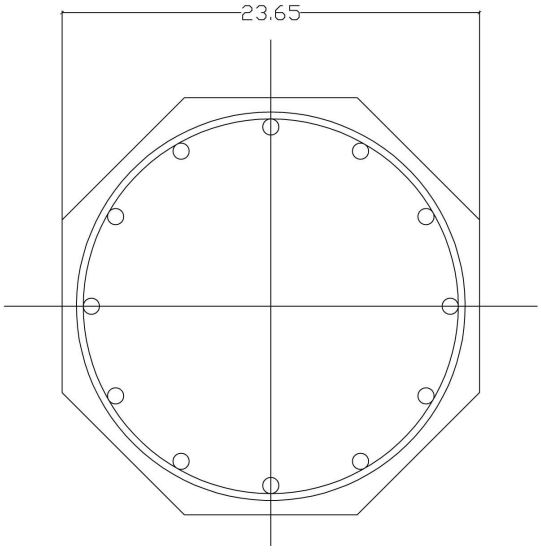

Figure 5-45 Cross section for the column used to compare Mander model to Eccentricity based model

It is evident from the comparison, shown in Figure (5-45), that the present model is very accurate and just conservative enough compared to the experimental point. On the other hand, the Mander model is shown to be accurate as well but not conservative enough relative to the experimental point

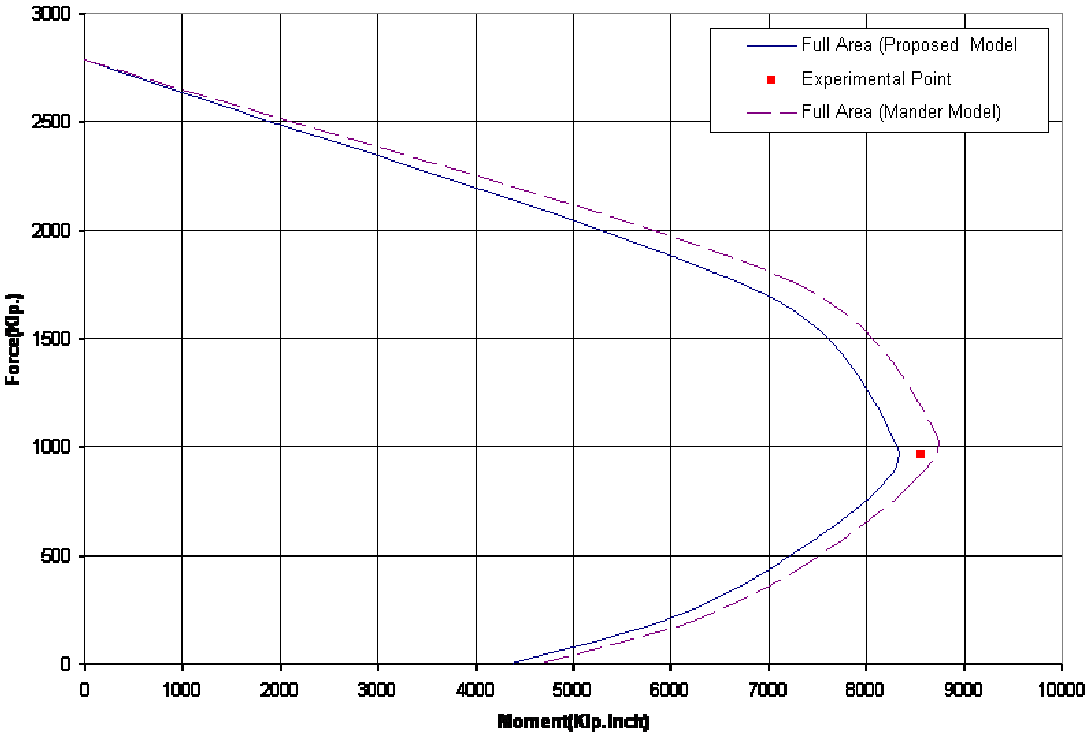

Figure 5-46 Interaction diagrams by the present model and Mander Model

To show this comparison when the confinement is more pronounced, another example column is analyzed by the two models. The column parameters are:

Column Diameter (H) : 12 in

Clear Cover : 1 in

Longitudinal Reinforcement: 8#7

f'_c : 4 ksi

f_y : 60 ksi

f_{yh} : 60 ksi

Transverse Reinforcement

Spiral Diameter : #5

Spiral Spacing : 1 in

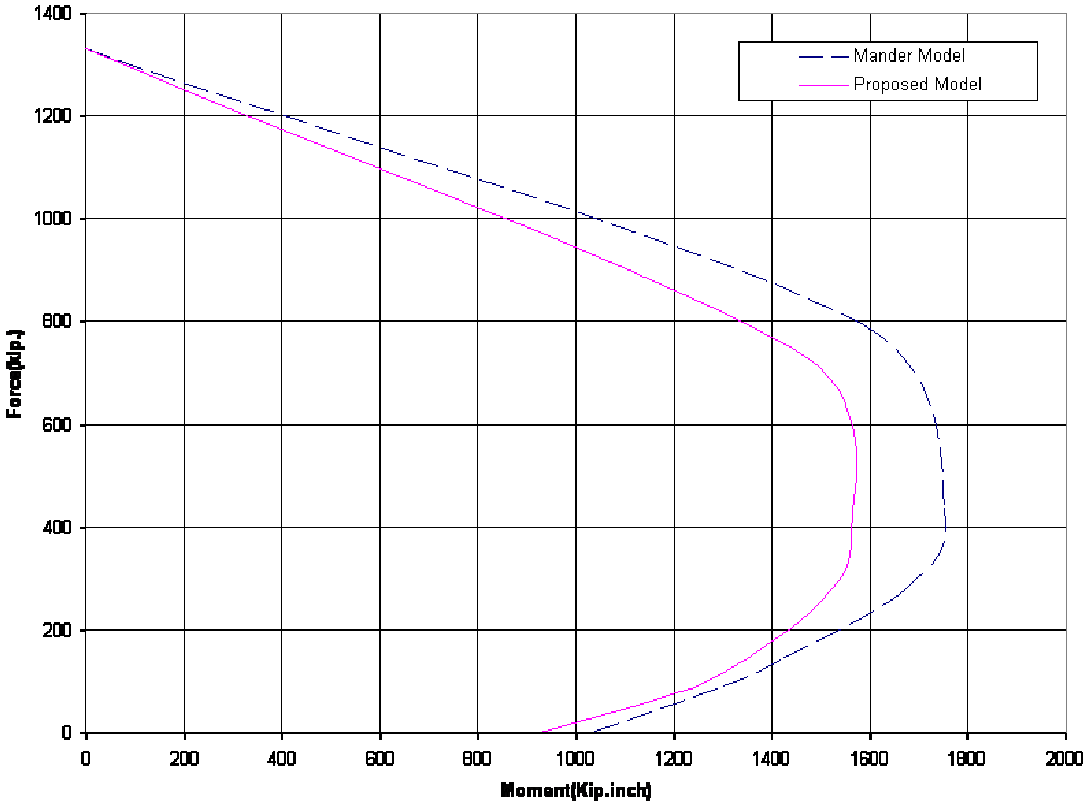

Figure 5-47Comparison between the present and Mander model

It is clear from Figure (5-41) that the present analysis is significantly more conservative than that of Mander model that indicates that the eccentricity based model is necessary, especially in confinement critical columns

5-4 Comparison of extreme cases

Two extreme cases are compared to show the increase in column capacity, by considering the confinement effect; the parameters for the two cases are constant, except for those related to transverse steel reinforcement. Steel #3 with spacing of 3 in (maximum allowed by AASHTO code) is used in the first case, while the second case has steel #5 and spacing equal to 1 in (minimum allowed by AASHTO code). The parameters used are:

Case 1:
Column Diameter (H) : 12 in
Clear Cover : 1 in
Longitudinal Reinforcement: 8#7
f'_c : 4 ksi
f_y : 45 ksi
f_{yh} : 45 ksi
Transverse Reinforcement
Spiral Diameter : #3
Spiral Spacing : 3 in

Case 2:
Column Diameter (H) : 12 in
Clear Cover : 1 in
Longitudinal Reinforcement: 8#7
f'_c : 4 ksi
f_y : 45 ksi
f_{yh} : 45 ksi
Transverse Reinforcement
Spiral Diameter : #5
Spiral Spacing : 1 in

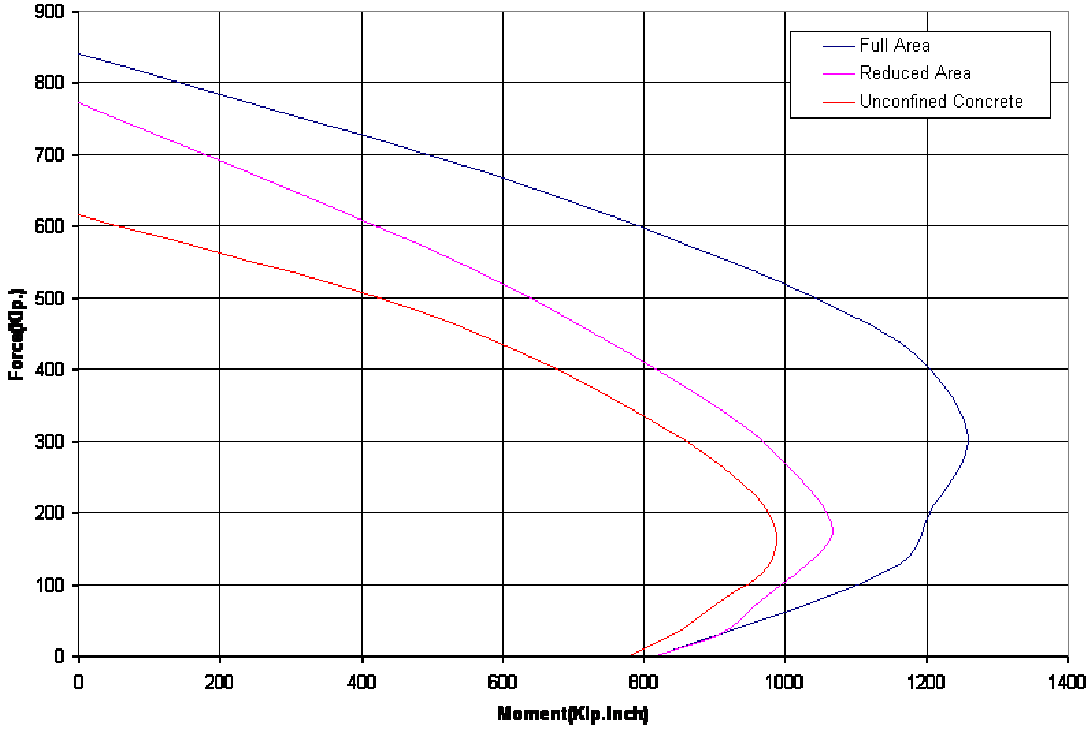

Figure 5-48 Interaction diagrams for case 1(without strain hardening)

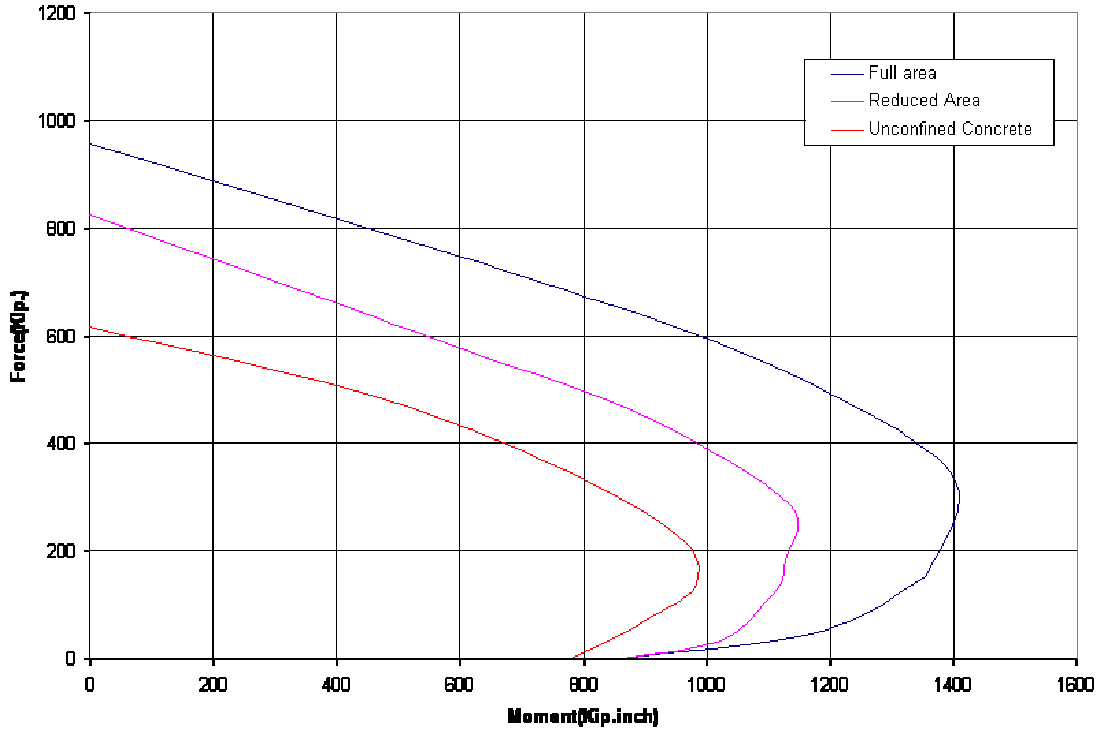

Figure 5-49 Interaction diagrams for case 1 (with 5% strain hardening)

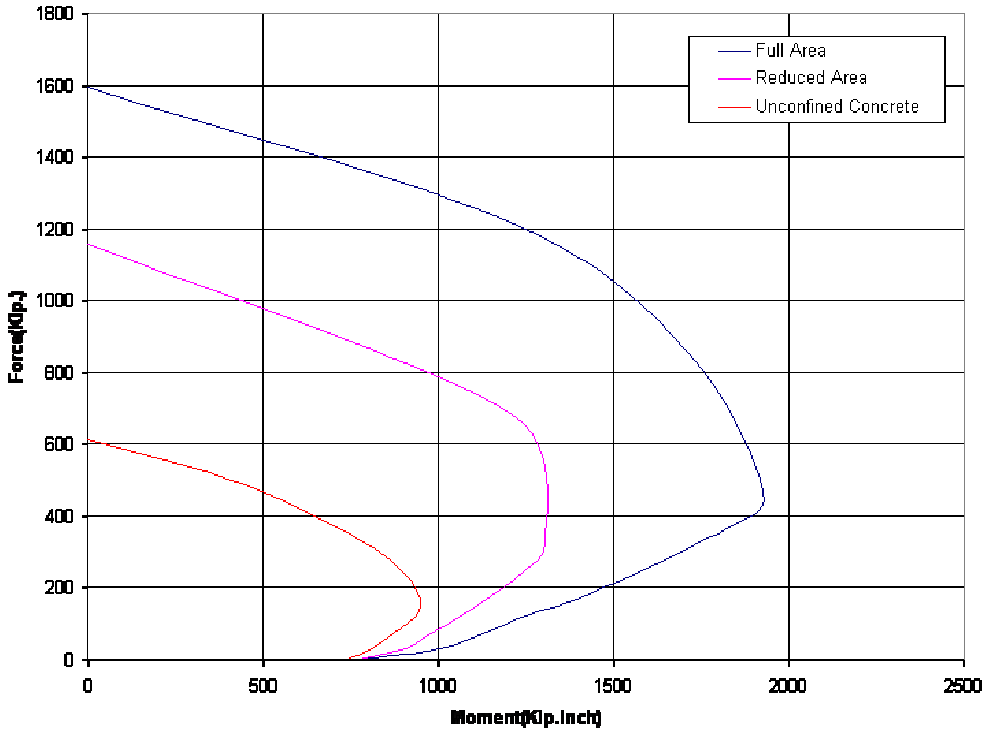

Figure 5-50 Interaction diagrams for case 2 (without strain hardening)

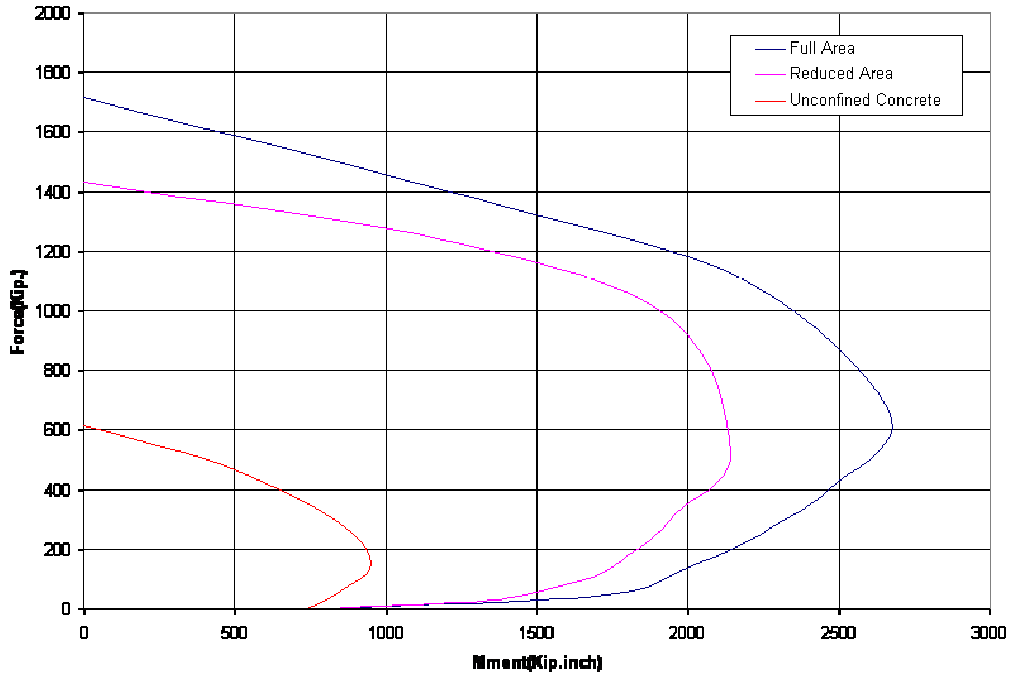

Figure 5-51 Interaction diagrams for case 2 (with 5% strain hardening)

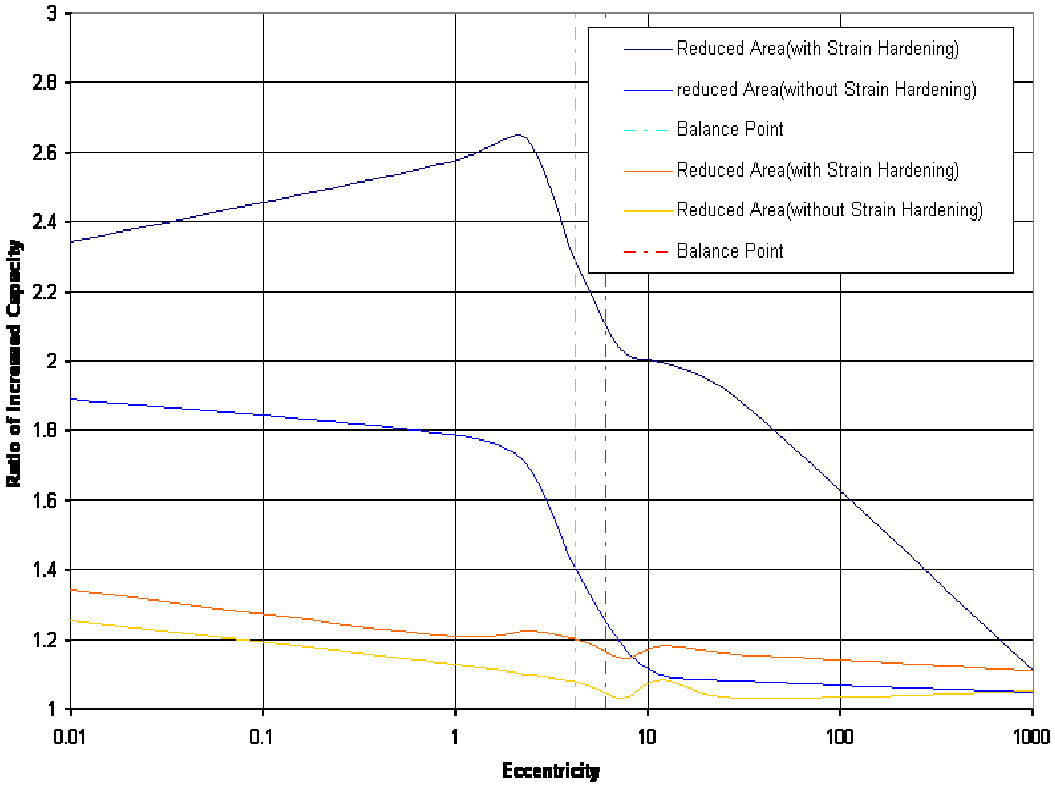

Figure 5-52 Increased Strength of Confined Columns with respect to Unconfined Capacity for case 1 and 2.

Figure (5-52) illustrates the huge increase of confined column capacity, when the actual behavior is analyzed. In case 1, the ratio of increased capacity, with strain hardening, reaches around 190% more than that of unconfined concrete. In case 2, 230% increase in column capacity is achieved relative to the unconfined case. In case 1, the maximum gain in capacity takes place at the point of pure axial compression. In case 2, the maximum gain in capacity happens near the location of balanced point. Also it can be seen that the two curves, with strain hardening and without strain hardening for each case converge at the same point for the pure bending case as the effect of the lateral confinement vanishes.

5-5 Benchmarking of confined analysis with zero f_{yh}

This comparison was pursued to compare the baseline results of the confinement analysis algorithm by assuming the yield strength in the lateral confinement to be zero, and the unconfinement computations.

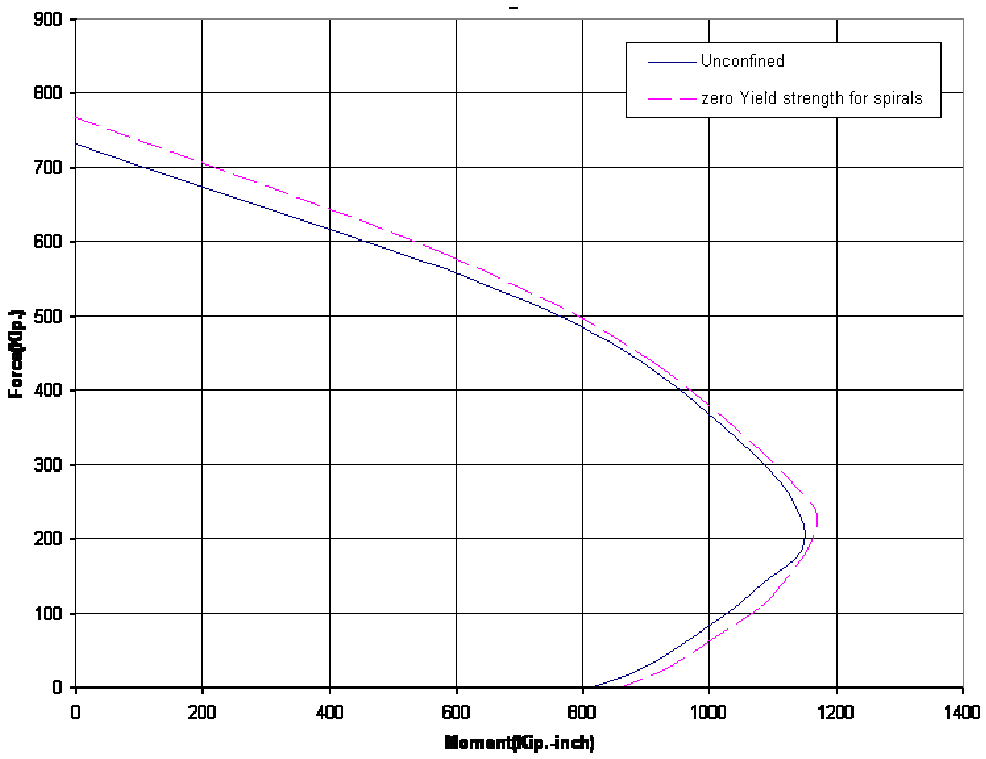

Figure 5-53 Interaction diagrams for unconfined and confined analysis (with assuming f_{yh} = 0)

It is obvious in Figure (5-47) the excellent correlation between the two curves. This comparison evidently suggests the accuracy of the confined analysis algorithm.

5-6 Studying column different parameters relationships

This set of results is generated using the following parameters:

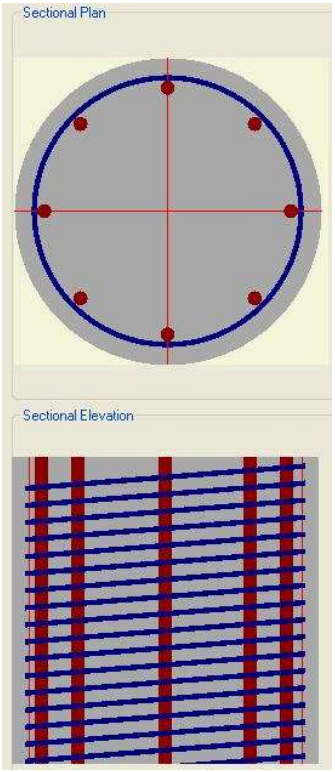

Column Diameter (H) : 36 in

Clear Cover : 2 in

Longitudinal Reinforcement: 8#14

f'_c : 5 ksi

f_y : 60 ksi

f_{yh} : 60 ksi

Transverse Reinforcement

Spiral Diameter : #5

Spiral Spacing : 2 in

Figure 5-54 Cross section for the column used to generate different parameters relationships

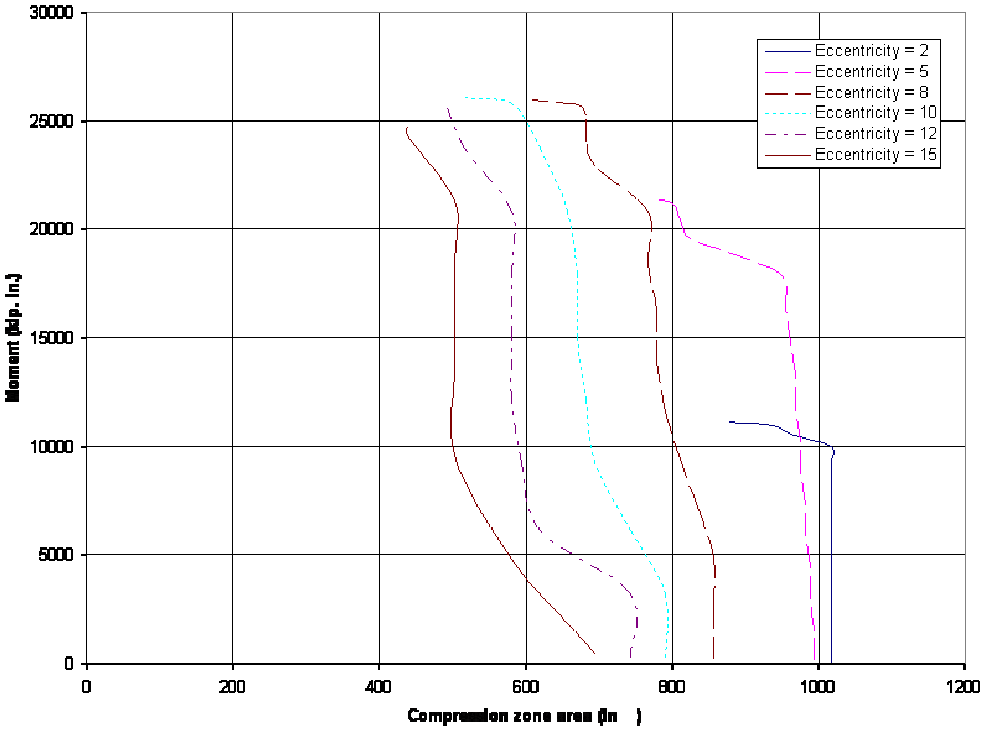

Figure 5-55 Change of area of compression zone with moment

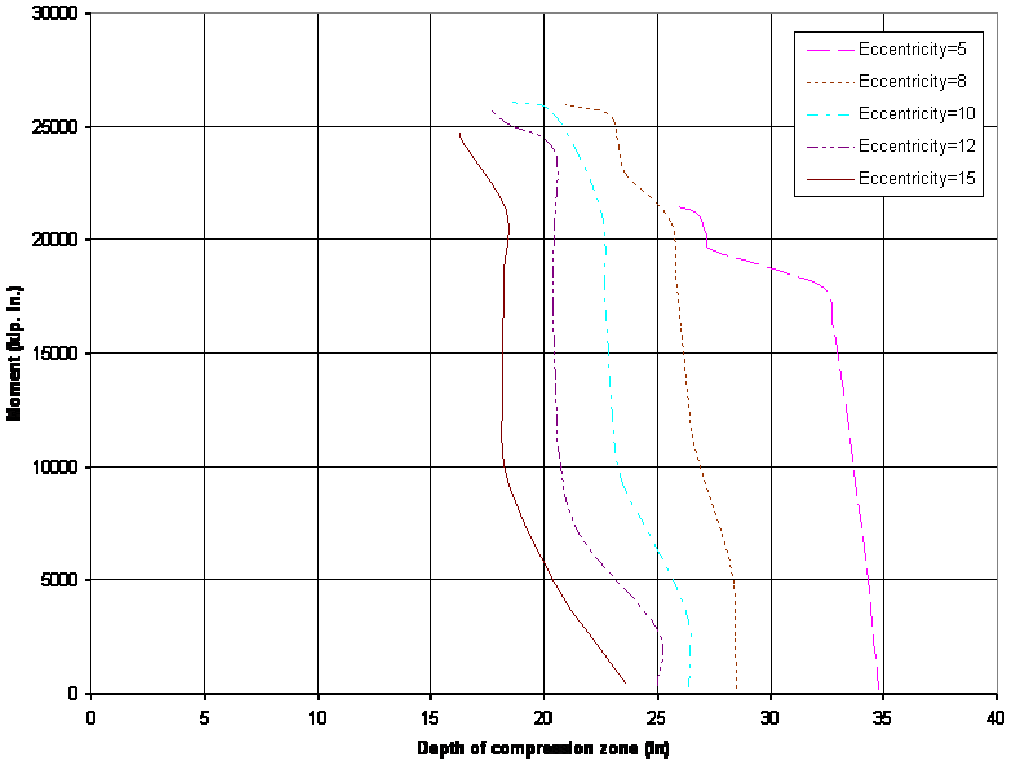

Figure 5-56 Change of compression zone depth with moment

It can be shown from Figure (5-55) and (5-56) that the depth of compression zone correlates well on most of the loading history. That is evident of the accuracy of the eccentricity based model. Accordingly the depth of compression zone can be related directly to eccentricity. It can be seen also that the curves deviate near the failure loading.

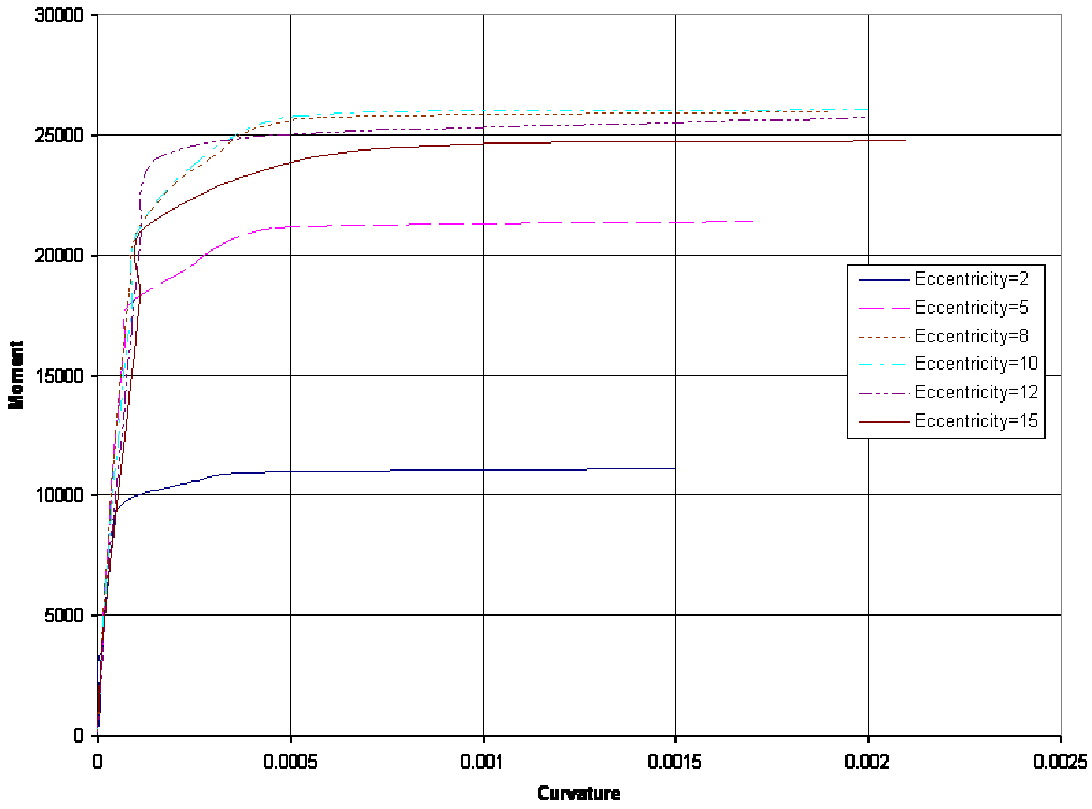

Figure 5-57 Moment- curvature relationships

It is evident from Figure (5-57) that the moment-curvature relationship is similar for the entire range of eccentricities. The overall relationship may be approximated by a trilinear response. The first linear portion is the same for all eccentricities indicating the same initial and subsequent EI. It can also be seen that the ultimate curvature increases steadily from near axial compression to near pure bending cases.

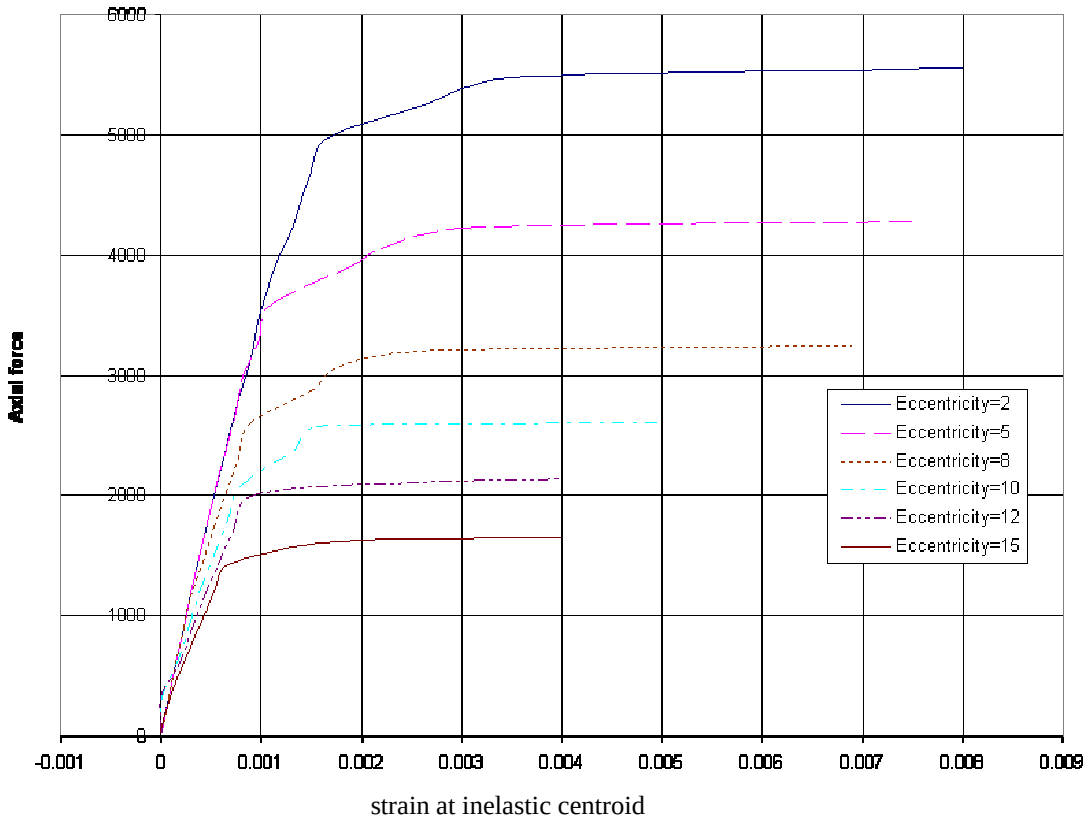

Figure 5-58 Axial force – strain at inelastic centroid relationship

It is evident from Figure (5-58) that P-ε_o relation ship is also closely trilinear for all eccentricities. However, the ultimate strain is greatest at near axial compression case and decreases gradually up to the case near pure bending. This is obviously the opposite of the observation of moment-curvature relationships. This is attributed to the fact that the curvature and ε_o are inversely proportional at ultimate failure since they are related through the linear strain distribution.

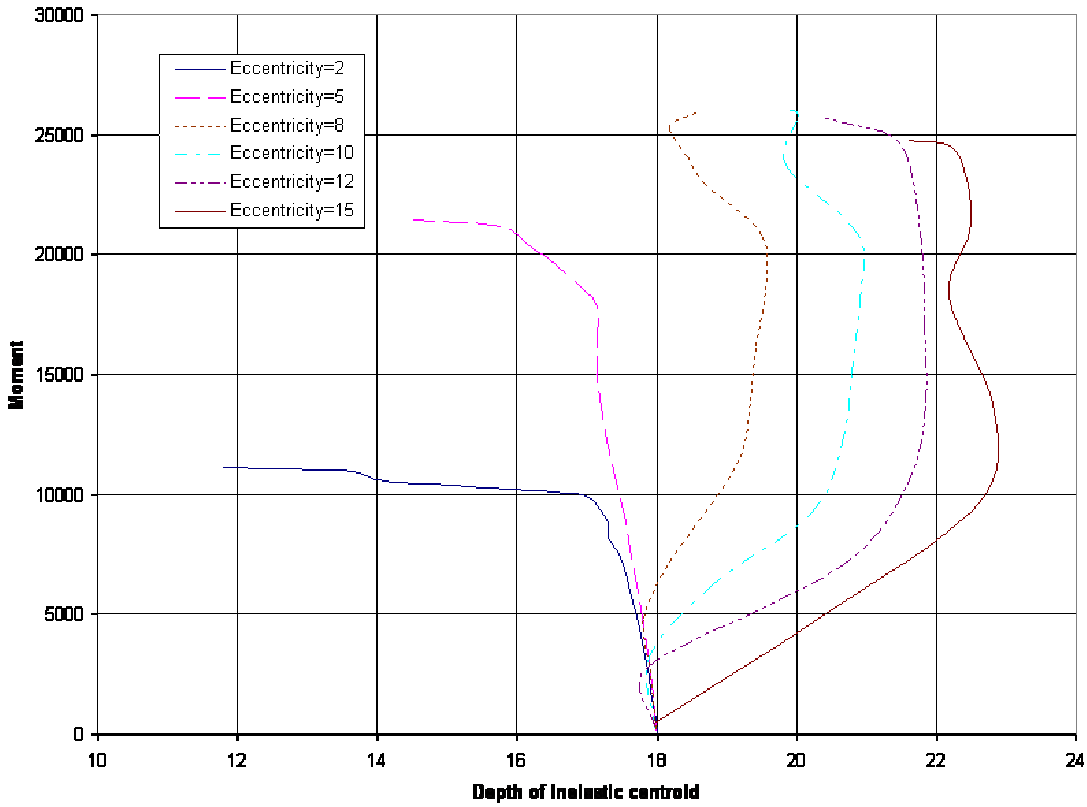

Figure 5-59 Change of inelastic centroid depth with moment

It can be shown from Figure (5-62) that for compression controlled cases(small eccentricities) the depth of inelastic centroid decreases with increasing the load. While for tension controlled cases (big eccentricities) the depth of inelastic centroid increases with load increasing.

CHAPTER 6 - Software Development

6-1 Introduction

The software prepared using the object oriented programming “OOP”, within the framework of the visual C++ language, that is a useful tool to organize the program in different classes, and generate objects from these classes. This procedure is adaptable to simulate the real process, as well as it is flexible enough for modification and addition to the program

As shown in Figure (6-1), the main two classes are material, which has concrete and steel inherited from it, and shape that define the cross section. The reinforced circular cross section class was generated by combining the three classes; concrete, steel and circle. Then, any analysis

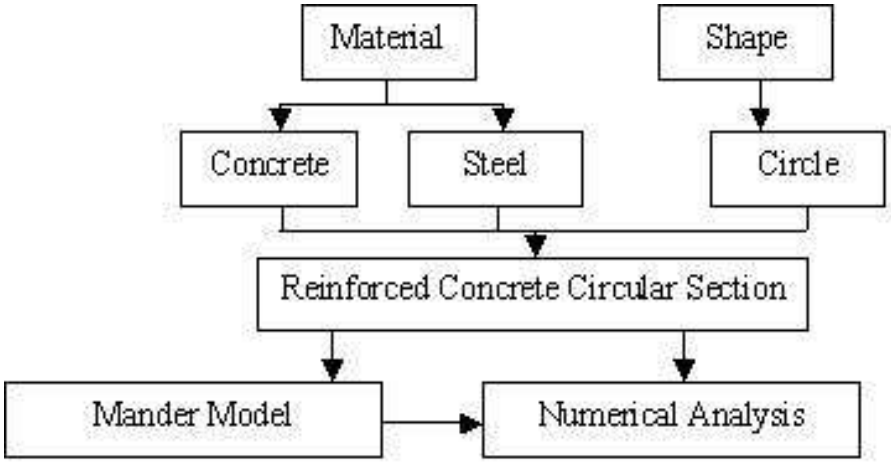

can be applied on this class.

Figure 6-1 Classes Used in program structure

6-2 Interface Design

The interface was generated using the graphical user interface “GUI” which is a convenient communication tool between the user and the program. The interface is divided into five sections as shown in Figure (6-2):

1- Data Input

Figure (6-3) shows the four sub-sections; Geometric properties, concrete properties, longitudinal steel properties and transverse steel properties.

2- Graphics Input representation

This section automatically generates sectional plan view and elevation view of the cross section, which is input in the Data Input section. It gives the user an indication of how the cross section looks like, and the properties of different component in order to avoid unrealistic errors in inputs.

3- Plotting area (output)

The plotting area section shows the required results curve/s.

4- Selection tools (input)

This section has different buttons which control with plotting interaction diagram curve/s as depicted in Figure (6-5):

Plotting the three curves; confined concrete, unconfined concrete and design curves

Plotting any one of the previous curves separately.

Plotting a series of design curves for the full range of reinforcement ratio..

It has also buttons for optionally save or load cases defined in the “Data Input” section and print the “plotting area” section view

5- Projection points input

This section enables the user to input any numbers of points up to a minimum of 25, which show up immediately on the plotting area along side with the existing curve/s.

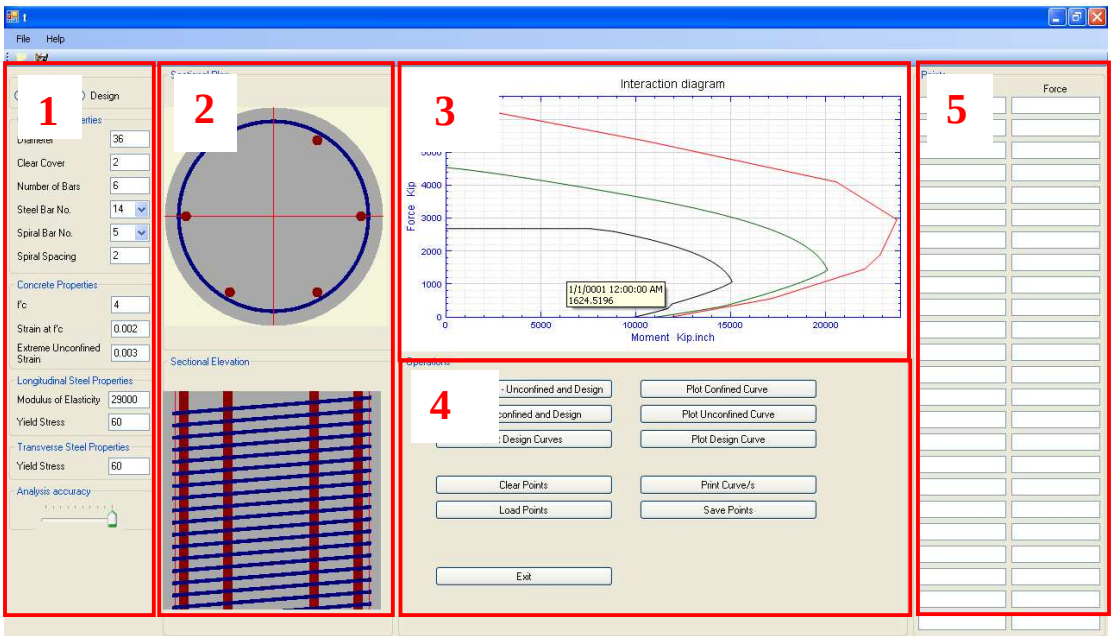

Figure 6-2 Interface main sections

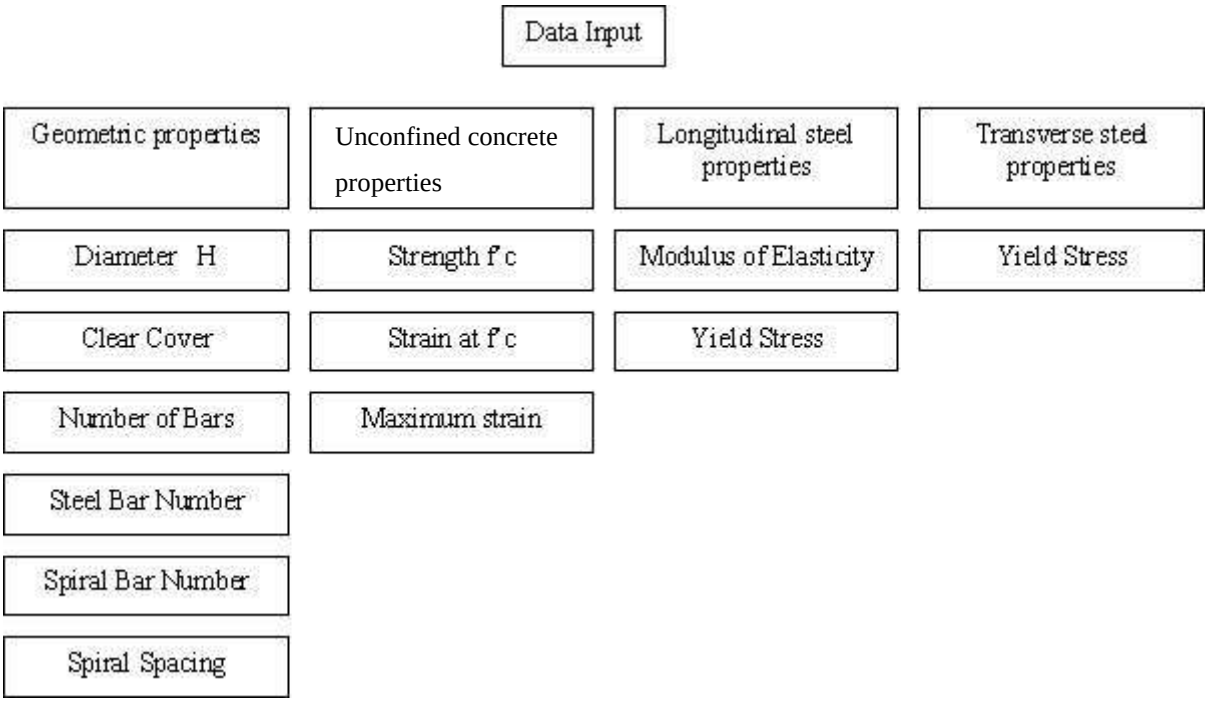

Figure 6-3 Different Sub-Sections under the "Data Input" Section

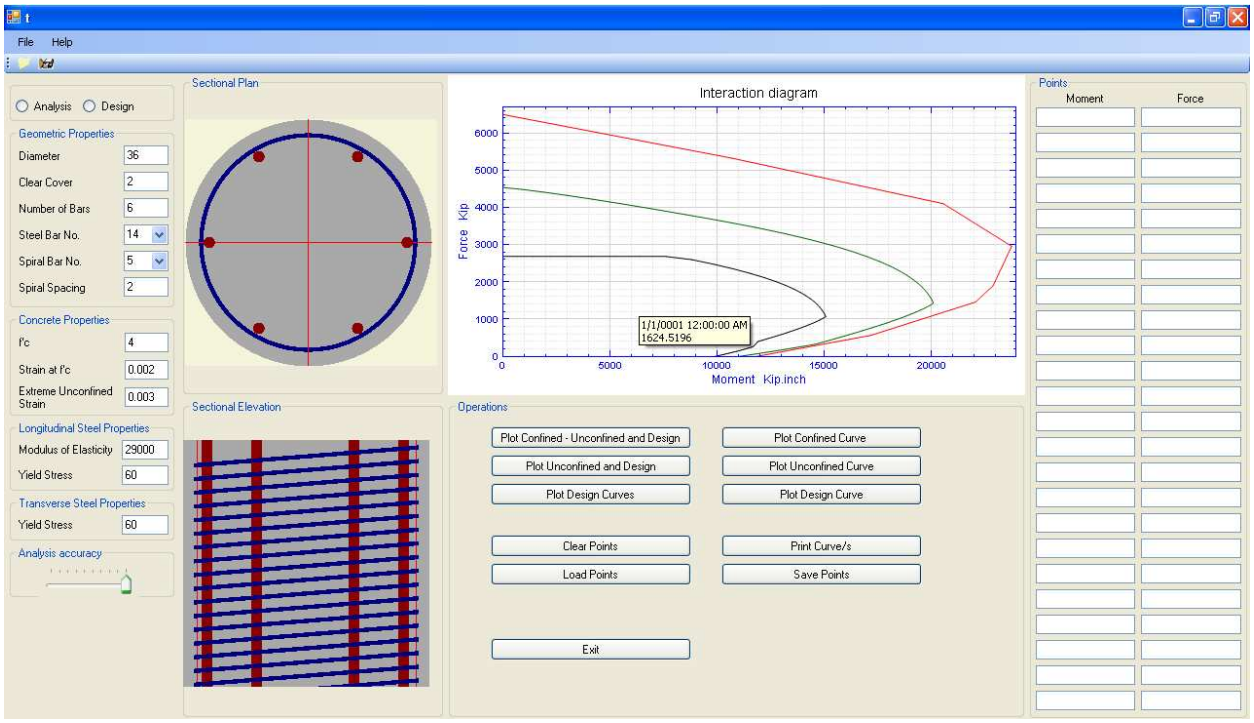

Figure 6-4 Interface view

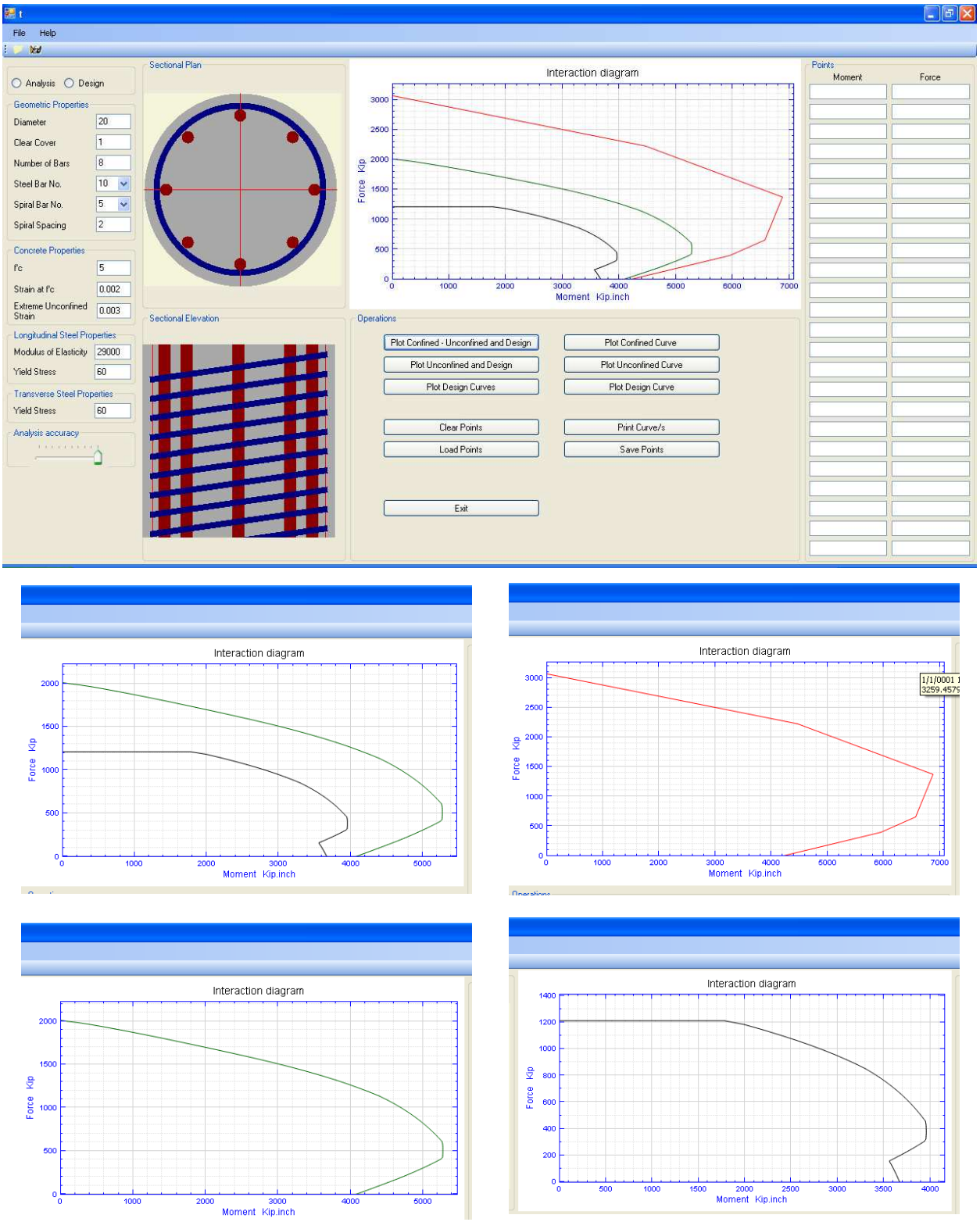

Figure 6-5 Different views of the “plotting area” section

6-3 Analysis features

As shown in figure (6-5), the program is capable of analyzing the circular cross section in a variety of ways. The actual capacity of the cross section is analyzed taking into account spiral confined effect, and generates interaction diagrams for the confined concrete and the unconfined concrete.

6-4 Design features

The software has the ability to plot design interaction diagrams according to AASHTO-code, which disregard the confinement effect. As figure (6-6) illustrates, six design curves are generated with different ratio of steel to the gross section. This feature is a useful design tool that enables the user to select the proper ratio of steel.

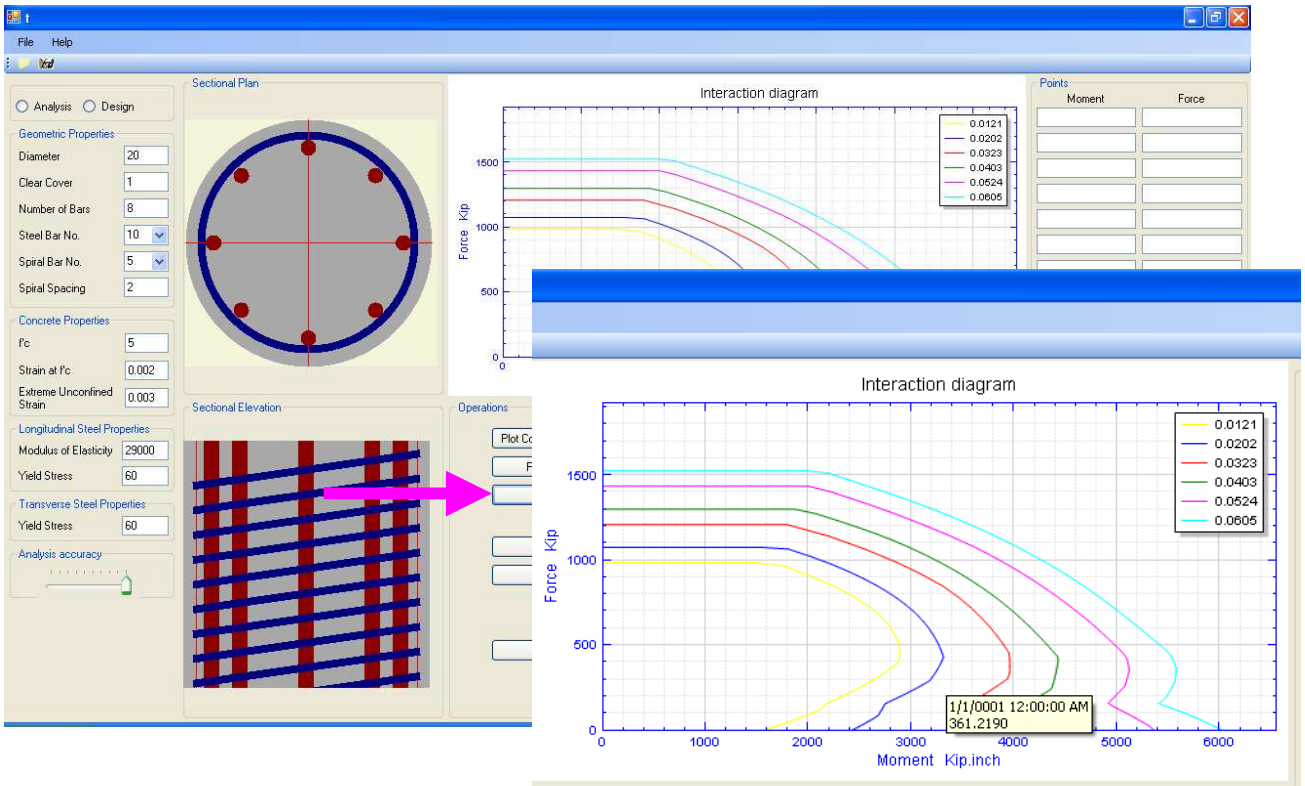

Figure 6-6 Design curves generated in the “plotting area” section

The software also has the option of plotting up to 25 points on top of the design curves, as a convenient tool for design as shown in figure (6-7).

The program is expandable to include any cross section, as well as any model or analysis to be applied to any cross section. It is also adaptable for considering any type of external confining like steel tubes and FRP wrapping.

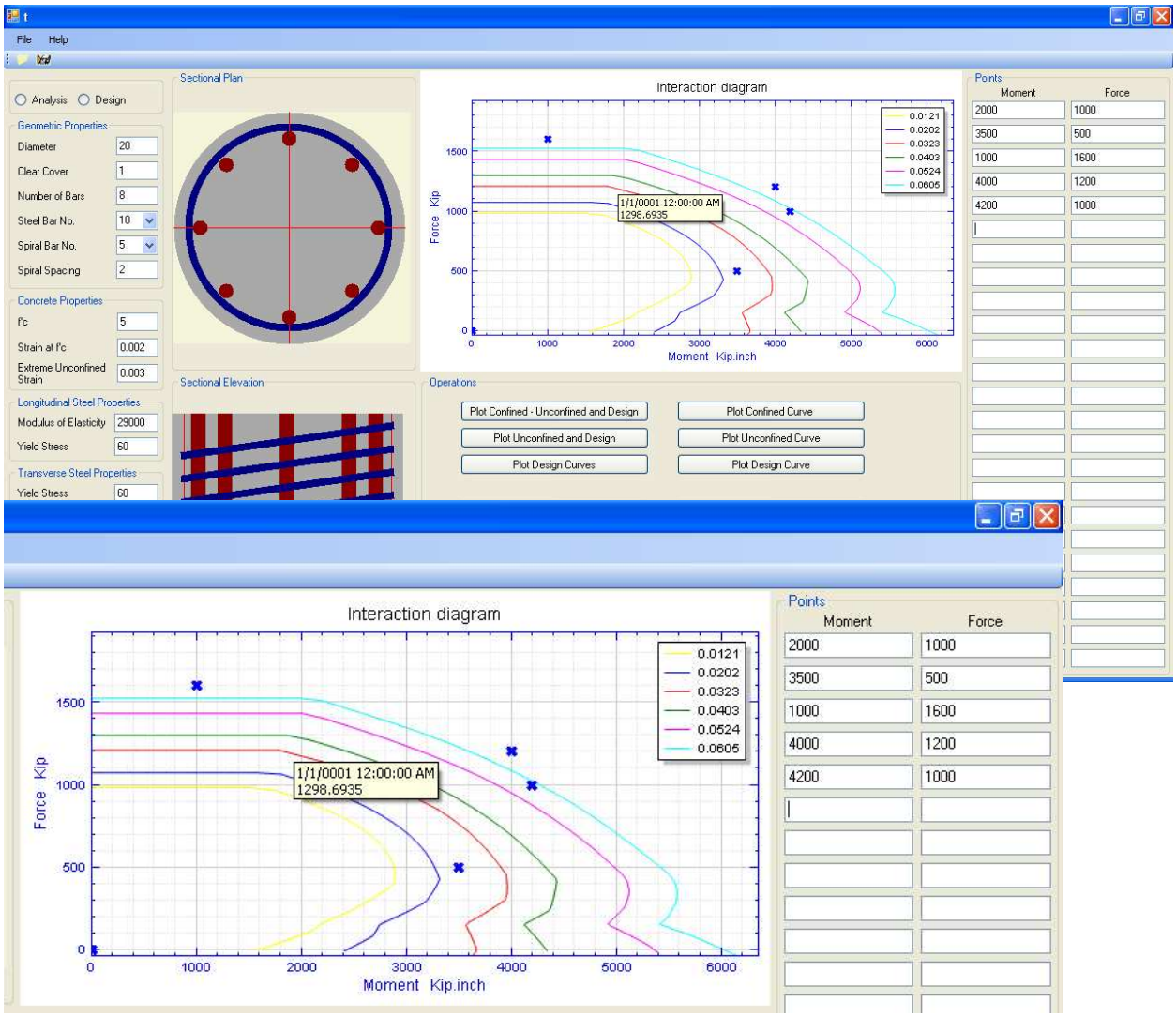

Figure 6-7 Design curves with points

CHAPTER 7 - Conclusions and Recommendations

7-1 Conclusions

This thesis accomplished several objectives at the analysis, material modeling, design implications and software development levels. It may be concluded that:

1- The new eccentricity-based model predicted the results accurately compared to the concentric type models for the entire range of eccentric loading.

2- The unconfined concrete assumptions at pure bending are accurate as evidenced by comparisons to experimental results.

3- The fully confined concrete assumptions at pure axial compression are accurate when the clear cover is removed as evidenced by close comparison to experimental results.

4- The unconfined concrete analysis is benchmarked successfully against well-established software for a range of design parameters.

5- The confined concrete analysis procedure is completely different from the solution strategy of unconfined concrete analysis. To benchmark an extreme case of confined analysis, f_{yh} is set to zero to match the results of unconfined analysis.

6- The partial confinement utilization is examined against e/H ratio at various loading levels to generate insights on the effectiveness of the eccentricity-based model.

7- Extreme confinement design parameters are selected to study the improvements of confined to unconfined behavior under different eccentricities.

8- The Mander model is shown ineffective when the hoop (or spiral) reinforcement diameter is very small. This was evidence by having the experimental data points scatter around the unconfined interaction diagram.

9- The software is developed effective for preliminary design when the options of interaction diagrams of various reinforcement ratios are plotted against the demand.

10- The software developed is effective for assessment of ultimate capacity for extreme load cases as compared to unconfined results. The graphs are readily available against the actual demand as well.

11- The strain hardening feature is added to push the ultimate analysis to simulate the actual case especially when higher strength steel is used for longitudinal reinforcement

7-2 Recommendations

This work should be extended to address the following areas:

1- Model FRP wrapping on confinement effects for circular columns.

2- Model cover spalling and corrosion of longitudinal and transverse steel for circular columns

3- Model the unconfined, confined and design interaction curves for rectangular columns under axial load and biaxial bending.

4- Model FRP wrapping on confinement effects for rectangular columns.

5- Model cover spalling and corrosion of longitudinal and transverse steel for rectangular columns.

References

Ahmad, S. H., and Shah, S. P. (1982). “Complete Triaxial stress-strain curves for concrete.” ASCE J., 108(ST4),April 1982 728-743.

Ahmad, S. H., and Mallare, M. P. (1994). “A Comparative study of models for confinement of concrete by circular spirals.” Magazine of concrete research 46(166), 49-56.

Ahmad, S. H., and Shah, S. P. (1982). “Stress-Strain Curves of Concrete Confined by Spiral Reinforcement.” ACI J., 79(6), 484-490.

Assa B., Nishiyama, M., and Watanabe, F.(2001). “New Approach for Modeling Confined Concrete. I: Circular Columns.” J. Struct. Eng., 127(7), 743-750.

Attard, M. M., and Setunge, S. (1996). “Stress-Strain Relationship of Confined and Unconfined Concrete.” ACI Mater. J., 93(5), 432-442.

Bazant, Z. P., and Bhat, P. D. (1976). “Endochronic Theory of Inelasticity and Failure of Concrete.” J. Engrg. Mech. Div., ASCE, 102(4), 701-722.

Bazant, Z. P., and Bhat, P. D. (1977). “Prediction of Hysteresis of Reinforced Concrete Members.” J Struct. Div., ASCE, 103(1), 153-167.

Bradford, M. A., and Gilbert, R. I. (1992). “Analysis of Circular RC Columns for Short and Long-Term Deformations.” J. Struct. Engrg., ASCE, 118(3), 669-683.

Breen, J. E. (1962) , “The Restrained Long Concrete Column as a Part of A Rectangular Frame.” Ph. D. Thesis Presented to The University of Texas, Austin, Tex.

Candappa, D. (2000). “The Constitutive Behavior of High Strength Concrete under Lateral Confinement.” PhD Thesis, Monash Univ., Clayton, VIC, Australia.

Candappa, D. P., Sanjayan, J. G., and Setunge, S. (2001). “Complete Triaxial Stress-Strain Curves of High-Strength Concrete.” J. Mater. Civ. Eng., 13(3), 209-215.

Candappa, D. P., Setunge, S., and Sanjayan, J. G. (1999). “Stress Versus Strain Relationship of High Strength Concrete under High Lateral Confinement.” Cem. Concr. Res., 29(12), 1977-1982.

Carreira, DJ., and Chu, K. H. (1985). “Stress-Strain Relationship for Plain Concrete in Compression.” ACI J., 83(6), 797-804.

Chan, W. W. L. (2002). “The Ultimate Strength and Deformation of Plastic Hinges in Reinforcement Concrete Frameworks” Magazine of Concrete Research (London), V. 128, No. 12 p. 1551-1564, December 2002.

Cusson, D. and Paultre, P. (1995). “Stress-Strain Model for Confined High-Strength Concrete” ASCE Journal of Structural Engineering, Vol. 121, No.3, p. 468-477.

Davalth, S. R. and Madugula M. K. (1988) “Analysis/design of reinforced concrete circula cross sections”, ACI J.

Davister, M. D. (1986). “A Computer Program for Exact Analysis,” Concrete International: Design and Construction, V. 8, No. 7, July 1986, pp. 56-61.

Dodd, L. L., and Cooke, N. (2000). “Capacity of circular bridge columns subjected to base excitation.” ACI J., 97(2), 297-308.

Ehsani, Mohammad R. (1986). “CAD for Columns,” Concrete International: Design and Construction, V. 8, No. 9, Step. 1986, pp. 43-47.

Eid, R. and Dancygier A. N. (2005) “Partially confined circular members subjected to axial compression: Analysis of concrete confined by steel ties” Structural engineering and Mechanics, Vol. 21, No. 6 p 737-765.

El-Dash, K. M., and Ahmad, S. H. (1995). “A Model for Stress- Strain Relationship of Spirally Confined Normal and High-Strength Concrete Columns.” Mag. Concrete Res., 47(171), 177-184.

Esmaily, A. and Xiao, Y. (2004). ”Behavior of Reinforced Concrete Columns under Variable Axial Load” ACI Structural Journal, V.101, Issue 1, p.124-132, January 2004.

Everand, Noel J., and Cohen, Edward. (1964). “Ultimate Strength Design of Reinforced Concrete Columns” ACI Special Publication, SP-7, 182 p, Detroit.

Everand, Noel J., (1997). “Axial load moment interaction for cross sections having longitudinal reinforcement arranged in a circle” ACI J, V. 94, No. 6, December 1997.

Fam, A. Z., Flisak, B., and Rizkalla, S. H., (2003). “Experimental and Analytical Modeling of Concrete-Filled Fiber-Reinforcement Polymer Tubes Subjected to combined Bending and Axial Loads”. ACI Structural Journal, V.100, Issue 4, p.499-509, August 2003.

Fafitis A., and Shah, S.P. (1985). “Lateral Reinforcement for High-Strength Concrete Columns” ACI Special Publication, SP 87-12, p.213-232.

Furlong. R. W. (1961), “Ultimate strength of square columns under biaxially eccentric loads”, Journal of the American Concrete Institute, No 57-53, P1129-1140

Gunnin, B. L., Rad, F. N., and Furlong, R. W. (1979). “A General Nonlinear Analysis of Concrete Structures and Comparison With Frame Tests,” Computers and Structures, V. 105, No. 2, Apr. 1979, pp. 297-315.

Hognestad, E. (1930) “A study of combined bending and axial load in reinforced concrete members”, University of Illinois, Urbana.

Hoshikuma, J., Kawashima, K., Nagaya, K., and Taylor, A. W. (1997). “Stress-Strain Model for Confined Reinforced Concrete in Bridge Piers.” J. Struct. Eng., 123(5), 624-633.

Hsu, L. S., and Hsu, C. T. T. (1994). “Complete Stress-Strain Behavior of High-Strength Concrete under Compression.” Mag. Concrete Res., 46(169), 301-312.

Kent, D. and Park, R. (1971). “Flexural Members with Confined Concrete” Journal of Structural Division. Proceedings of the American Society of Civil Engineers. V.97, No.ST7, p 1969-1990, July 1971.

Kroenke, W. C., Gutzwiller, M. J., and Lee, R. H. (1973). “Finite Element for Reinforced Concrete Frame Study.” Journal of Structural Division, ASCE, V. 99, No. ST7, July 1973, pp. 1371-1390.

Lazaro, A. L., and Richards, Jr., r. (1974). “Full Range Analysis of Concrete Frames.” Journal of Structural Division, ASCE, V. 100, No. ST12, Dec. 1974, pp. 2419-2432.

Lokuge W. P. , Sanjayan J. G. and Setunge S. (2005) “Stress strain model for laterally confined concrete”. Journal of materials in civil engineering,ASCE, Vol. 17, No. 6 p607-616, December 2005

Lucio, K. (2004) “Analytical performance of reinforced concrete sections using various confinement models” , master thesis, Kansas State University 119 p.

Mander, J.B., Priestley, M.J.N., and Park, R. (1988). ”Theoretical Stress-Strain Model for Confined Concrete” Journal of Structural Engineering, ASCE, V.114, No. 8, p. 1827-1849, August 1988.

Mander, J.B., Priestley, M.J.N., and Park, R. (1988). ”Observed stress strain behavior of confined concrete” Journal of Structural Engineering, ASCE, V.114, No. 8, p. 1804-1825, August 1988.

Mander, J. B. (1983). “Seismic design of bridge piers” PHd thesis. Uniersity of Canterbury, New Zealand, 442 p.

Mansur, M.A., Chin, M. S., and Wee, T. H. (1997). ”Stress-strain relationship of confined high strength plain and fiber reinforcement” Journal of Materials in civil engineering, V.9, No. 4, p. 171-179, November 1997.

Martinez, S., Nilson, A. H., and Slate, F. O. (1984). “Spirally reinforced High-Strength Concrete Columns.” ACI J., 81(5), 431-442.

Medland, I. C., and Taylor, D. A. (1971). “Flexural Rigidity of Concrete Column Sections.” Journal of Structural Division, ASCE, V. 97, No. ST2, Feb. 1971, pp. 573-586.
Najami, A., and Tayem, A. (1996). “Design of round reinforced concrete columns.” J. Struct. Engrg., ASCE, 122(9), 1062-1071.

O’shea. M. D. and Bridge, R. Q. (2000) “Design of circular thin walled concrete filled steel tubes” ASCE, vol 126, No 11,p1295-1303, November 2000

Popovics, S. (1973). “A Numerical Approach to the Complete Stress-Strain Curves of Concrete.” Cem. Concr. Res., 3(5), 583-59.

Rasheed, H. A. and Dinno, K. S. (1994) “An efficient nonlinear analysis of RC sections”., Computers and structures Vol 53, No. 3 P613-623

Razvi, S., and Saatcioglu, M. (1999). “Confinement Model for High-Strength Concrete.” J. Struct. Eng., 125(3), 281-289.

Richart. F. E., Brandtzaeg, A., and Brown R.L. (1982). “A Failure of Concrete under Combined Compressive Stress.” Bulletin No. 185, Engineering Station, University of Illinois, Urban.

Roy, H. E. H. and Sozen, M. A. (1965). “Ductility of Concrete” Flexural Mechanics of Reinforced Concrete, SP-12, American Concrete Institute/American Society of Civil Engineers, Detroit, pp. 213-224.

Saatcioglu, M., and Razvi, S. R. (1992). “Strength and Ductility of Confined Concrete.” J. Struct. Eng., 118(6), 1590-1607.

Saatcioglu, M., Salamt, A. H. and Razvi, S. R. (1995). “Confined columns under eccentric loading.” J. Struct. Eng., 121(11), 1547-1556.

Samra R. M., Deeb,N. A. and Madi, U. R. (1996), “Transverse steel content in spiral concrete columns subject to eccentric loading”, ACI j. v93, No. 4, August 1996.

Sargin, M. (1971). “Stress-Strain Relationships for Concrete and the Analysis of Structural Concrete Sections” Solid Mechanics Division, University of Waterloo, Study No. 4.

Scott, B. D., Park, R., and Priestley, N. (1982). “Stress-Strain Behavior of Concrete Confined by Overlapping Hoops at Law and High Strain Rates.” ACI J., 79(1), 13-27.

Sheikh, S. A., and Uzumeri, S. M. (1982). “Analytical Model for Concrete Confinement in Tide Columns” Journal of Structural Engineering, ASCE, V.108, No.ST12, P.2703-2722, December 1982.

Sheikh, S. A., and Toklucu, M. T. (1993). “Reinforced concrete columns confined by circular spirals and hoops” ACI J., 90(5), 542-553.

Soliman, M. T. M. and Yu, C. W. (1967). “The Flexural Stress-Strain Relationship of Concrete Confined by Rectangular Transverse Reinforcement” Magazine of Concrete Research (London), V.19, No.61, pp. 223-28, Dec. 1967.

Vallenas, J., Bertero, V. and Popov, E. (1977). ”Concrete Confined by Rectangular Hoops and Subjected to Axial Loads” Research Center Report UCB/EERC-77-13, University of California at Berkeley, August, 1977.

Wang, G. G., and Hsu, C. T. (1992). “Complete Biaxial Load-Deformation Behavior of RC Columns.” J. Struct. Engrg., ASCE, 118(9), 2590-2609.

Wang, P. T., Shah, S. P., and Naaman, A. E. (1978). “Stress-Strain Curves of Normal and Lightweight Concrete in Compression." ACI J., 75(11), 603-611.

Wee, T. H., Chin, M. S., and Mansur, M. A. (1996). “Stress-Strain Relationship of High Strength Concrete in Compression.” J. Mater. Civ. Eng., 8(2), 70-76.

Yong, Y-K, Nour, M.G. and Nawy, E.G. (1998). “Behavior of laterally Confined High-Strength Concrete under Axial Loads” Journal of Structural Engineering, V.114, No.2, P.332-351 , February 1998.